Monitoring ecosystem dynamics in semi-arid environments using multi-sensor Earth-observation

Thomas Phillip Higginbottom

School of Science and the Environment

Manchester Metropolitan University

A thesis submitted in partial fulfilment of the requirements of the Manchester Metropolitan University for the degree of

Doctor of Philosophy

2018

"We've grown used to wonders in this century. It's hard to dazzle us. But for twenty-five years the United States space program has been doing just that. We've grown used to the idea of space, and, perhaps we forget that we've only just begun. We're still pioneers..."

President Ronald Reagan. Address to the Nation following the Space Shuttle Challenger disaster - 28th January 1986

Abstract

Climate change and a growing human population are instigating major changes on the Earth's surface. Monitoring and understanding these changes as they unfold is critical for society and the environment. Satellite remote sensing provides the only means of achieving this over large spatial and temporal scales, and major progress in the application of Earth-observation imagery has been made since the beginning of the space age in the mid-20th century. However, savannahs - dynamic systems comprised of shrubs, trees, and grass species - have proved challenging for EO-based monitoring. Yet, these ecosystems cover almost 25% of the Earth's surface and are home to some of the poorest people on the planet. This thesis investigates the use of EO for monitoring ecosystem dynamics in African savannahs, focussing specifically on woody cover and biomass provision.

One of the most common Earth-observation (EO) based tools for monitoring vegetation is the Normalised Difference Vegetation Index (NDVI). A detailed review of the application of NDVI for monitoring land degradation was undertaken. This covered the historical context and ongoing debates around NDVI analyses, and highlighted key research gaps. NDVI was then used to map grass biomass for the Kruger National Park in South Africa, by combining *in situ* data with a downscaled NDVI dataset in a machine-learning framework. These predictions highlighted that the NDVI-biomass relationship is vulnerable to overfitting in space and time, due to spatial autocorrelation and a variable species composition, respectively.

The NDVI was further explored at the continental scale using multiple time-series analyses. These revealed that a majority of African savannahs have only experienced vegetation greening in the 1982-2016 period. Areas of declining vegetation, or changes in the trend direction,

were associated with phenological changes (i.e. a shrinking growth season), woodland degradation, or population increases.

Finally, fractional woody vegetation cover was mapped for the Limpopo province of South Africa using Landsat spectral metrics and ALOS PALSAR radar imagery and a series of Random Forest regression models. The most accurate models combined multi-seasonal Landsat data and the radar layers. However, this was only marginally more accurate than just using dry and wet season metrics alone. When using a single season of imagery, the dry season preformed best. These results were reaffirmed for categorical savannah land-cover classifications, highlighting the importance of multi-sensor and multi-temporal data.

The thesis contributes new insights for monitoring savannahs using EO imagery. By combining EO data with modern statistics and machine-learning methods novel insights to ecological and environmental issues can be gained. In the coming years, the increasing number of operational sensors and the volume of data collected will be of great benefit for environmental monitoring, especially in savannahs.

Acknowledgement

Contents

List of Figures

List of Acronyms

+

AGB	Above-Ground Biomass
AOT	Aerosol Optical Thickness
ALOS	Advanced Land Observing Satellite
APAR	Available Photosynthetically Active Radiation
ASTER	Advanced Spaceborne Thermal Emission and Reflection Radiometer
AVHRR	Advanced Very-High-Resolution Radiometer
BFAST	Breaks For Additive Season and Trend
CPU	Central Processing Unit
CV	Cross Validation
Envisat	Environmental Satellite
EO	Earth-observation
EOF	Empirical Orthogonal Function
EOT	Empirical Orthogonal Teleconnections
ERTS	Earth Resources Technology Satellite
ESA	European Space Agency
ETM+	Enhanced Thematic Mapper Plus
FASIR	Fourier-Adjustment, Solar zenith angle corrected, Interpolated Reconstructed
FAO	Food and Agriculture Organisation
FFS	Forward Feature Selection
FLEX	Fluorescence Explorer
FPAR	Fraction Photosynthetically Active Radiation
GAM	Generalised Additive Model
GDP	Gross Domestic Product
GIMMS	Global Inventory Monitoring and Modeling System

GLADA	Global Assessment of Land Degradation and Improvement
GVI	Global Vegetation Index
HDI	Human Development Index
HH	Horizontal-Horizontal Polarization
HV	Horizontal-Vertical Polarization
ISRIC	International Soil Reference and Information Centre
JAXA	Japan Aerospace Exploration Agency
JERS	Japanese Earth Resources Satellite
LAI	Leaf Area Index
LIDAR	Light Detection And Ranging
LLO	Leave Location Out
LLTO	Leave Location and Time Out
LTDR	Land Long Term Data Record
LTO	Leave Time out
LUE	Light Use Efficiency
LULCC	Land use/land cover change
MAE	Mean Absolute Error
MAP	Mean Annual Precipitation
MERIS	Medium Resolution Imaging Spectrometer
ML	Machine Learning
MLC	Maximum Likelihood Classifier
MODIS	Moderate Resolution Imaging Spectroradiometer
MSS	Multi-spectral Scanner System
NASA	National Aeronautics and Space Administration
NDVI	Normalized Difference Vegetation Index
NPP	Net Primary Productivity
NIR	Near Infrared
NOAA	National Oceanic and Atmospheric Administration
OLI	Operational Land Imager

PAR	Photosynthetically Active Radiation
PAL	Pathfinder AVHRR Land-record
PALSAR	Phased Array type L-band Synthetic Aperture Radar
PCA	Principle Components Analysis
PMR	Precipitation Marginal Response
RESTREND	Residual Trends
RFE	Recursive Feature Elimination
RMSE	Root Mean Squared Error
RUE	Rain Use Efficiency
SAR	Synthetic Aperture Radar
SeaWiFS	Sea-Viewing Wide Field-of-View Sensor
SLC	Scan Line Corrector
SPOT	Satellite Pour l'Observation de la Terre
SRTM	Shuttle Radar Topography Mission
TAMSAT	Tropical Application of Meteorology Using Satellite Data and Ground-Based Observations
TOA	Top of Atmosphere
TOC	Top of Canopy
TM	Thematic Mapper
TVI	Transformed Vegetation Index
UN	United Nations
UNCCD	United Nations Convention to Combat Desertification
USGS	United States Geological Survey
VCA	Veld Condition Assessment
VVI	Visible Vegetation Index
WRS	World Reference System

Chapter 1

Introduction

1.1 Motivation

In July 2018, the human population of the Earth surpassed 7.6 billion persons, co-inciding with an atmospheric carbon dioxide concentration of $>$ 410 ppm. Both these records are a testament to anthropogenic manipulation of the Earth's surface and harnessing of ecosystem service production. By the early 21st century, humans had directly modified 75% of the Earth's ice-free surface and appropriated over 25% of primary production annually for food, fuel, and fibre (Krausmann et al. 2013, Ellis et al. 2010). In addition to these anthropogenic pressures, the biosphere is increasingly affected by climatic change as temperature and rainfall regimes are altered. Over the coming decades, both human and climatic affects are likely to increase, making it essential that ecosystem dynamics - how ecosystems function and change - are well understood.

The most obvious ecosystem function changes are abrupt transformations, such as deforestation or urbanisation. Less apparent are changes occurring in systems such as savannahs, defined as heterogeneous mosaics of grass, shrub, and tree species. However, these ecosystems cover 20% of the Earth surface, including a majority (65%) of the African continent (Figure 1.1), and are cumulatively the largest terrestrial vegetation carbon stock (Archibold 2012).

Savannahs are critical for both the ecosystem services they provide to some of the world's poorest people, and for their unique and endangered biodiversity. Furthermore, over the coming decades they are projected to experience increasing ecological, climatic, and human pressures. This makes it imperative that shifts in their ecosystem functionality are monitored and understood, to better enable their appropriate management. However, savannahs are difficult systems to monitor,

due to their heterogeneity and large spatial coverage. It is this difficulty that the research presented here attempts to elucidate, by focusing on the use of Earth-observation to monitor and understand the ecosystem dynamics of African savannah systems.
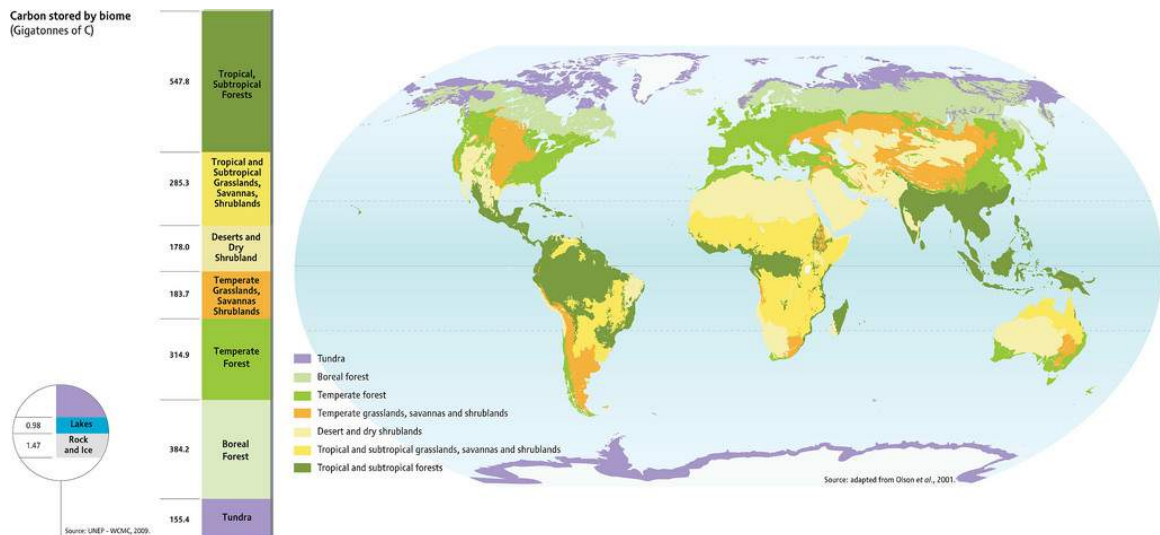
Figure 1.1: Global distribution of biomes and their Carbon stocks. Source UNEP, after Olson et al. (2001)

Why African Savannahs?

It has been argued that nowhere is ecosystem monitoring more important, for both social and environmental concerns, than Africa (Reynolds et al. 2011). No African nation appears in the top third of the global Human Development Index (HDI) rankings, with only five countries (Seychelles, Mauritius, Algeria, Tunisia, and Libya) obtaining a 'high' classification (UN 2016) . In particular, sub-Saharan Africa is afflicted by low development, with 389 million people (41%) currently living in extreme poverty on less that int.$1.90 per day: a proportion that has declined at a far slower rate than other regions over the past 30 years (Figure 1.2).

The low development of sub-Saharan Africa coincides with a high dependency on ecosystem services for livelihoods, particularly within rural populations. A majority of sub-Saharan residents (80%) depend on wood collection for fuel (IEA 2010); even in relatively developed South Africa, 54% of rural households use biomass fuel (Pereira et al. 2011). The woody components of savannahs and sparse woodlands are therefore crucial for local inhabitants. Concurrently, rearing livestock, such as
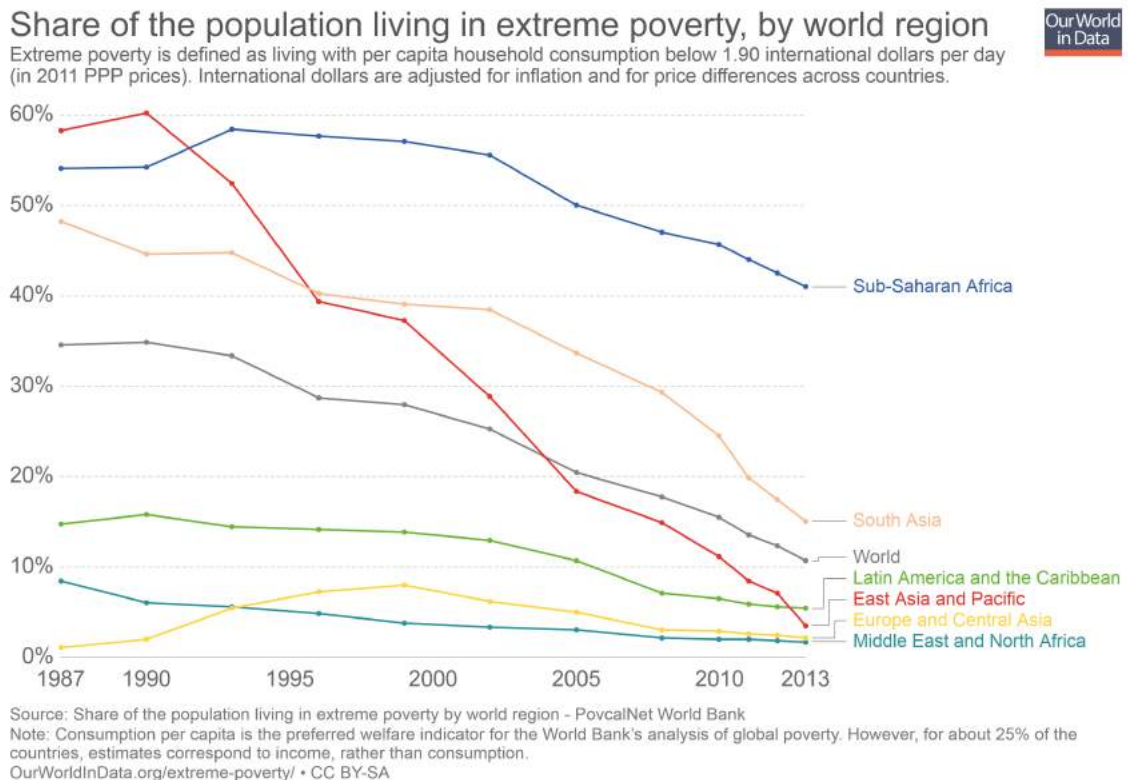
Figure 1.2: Proportion of people living in extreme poverty by continent. Source: https://ourworldindata.org/extreme-poverty

goats and cattle, is an important source of food and income for rural residents, especially in arid regions where arable agriculture is less feasible. Pastoralism is, inherently, dependent upon the availability of forage in the form of grass; reductions in grass cover, for either bare ground or woody cover, can incur major economic consequences (Anadón et al. 2014).

The biodiversity of Africa and it's savannah regions is globally unique. Megafauna, particularly large mammals, are present across vast areas of African savannahs in densities and diversity not found on other continents. In addition, Africa possess large number of endemic mammals, birds, and reptiles (Figure 1.3). The continued sustainability of this biodiversity is dependent upon the existence of sufficient quantity and quality of appropriate habitat. This requirement is amplified by the large migrations undertaken by many animals, as herds follow seasonal rains and vegetation. In addition to its intrinsic value, African biodiversity is a major generator of tourism revenue. Despite poor infrastructure, in 2012 alone the 33.8 million visitors in sub-Saharan Africa generated $36 billion (2.8% of GDP) (World Bank 2013).
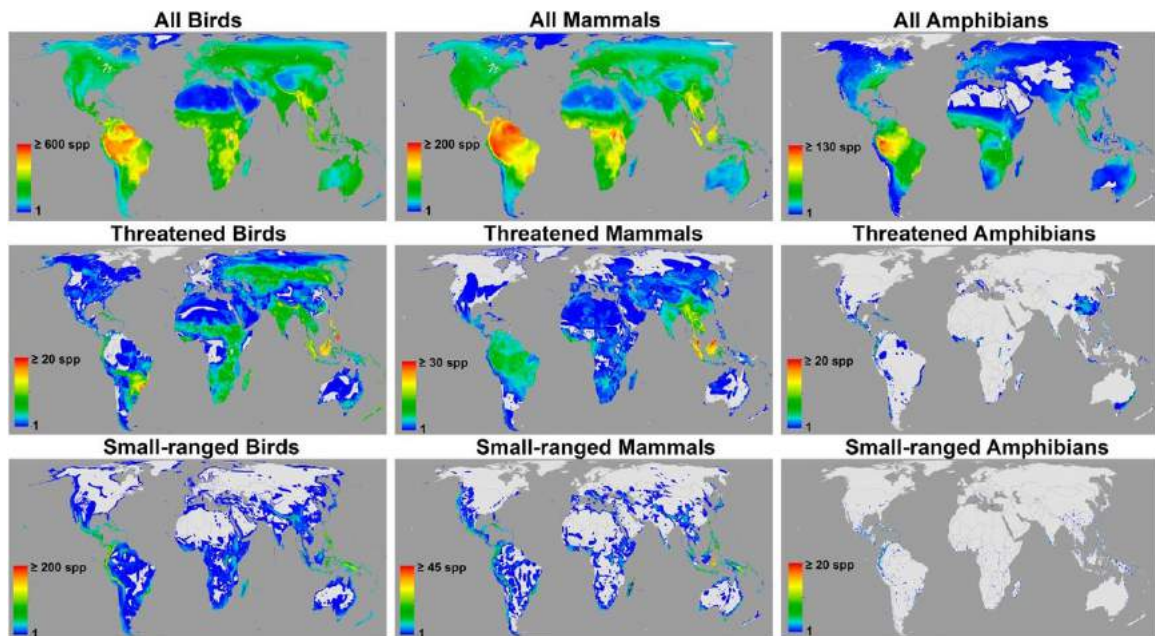
Figure 1.3: Global distribution of species richness for different categories of species. Top row: all species in taxon. Middle row: only threatened species (vulnerable, endangered, or critically endangered in the IUCN Red List). Bottom row: only species with a geographic range less than the median range size for that taxon. Source Jenkins et al. (2013)

Any plans to accelerate development and reduce food insecurity in sub-Saharan Africa necessitate a focus on agriculture, a goal that has historically been hampered by a proliferation of civil conflict and limited infrastructure, making sub-tropical Africa one of the least integrated agricultural markets in the world, with a limited presence of international trade. This situation in liable to imminent change. An ongoing decrease in conflict is co-occurring with displacement of agriculture from South America, due to regulation and rising land prices, spurring agricultural investments. Furthermore, large-scale Chinese infrastructure projects are opening up inland areas once too isolated for international trade. Large areas of savannahs are, therefore potentially vulnerable to agricultural conversion, particularly for soy beans. Although these developments have great potential to reduce poverty and food insecurity, novel and biodiverse ecosystems could become threatened.

1.2 Using Remote Sensing to Monitor Ecosystem Dynamics

Global environmental problems require data at large spatial and long-term temporal scales. For many, if not all, regions the only data source meeting these requirements is Earth-observation (EO) satellites. The first bespoke Earth-observation satellite was launched in 1972, as the Earth Resources Technology Satellite 1. This was the first component of what was to become the Landsat series, now the longest continually operational Earth-observation mission. The 46 plus years of imagery collected by the seven (successfully launched) Landsat sensors is arguably the most comprehensive evidence of changes occurring on the Earth's surface over a period in which the human population has doubled and global warming has become apparent (Kennedy et al. 2014) (Figure 1.4).
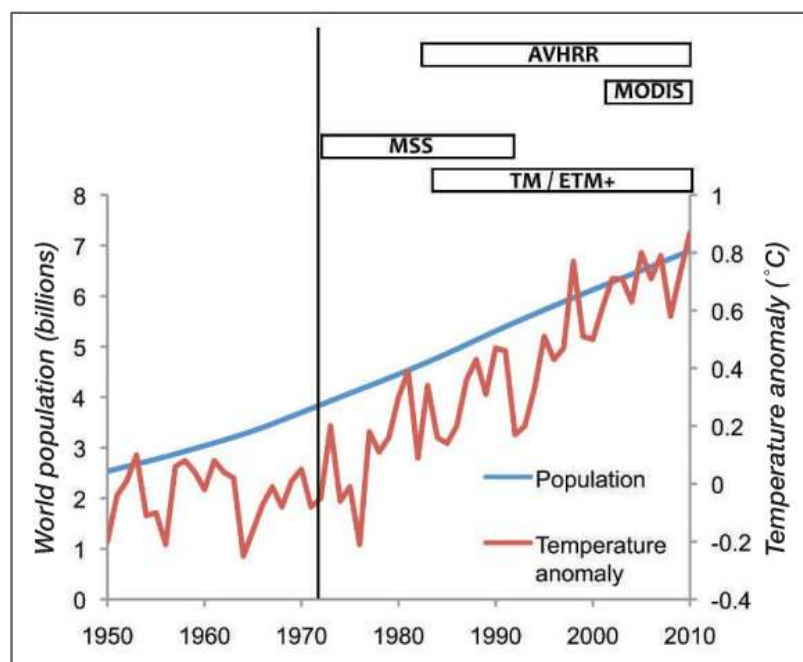
Figure 1.4: Periods covered by the most commonly-used Earth-observation sensors, corresponding to human population and global temperature, source Kennedy et al. (2014)

Earth-observation sensors can broadly be categorised into two types: passive or active. Active, such as radar or lidar, sensors emit radiation towards a target and measure the reflected (or returned) energy. Conversely, passive (i.e optical) sensors lack a method for generating radiation, and measure the reflected energy emitted by a third party source (i.e. the Sun) (Warner et al. 2009). These differences

in operation result in the data provided by both systems possessing different advantages and limitations. Active sensors are not limited to the radiation wavelengths present within sunlight; they operate with radar wavebands which can penetrate clouds and vegetation canopies be to used. Passive sensors, on the other hand, rely on sunlight which can be blocked by clouds, but negates the need for an energy source, making them cheaper and operational for longer.

This PhD was undertaken at an especially opportune time for Earth-observation, benefiting from two major advances: open-data policies and increases in computation power. Firstly, in 2008, the US government made their historic and future Landsat collections freely available and began efforts to collect and centralise image collections held around the world (Woodcock et al. 2008, Wulder et al. 2016). These efforts have enabled Landsat-based analyses to use an amount of imagery that would have been economically unfeasible under a commercial distribution model (Wulder et al. 2012, Kennedy et al. 2014). Traditional studies would typically use a single image to map land cover, and a handful of images to monitor change (Singh 1989, Lunetta and Elvidge 1999). It is now possible to use dense stacks of imagery to map ecosystem properties and change at large spatial and regular temporal scales (Griffiths et al. 2013, Kennedy et al. 2010, Roy, Ju, Kline, Scaramuzza, Kovalskyy, Hansen, Loveland, Vermote and Zhang 2010). Secondly, computing power has become considerably cheaper and more accessible in recent years, for both desktop computers and cloud services. This is exemplified by Hansen et al. (2013) who analysed 654,178 million Landsat scenes (143 billion 30m pixels) to generate the first high-resolution, global maps of forest cover and change. This was possible due to Google Earth Engine, a cloud-based server developed by Google inc. in California (Gorelick et al. 2017). By hosting the entire Landsat (and other imagery) archive on an accessible and freely-available cloud server it is now possible to perform computationally demanding calculations that would previously have taken months or years to complete; e.g. Hansen et al. (2013) would have required one million CPU-core hours on 10,000 PCs. This typifies a 'take the methods to the data' approach, where the time and money consuming process of data processing is completed remotely, and researchers instead move their analysis codes to where the data is located.

This thesis focuses, in particular, on two ecosystem attributes that are key for savannahs: woody coverage, and biomass. The woody cover component of savannahs is the top-down 2-dimensional proportion (%) of ground covered by the

canopies of woody plants, including trees and shrubs. Biomass is the vegetation carbon content (Kg ha^{-1}) accumulated through Net Primary Production (NPP). These attributes were chosen as they are fundamental to ecosystem service provision, and are key indicators of environmental change (Running et al. 2004, Eldridge et al. 2011, Myneni et al. 1997).

Land Cover Mapping

The woody cover chapters of this thesis are, fundamentally, concerned with the mapping of land cover. Classifying imagery into maps of land use or land cover has been one of the primary applications of Earth-observation since the launch of Landsat 1- then known as the Earth Resources Technology Satellite 1. The classification of satellite imagery involves three stages: the collation of training pixels that are of a known class; the acquisition of some satellite-derived variables that are to be classified, and finally, the application of a statistical model to generate predictions for pixels not included in the training data. Although these components have been consistent since the 1970s, major developments have occurred in the types of predictors and statistical models available.

Early land cover studies relied heavily on Maximum Likelihood Classification (MLC), a Bayesian approach that uses the class-level mean and standard deviation of the predictor variables to assign probabilities of class membership to pixels. However, as MLC is based on the mean of the training data, each predictor band per class must be normally distributed. Other classification methods used in early studies include minimum distance, decision trees, and parallelepiped. All of these techniques benefit from being computationally light, a key requirement when dealing with what was until recently considered sizeable datasets. However, these methods generally preform sub-optimally when compared with statistical techniques developed in the 2000s. Therefore, the most commonly used classifiers for contemporary studies are generally derived from machine learning, such as Random Forests (James et al. 2013, Kuhn and Johnson 2013).

Random Forests are an extension of the simpler decision tree technique. In decision trees, the outcome class (or leaf) is determined based on a series of rules splitting the predictor variables (nodes). This method is easily interpretable and quick to compute. However, small shifts in the training data can produce markedly different trees- they have high variance but low bias, making their predictive power

over unseen data rather weak. Random Forests overcome this weakness of decision trees by iteratively sampling from the full dataset, generating a decision tree and validation against the withheld sample. This process can be repeated multiple times, with a final prediction based on an average of these trees.

Improvements in statistical models has allowed a proliferation in the number of predictors that can be applied. Traditional classifiers behave poorly when the number of predictor variables increases, as the dimensionality of the feature space expands (i.e. the 'curse of dimensionality') (Guyon et al. 2002, Guyon and Elisseeff 2003). This development has also coincided with improvements in open-data policies and data availability. Therefore, inputs to classification models are no longer limited to single date cloud-free images, and instead can be derived from large numbers of candidate images. Roy, Ju, Kline, Scaramuzza, Kovalskyy, Hansen, Loveland, Vermote and Zhang (2010), Griffiths et al. (2013) developed the concept of best available pixel compositing. The approach takes all available Landsat images and selects the optimum pixel based on a series of criteria, e.g. target date, year, proximity to clouds, or radiometric quality. A simpler process of generating spectral-temporal variability metrics has also proved popular. This method generates summary statistics (e.g. mean, standard deviation, percentiles) on a pixel-level basis from all cloud-free observations (Müller et al. 2015). These statistics have the benefit of conveying information on the temporal variability of a pixel, which can be informative for many land cover types. Further temporal parameters can be derived from fitting statistical curves to raw observations. This is a desirable option, as many land cover types are distinctive in their temporal evolution (Brandt et al. 2016, Zhang et al. 2014). However, for reliable curves to be fit there must be sufficient data points present, a requirement that is not typically met for many areas outside of the United States.

In many environments, mapping land cover as a single class is not an ideal strategy, as habitats may be heterogeneous at the pixel scale. In these regions, mapping the sub-pixel or fractional cover of different land cover types is more appropriate. This can be achieved through a variety of methods such as spectral unmixing, whereby a spectrum is decomposed into contributions from pure spectra (endmembers) (Lillesand et al. 2004); alternatively, regression analysis can predict coverage based on training data that quantifies the subpixel content. Fractional land cover maps can be more ecologically relevant especially where one class is of particular concern (Naidoo et al. 2015).

8

Biomass and Primary Production

The first step towards the accumulation of vegetation biomass is photosynthesis; where water (H_2O) and carbon dioxide (CO_2) are combined with sunlight in the form of photons (γ), to produce carbohydrates (CH_2O_n) and oxygen (O_2); Equation 1.1).

$$2nCO_2 + 2nH_2O + \gamma = 2(CH_2O)_n + 2nO_2 \qquad (1.1)$$
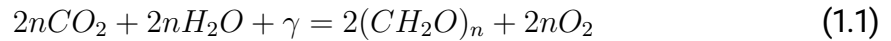
In nearly all plants and algae, the chlorophyll pigment within chloroplasts is responsible for the absorption of sunlight and the operation of photosynthesis. The biomass accumulated over a period of time is referred to as *Gross* Primary Production (GPP), a portion of which is used by plants for maintenance of cells and respiration, with the remainder constituting NPP. The main wavelengths of light absorbed by photosynthesis are the red and blue spectra, which gives vegetation it's characteristic green colouring (Figure 1.5.A). Collectively, this spectral region that is available for photosynthesis is the Photosynthetically Active Radiation (PAR), i.e. the ratio of NPP to PAR, which quantifies the efficiency of the photosynthesis that has occurred. The later is referred to as Light Use Efficiency (LUE).

The first attempts to model NPP at large-scales were the empirical equations developed by Whittaker and Marks (1975). Globally distributed weather data were used to estimate actual evapotranspiration (AET), which was then regressed against a small number of NPP crop field sites. The resulting equation (Equation 1.2),

$$NPP = 3000\{1 - \exp[-0.000995(AET - 20)]\} \qquad (1.2)$$

when applied to the extrapolated AET estimates, produced a global NPP value of 118 billion metric tons of carbon per annum. Climate-based methods of estimating NPP were, for many years, the only method of large-scale analysis. However, they have fundamental constraints for monitoring purposes, as weather data are limited in spatial coverage and resolution (Running et al. 2004). Furthermore, this approach assumes that the only limitation to NPP is climate, with no quantification of the role played by nutrients, management, or most importantly varying LUE. An ideal option would be the monitoring of photosynthesis directly, i.e. without having to not rely on climatic constrains. This aim has been the focus of much work using optical remote sensing, with varying degrees of success (Eisfelder et al. 2012, Wessels et al. 2006), .

As photosynthesis is fundamentally a process of the absorption and processing of sunlight, it is reasonable to assume that optical-based EO has good potential for monitoring or modelling the process. The most common, and simplest method for achieving this is the use of broad-band vegetation indices, the most ubiquitous of which is the Normalised Difference Vegetation Index (NDVI):

$$NDVI = \frac{(\rho NIR - \rho Red)}{(\rho NIR + \rho Red)} \tag{1.3}$$

where ρNIR is reflectance in the 0.7-1.3μ near infra-red wavelength range, and ρRed is reflectance in the visible red spectra, around 0.67μ (Tucker et al. 1973). This formulation takes advantage of the 'red-edge' phenomena of vegetation spectra, where the reflectance of healthy plants increases sharply between 0.68 and 0.73μ (Figure 1.5.A). This is the threshold at which sunlight transitions from being beneficial to plants and absorbed for photosynthesis, to being potentially harmful by causing overheating and cell damage, and is reflected (Prince 1991, Warner et al. 2009).

NDVI is not a direct measure of either biomass or NPP; it does however, show a strong linear relationship to both of these variables in low-to-moderately productive environments (Prince 1991). In practice, NDVI can more broadly be considered a proxy of vegetation vigour or greenness, not a strict ecological parameter. As it is most sensitive to variations in the vegetation of low-to-moderate systems, it is commonly used in semi-arid area,; where it is one of, if not the most, common methods of monitoring biomass fluctuations over large areas (Eisfelder et al. 2012).

NDVI can be calculated from any sensor that collects red and infra-red wavebands, whether aboard a satellite, an aircraft, a drone, or ground based. After being conceived using ground-based spectroradiometers, the first space-borne application of NDVI used imagery from the newly launch Landsat 1 (Tucker et al. 1973, Prince and Astle 1986). However, the key breakthrough for ecosystem monitoring came in 1981 when modifications to the Advanced Very High Resolution Radiometer (AVHRR) sensor aboard the 7th instalment of the National Oceanic and Atmospheric Administration's (NOAA) polar orbiting platforms shifted the near-infared channel, allowing the detection of vegetation (Tucker 1979, Cracknell 2001). Although AVHRR imagery were coarse resolution (8 km pixels), even by the standards of the 1970s and 1980s (Landsats 1-4 were 60 m), it had the benefits of being an operational mission with two sensors continuously in orbit, resulting in rapid repeat coverage of the whole Earth. This enabled the imagery to be composited at regular
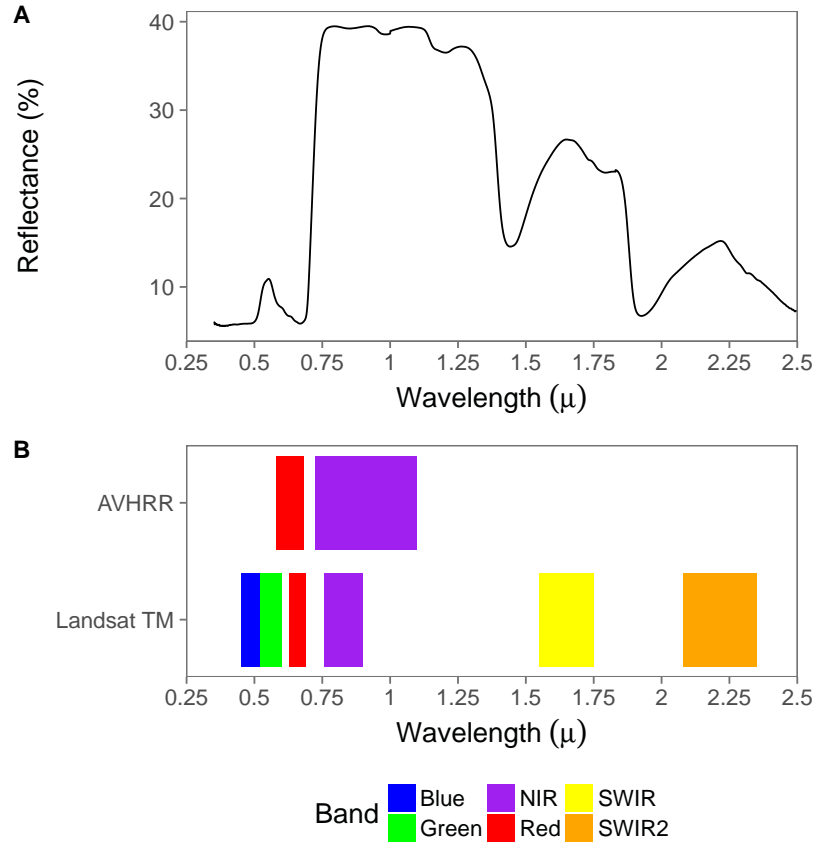
Figure 1.5: A) Spectral profile of a healthy oak tree (ASTER library), B) respective wavebands for Landsat and AVHRR)

intervals such as monthly or bi-monthly (15-day) periods across entire continents, a spatial and temporal scale unimaginable using Landsat imagery at the time (Tucker et al. 1986, Prince and Tucker 1986). The NDVI data produced by AVHRR were fundamental in the development of global ecological science, providing the ability to undertake large-scale analyses to issues typically studied at small-scales: including deforestation in the Amazon, desertification in the Sahel, and studying phenological cycles (Tucker et al. 1991, Skole and Tucker 1993, Tucker, Townshend and Goff 1985).

It is possible to deterministically convert NDVI to NPP. However, this process requires a number of additional stages. The Moderate resolution imaging spectrometer (MODIS) NPP product (MOD17A3) achieves this by the following stages (Running et al. 2004): firstly, NDVI is used as a measure of the *Fraction* of PAR (FPAR) according to:

$$APAR/PAR \approx NDVI \approx FPAR \qquad (1.4)$$

Secondly, GPP is estimated according to:

$$GPP \approx \varepsilon \times FPAR \approx \varepsilon \times NDVI \times PAR \qquad (1.5)$$

where ε is a landcover-specific conversion efficiency value, analogous to a simple LUE score. Thirdly, the daily GPP is converted to *net* photosynthesis (PSN$_{net}$) by deducting a 24-hour estimate of maintenance costs (R$_{lr}$):

$$PSN_{net} = GPP - R_{lr} \qquad (1.6)$$

Finally, the daily GPP is summed to NPP after removing annual maintenance costs for leaves and roots (R$_g$ and R$_m$):

$$NPP = \sum (PSN_{net} - R_g - R_m) \qquad (1.7)$$

This approach requires a number of assumptions, such as the parametrisation of ε and R_{lr} that are problematic in many regions. In particular, using a landcover-derived ε has proved flawed in semi-arid African ecosystems, which are highly heterogeneous at the 1 km scale of MODIS land cover products (Fensholt et al. 2006). Therefore, for semi-arid regions, NDVI is often considered preferential to NPP models, due to simplicity, historical usage, and fewer assumptions.

1.3   Aims

The overarching aim of this thesis is to improve the capacity of Earth-observation for monitoring the ecosystem dynamics and health of semi-arid savannah ecosystems. This is aim is envisioned as a precursor to potential operational monitoring systems. The following research questions contribute towards this aim:

1. What is the current status and potential limit of land degradation monitoring frameworks?

2. Can grass biomass be reliably mapped using coarse-resolution NDVI data?

3. What is the most accurate method for mapping the fractional woody cover of savannahs?

4. How has regional-scale woody cover changed in northern South Africa since 1984?, and what are the drivers of this change?

5. What are the continental-scale trends in vegetation greenness since 1982 for Africa?

1.4   Thesis Structure

This thesis is presented as five stand-alone papers, which have either been published, are undergoing peer review, or pending submission. These chapters are independent but have a common theme of using remote sensing for monitoring savannah ecosystems.

Chapter Two is a review paper, providing an in-depth summation on the use of vegetation indices for monitoring land degradation (Higginbottom and Symeonakis 2014). Coarse resolution indices, such as the NDVI, are arguably the most common method for assessing savannah ecosystem dynamics having been used in the Food and Agriculture Organisation's (FAO) Global Assessment of Land Degradation and Improvement (GLADA) project (Bai et al. 2008). As a concept, using a proxy of photosynthesis to monitor the condition of ecosystems appears simple and appealing. However, the theoretical and methodological implementation of this theory is highly controversial, with a long history of contentious debate. This chapter summarises the historical background and academic debates concerning the use of NDVI for degradation monitoring, and provides a number of recommendations for future study.

Chapter Three presents a statistical study on the relationship between NDVI and grass biomass, for the Kruger National Park South Africa. This relationship has been acknowledged and studied for 40 years, providing the basis for many applications (as discussed in Chapter Two). Yet there is a lack of robust spatio-temporal analysis on how reliable this relationship and what factors have influence. In this study, machine learning methods are combined with target-orientated, spatio-temporal, cross validation procedures to test how reliable and transferable NDVI-biomass relationships are.

Chapter Four is a methodological study on mapping the *fractional* woody cover of savannahs (Higginbottom et al. 2018). This paper tests the ability of radar and optical data to generate large-area woody cover maps for the Limpopo province of South Africa. A variety of multi-sensor datasets are used including: a pre-processed L-band radar mosaic, a series of multi-seasonal spectral-temporal metrics derived from large volumes of Landsat imagery, and high-resolution aerial imagery. These

data are combined in a machine learning framework to identify the benefits and limitations of different seasonal and sensor combinations for fractional woody cover mapping.

Chapter Five extends the approach developed in Chapter Three into a multi-temporal study. Landsat metrics are classified into maps of woody cover change, for two northern South African provinces from 1986-2012. This change data is then used to test three theories on the causes of shrub encroachment. There are three competing theories to explain woody cover changes: i) land managment and grazing, ii) atmospheric carbon fertilisation, and iii) rainfall variation. Considering these possible explanations, a series of variables were compiled and used in a modelling framework to test which of these proposal works best in South Africa.

Chapter Six builds on some of the issues raised in Chapter Two, by examining vegetation greenness in African savannahs, using a variety of methods. A 34 year NDVI time-series is aggregated into two annual metrics: maximum and sum. These metrics are used as inputs into both linear and piecewise, time-series regression models. By using two metrics and two analyses, it is possible to infer ecological driver throught the similarities and differences of the results.

Chapter 2

Assessing Land Degradation and Desertification Using Vegetation Index Data: Current Frameworks and Future Directions

Citation

This chapter has been published as a review paper in the following journal article:

2.1 Abstract

Land degradation and desertification has been ranked as a major environmental and social issue for the coming decades. Thus, the observation and early detection of degradation is a primary objective for a number of scientific and policy organisations, with remote sensing methods being a candidate choice for the development of monitoring systems. This paper reviews the statistical and ecological frameworks of assessing land degradation and desertification using vegetation index data. The development of multi-temporal analysis as a desertification assessment technique is reviewed, with a focus on how current practice has been shaped by controversy and dispute within the literature. The statistical techniques commonly employed are examined from both a statistical as well as ecological point of view,

and recommendations are made for future research directions. The scientific requirements for degradation and desertification monitoring systems identified here are: (I) the validation of methodologies in a robust and comparable manner; and (II) the detection of degradation at minor intensities and magnitudes. It is also established that the multi-temporal analysis of vegetation index data can provide a sophisticated measure of ecosystem health and variation, and that, over the last 30 years, considerable progress has been made in the respective research.

2.2 Introduction

The United Nations Convention to Combat Desertification (UNCCD), ratified by 195 countries, identifies land degradation and desertification as one of the most pressing environmental concerns of our times (UNCCD 1994, 2002). Furthermore, the UN Conference on Sustainable Development ("Rio + 20") has called for a target of *"zero net land degradation"*, whereby the rate of deteriorating lands would be counterbalanced by the rate of land improvement. These political frameworks, whilst admirable, require sound scientific evidence for effective implementation (Grainger 2015). However, in spite of political and scientific recognition of the importance of land degradation, current estimates of its extent and severity are highly unreliable and spurious. The often quoted statistics that 15% of the Earth's surface and 60% of drylands are degraded (Oldeman et al. 1991), are acknowledged as qualitative and unsubstantiated (Nicholson et al. 1998, Thomas et al. 1994). These estimates, based on coarse resolution expert opinions, are not suitable for policy making or for scientific investigations into the potential remediation of degraded lands (Glenn et al. 1998).

The timely and early detection of degradation processes is necessary to prevent the continuing deterioration of land condition. The lack of authenticated evidence on the magnitude of desertification has led to questions over the very existence of a global degradation problem (Fensholt et al. 2012, Helldén and Tottrup 2008), with large-scale studies frequently at odds with plot and field-scale studies (Miehe et al. 2010, Hein et al. 2011). There is a pressing need, therefore, for accessible and accurate measurements on the extent of degradation and desertification for policy, natural resource management and scientific research needs (Glenn et al. 1998, Verrôn et al. 2006). Given the temporal nature of land degradation, it is paramount that measurements adhere to the principles of repetitiveness, objectivity and consistency (Hill et al. 2008). These requirements, combined with the size of the land

occupied by semi-arid regions and the degree of development of many vulnerable nations, make Earth Observation (EO)-based systems a candidate choice for establishing monitoring networks (Bai et al. 2008, Symeonakis and Drake 2004). So far, the most frequently utilised method employing EO datasets is trend analysis of vegetation index data, most commonly the Normalised Difference Vegetation Index (NDVI), as a proxy for Net Primary Production (NPP).

Land degradation and desertification is a complex area of scientific research. This complexity partly arises from an open discussion on the definition of what actually constitutes degradation. This confusion occurs due to the interdisciplinary nature of desertification, encompassing geographical, ecological, meteorological and social perspectives, all of which can have regionally specific interpretations (Warren 2002). Early observations, provided by European foresters in 1930's West Africa, classified desertification as the consequence of desert boundary displacement (Stebbing 1935). This viewpoint was later adapted to cover a variety of mechanisms that would result in a detrimental impact upon *"the physical, chemical or biological status of land which may also restrict the land's productive capacity"* (Chartres 1987). Quantifying desertification by measurements of vegetation productivity and cover has led to long running debates concerning both the acknowledgement and inference of climatic influence on semi-arid ecosystems, with the UNCCD acknowledging that degradation can result from *"various factors including climate variations and human activities"* (UNCCD 1994). For a comprehensive review of the various definitions and their contexts see reviews by (Nicholson et al. 1998, Thomas et al. 1994, Herrmann and Hutchinson 2005). For the purpose of this article, we follow the definition used by the Millennium Ecosystem Assessment (Safriel and Adeel 2005), which refers to land degradation as *"the reduction in the capacity of the land to perform ecosystem goods, functions and services that support society and development"*, and to desertification as the same process in arid and semi-arid environments (collectively, the drylands). Hence, we use the terms desertification and degradation interchangeably. This definition considers the ability of land to support primary production as key ecosystem service, and its adoption implies that a reduction in the measured NPP at a site can potentially be viewed as land degradation (Wessels et al. 2012). This notion forms the theoretical framework on which the majority of EO-based assessments of degradation are founded, e.g., Symeonakis and Drake (2004), Bai et al. (2008), Prince et al. (1998). The potential of vegetation index variation as a measure of ecosystem health has been acknowledged for nearly 30 years (Tucker et al. 1986), yet in spite of this simple concept, the subject

has become extremely controversial within the scientific literature (Bai et al. 2008, Prince et al. 2007, Wessels 2009). This controversy prevents the realisation of land degradation early warning and monitoring systems, which have been postulated for some time (Symeonakis and Drake 2004).

In this paper, we review the theoretical and statistical frameworks used for assessing land degradation with vegetation indices with a view to clarify current understandings and to highlight avenues for future research. Our specific objectives are to provide:

1. A brief review of the origin of NDVI and the association of multi-temporal analysis in an land degradation framework;

2. An evaluation of the current methods used to assess degradation and desertification through vegetation indices;

3. An assessment of how these methods integrate into the wider debates on the mechanisms and processes of land degradation.

Although the focus of this review is the assessment of degradation and desertification in drylands, the frameworks discussed are by no means exclusive to this subject or environment, and are in many cases equally applicable to more wide-ranging global environmental change studies (Alcaraz-Segura, Chuvieco, Epstein, Kasischke and Trishchenko 2010).

2.3   NDVI: Origin and Data

NDVI is expressed as:

$$NDVI = \frac{NIR - Red}{NIR - Red} \tag{2.1}$$

where NIR and Red are reflectance values in the near-infrared and red wavebands, respectively. Thus, values range between -1 and 1 with an NDVI <0 indicating cloud or water and >0.7 dense canopy coverage. There is some confusion over the exact origin of the NDVI. Although frequently cited as the original record, both Deering (1978) and Rouse et al. (1973) used the *transformed* vegetation index ($TVI = \sqrt{NDVI + 0.5}$), *not* the NDVI. A number of ecology and spectroscopy studies through the late 1960s and 1970s used NDVI, with the original paper remaining elusive (Birth and McVey 1968, Jordan 1969, Pearson and Miller 1972). In light of

this confusion, the NDVI is most commonly credited to Tucker (1979) who compared field biomass data with various band combinations obtained from hand-held spectroradiometer readings.

NDVI is not a direct measure of vegetation or biomass, hence, it is not directly translatable into NPP. However, there is a considerable volume of literature reporting a close coupling between NDVI and in-situ NPP measurements (Tucker et al. 1986, Tucker, Vanpraet, Sharman and Van Ittersum 1985, Prince and Astle 1986, Wessels et al. 2006). For a full review of the advantages and limitations of vegetation index usage in dryland regions refer to Eisfelder et al. (2012) and references therein. A key limitation of NDVI in regions of sparse biomass is the influence of soil interference, thus it is not advisable to apply NDVI in regions with an average value of NDVI <0.1.

Time series analysis of NDVI can be applied using any system capable of measuring reflectances in the red and near infrared reflectance bands. However, long-term studies encounter data consistency and availability issues from a number of factors, including solar zenith angle, volcanic aerosols, sensor degradation and sensor compatibility. As such, analyses commonly utilise pre-processed datasets corrected for these issues (Table 1). The longest source of imagery available is obtained from the Advanced Very High Resolution Radiometer (AVHRR) sensor. Developed datasets include the 1981-2001 Pathfinder AVHRR Land-record (PAL) (Townshend 1994), the 1981-2006 Global Inventory Modelling and Mapping Studies (GIMMSg) (Tucker et al. 2005), and the 1981-2011 GIMMS3g (Pinzon and Tucker 2014) at 8 km resolutions A recent European consortium have merged AVHRR data with SPOT imagery generating a 5 km (1981-1998) and 1 km (1998-2012) product (Verger et al. 2012). The AVHRR-derived datasets, in particular the GIMMS and GIMMS3g products, continue as the most popular record, due to the unparalleled time span, in spite of the increasing availability of higher resolution products, such as SPOT (1 km), MERIS (1 km) and MODIS (500 m), all of which feature reduced time-spans. A comprehensive review of the available NDVI data sets is given in Pettorelli (2013).

2.4   Background of Multi-Temporal Analyses

The use of NDVI for assessing desertification originates in the Sahel region of sub-Saharan Africa, which experienced a prolonged reduction in rainfall between 1960 and 1990 (Figure 2.1), with particularly severe droughts in 1973, 1984, and 1990

Name	Sensor	Time-Span	Time-Step	Resolution
Pathfinder (PAL)	AVHRR	1981-2001	10-day	8 km
Global Vegetation Index (GVI)	AVHRR	1981-2009	7-day	4 km
LTDR	AVHRR	1981-2013	Daily	5 km
FASIR	AVHRR	1982-1998	10-day	0.125Âř
GIMMS	AVHRR	1981-2006	15-day	8 km
GIMMS3G	AVHRR	1981-2011	15-day	8 km
S10	SPOT-Vegetation	1998+	10-day	1 km
EM10	ENVISAT-MERIS	2002-2012	10-day	1/1.2 km
SeaWiFS	SeaWiFS	1997-2010	Monthly	4 km
MOD (MYD)13 A1/A2	Terra (Aqua)	2000+	16-day	500 m/1 km
MOD13 (MYD)A3	MODIS		Monthly	1 km
MOD13 (MYD)C1/C2			16-day/Monthly	5.6 km
MOD13 (MYD) Q1			16-day	250m
MEDOKADS	AVHRR	1989+	Daily	1 km

Table 2.1: A summary of commonly utilised Normalised Difference Vegetation Index (NDVI) datasets, FASIR - Fourier-Adjusted, Sensor and Solar zenith angle corrected,Reconstructed. Interpolated, LTDR - Land Long Term Data Record .

(Hulme 2001). These droughts represent the most dramatic climatic shift on modern record and resulted in widespread famine across the region (Hulme 2001). This ecological and meteorological transition was viewed as the consequence of anthropogenic desertification, supporting the "expanding deserts" paradigm (Stebbing 1935, Aubréville et al. 1949, Lamprey 1975). Desertification was understood to result from human alteration of land-atmosphere interactions (Figure 2.2) (D'Odorico et al. 2013). Reduced vegetation cover, initiated by increased grazing pressures (Sinclair and Fryxell 1985, Dregne 1986), was postulated to increase localised albedo and temperature, in turn reducing regional rainfall leading to further vegetation cover loss (Charney 1975, Charney et al. 1977). Thus, an increased anthropogenic pressure was attributed as the major driver of regional climate and land cover processes (Prothero 1974). This was in agreement with studies demonstrating the impact of intensive grazing on surface reflectance across the Negev-Sinai border (Tsoar and Karnieli 1996, Otterman 1981, Otterman and Tucker 1985). Conclusions regarding an expanding Sahara and encroaching dune systems, such as those proposed by Lamprey (1975) and Stebbing (1935), were heavily cited in both scientific publication and media outlets (Hellden 1991). More recent research heavily challenged this viewpoint and paradigm (Hellden 1984, Ahlcrona et al. 1988, Hanan et al. 1991, Nicholson et al. 1998). A number of studies in the Sudano-Sahelian region combined field surveys with aerial photography and multi-temporal NDVI. These

studies revealed little expansion of the Sahara, and a relatively minor human foot-print when compared to the climatic signal (Hanan et al. 1991). Other regional-scale analyses (Hellden 1991, Tucker et al. 1991) reinforced this conclusion, casting serious doubt on the expanding deserts paradigm (Thomas et al. 1994). The study of Tucker et al. (1991) was a seminal study in demonstrating the potential of EO for long-term regional-scale ecosystem studies. In combination with other studies in the tropics (Skole and Tucker 1993, Malingreau and Tucker 1988), Tucker et al. (1991) demonstrated the potential to apply time-series analysis on EO imagery for monitoring and assessing ecosystem processes.

The demonstration of the potential of multi-temporal NDVI imagery (Tucker et al. 1991), coupled with the development of pre-processed long-term data sets (Townshend 1994), resulted in an increase in the application of time-series analysis using NDVI. In the Sahel, a greening trend was observed by numerous studies (Eklundh and Olsson 2003, Herrmann et al. 2005, Huber et al. 2011, Fensholt and Rasmussen 2011). Herrmann et al. (2005) used the residual trend method (see Section 2.5) in combination with trend analysis on 19 years of monthly NVDI data to conclude that the region was, in general, greening with only localised degradation present. This analysis was reinforced by Huber et al. (2011) on an extended NDVI data set, in conjunction with soil moisture estimates, with similar conclusions. Process-based ecosystem-modelling studies reported an agreement between the observed NDVI patterns and climate model-based estimates (Hickler et al. 2005), with little influence from population or grazing pressures (Seaquist et al. 2009). Growing season NDVI was found to have increased by 0.09 units from 1981-2007 (Huber et al. 2011), although a reduction in the rate of greening was noted around 2000 (De Jong, Verbesselt, Zeileis and Schaepman 2013).This greening trend was found to be consistent across semi-arid regions globally, traditionally viewed as the hot-spots of land degradation (Donohue et al. 2009, de Jong, de Bruin, de Wit, Schaepman and Dent 2011, Helldén and Tottrup 2008). With comparable desert boundary variation also noted in Asian drylands (Piao et al. 2005, Jeong et al. 2011). Greening was found to occur through two mechanisms: a lengthening of the growing season through earlier springs and delayed senescence and an increase in the maximum amplitude of NDVI (de Jong, de Bruin, de Wit, Schaepman and Dent 2011, Heumann et al. 2007, Piao et al. 2006). Evidence of increased vegetation productivity accompanied a revised view of the cause of Sahelian rainfall fluctuations. Modelling studies revealed that the desiccation-vegetation feedback loop, theorised by Charney (1975), had been greatly exaggerated (Nicholson et al. 1998). Regional rainfall

variation is primarily related to external drivers, principally sea surface temperature in the low-latitudes (Giannini et al. 2003) but also northern hemisphere volcanic aerosol emissions (Haywood et al. 2013), with localised vegetation-atmospheric interactions playing a minor role (Giannini et al. 2003). The majority of vegetation greening, in the Sahel and globally, can be attributed to increased precipitation over the past 30 years (De Jong, Schaepman, Furrer, Bruin and Verburg 2013). However, the question of human influence on semi-arid ecosystems remains highly controversial (Bai et al. 2008, Wessels 2009). Furthermore, the sensitivity of trend methods to detecting degradation processes has been questioned (Wessels et al. 2012). Claims that current precipitation patterns may be disguising wide-spread degradation (Hein et al. 2011, Wessels et al. 2012) require urgent investigation. The consequences of this degradation would be severe when dry periods return to degrading or degradation-prone localities.

In arid regions, vegetation, and therefore NDVI, is highly correlated to rainfall (Nicholson et al. 1990), thus any variation in rainfall affects the NPP. Although temperature variation is also important in many regions (Jeong et al. 2011, Peng et al. 2011). Therefore, in order for any long-term permanent degradation to be detected, it is necessary to remove the influence of a precipitation trend. A number of methods have been proposed that aim to accomplish this. Le Houerou (1984) originally proposed the ratio of NPP to rainfall, the Rain-Use Efficiency (RUE), as an ecosystem indicator. It was suggested that arid lands would produce around 4 kg-dry matter/ha/year/mm rainfall, and that a reduced RUE indicated land degradation. Further analysis revealed that RUE values varied between regions Nicholson and Farrar (1994), Farrar et al. (1994). Consequently, temporal variation in RUE was proposed as an indicator of degradation (Prince et al. 1998). (Prince et al. 1998) investigated the regional RUE of the Sahel from 1982-1994, using seasonally integrated NDVI as a proxy for NPP. This analysis revealed little temporal variation in RUE across the region, thus indicating a consistent ecosystem dynamic through periods of droughts. However, the application of RUE as an indicator of land degradation has become highly controversial (Prince et al. 2007, Hein and De Ridder 2006, Wessels 2009). An explanation of the limitations and assumptions of RUE is given in Section 2.5. Statistical methods to separate NDVI from rainfall trends have also been proposed; these include the RESidual TRENDds (RESTREND) method (Evans and Geerken 2004, Archer 2004) and the Precipitation Marginal Response (PMR) (Verrôn et al. 2006). These methods both focus on detecting a shift in the statistical relationship between rainfall and NDVI. The proposed degradation mecha-
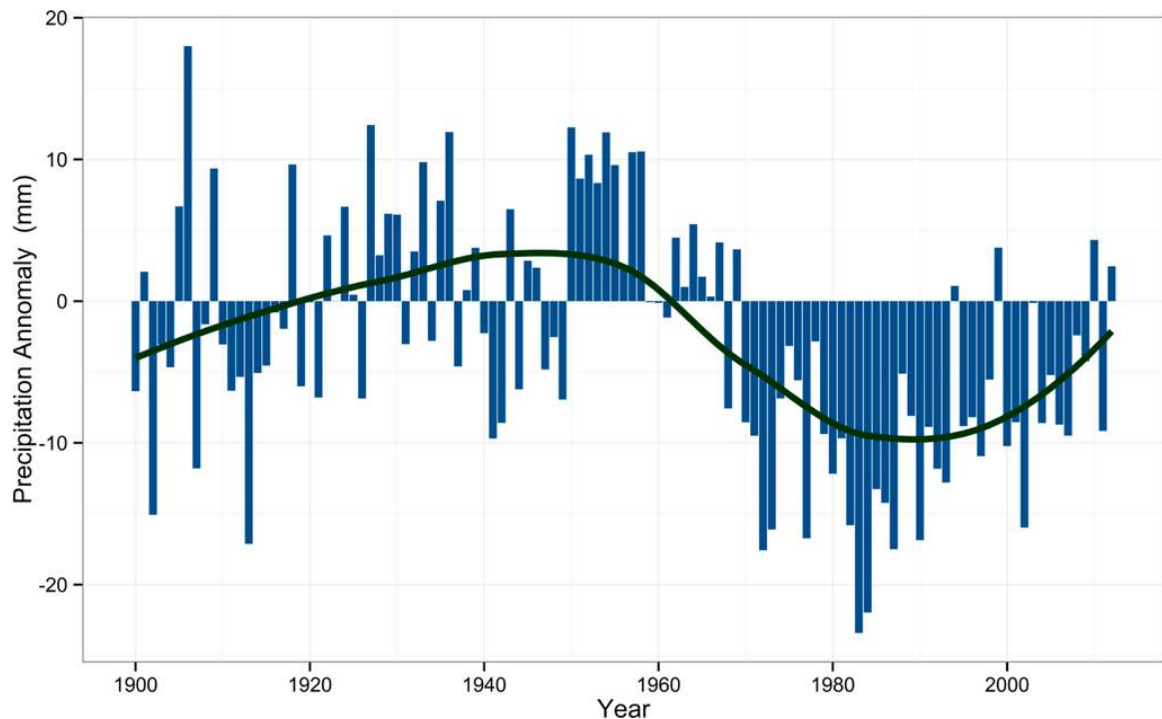
Figure 2.1: Time Series of the Sahel Precipitation Anomaly Index. Anomalies are with respect to the 1950 - 1979 period

nism is comparable to RUE: as degradation occurs, the usage of precipitation shifts, whereas meteorologically-induced degradation relationships stay constant (Evans and Geerken 2004, Archer 2004, Wessels et al. 2007).

2.5 Trend Analysis Frameworks

NDVI Trend Analysis

Time series techniques can be grouped into parametric and non-parametric methods. The application of these techniques on EO imagery has become a contentious issue due to the inherent limitations and assumptions; an overview of the most commonly used ones, is given below. Linear trend analysis applies a linear regression model to quantify change in the dependent variable, y (i.e., NDVI) against an independent variable, x (i.e., time). The direction and magnitude of change from this model thus explains the change in NDVI over the period analysed. This test has a number of assumptions that must be met in order to be considered robust (De Beurs and Henebry 2005):

1. independence of the dependent variable;
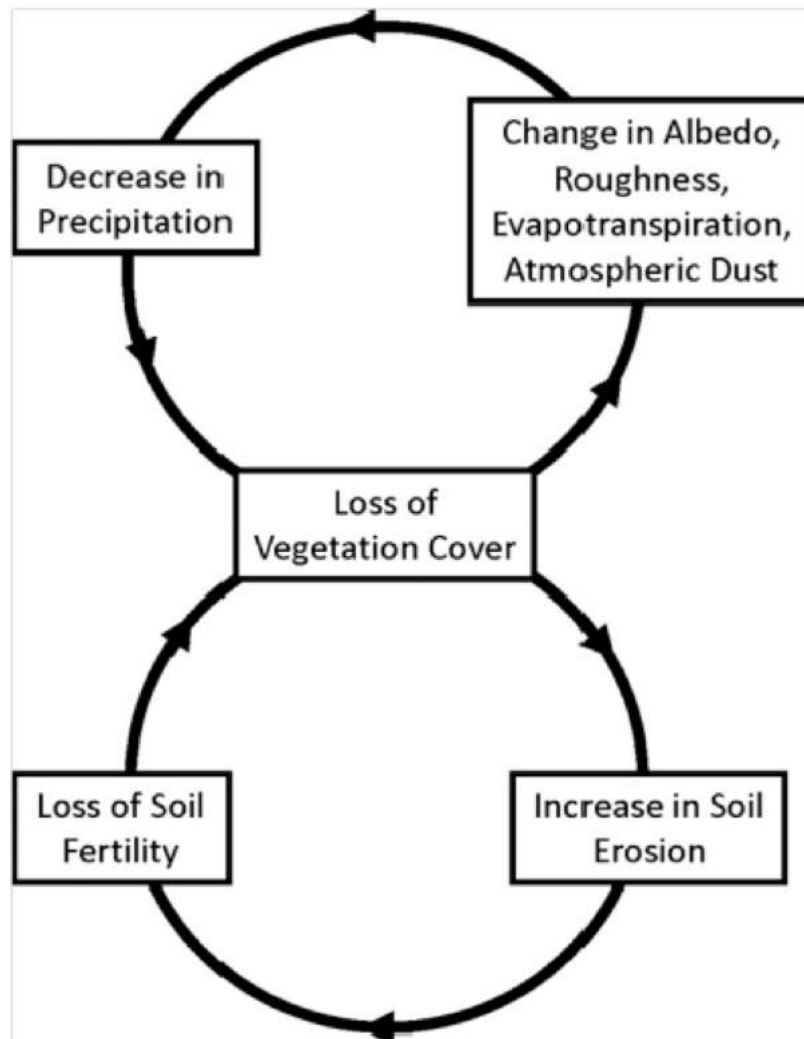
Figure 2.2: Representation of the positive feedback loop for desertification

2. normality in the model residuals

3. consistency in residual variance over time

4. independence in residuals

In addition to spatial autocorrelation functions present (Gaughan et al. 2012, Lennon 2000*a*), memory effects in dryland systems make inter- and intra-annual NDVI values strongly correlated (Martiny et al. 2006, Philippon et al. 2007, Richard et al. 2012). Thus, assumption one above and, commonly, four, are unlikely to be met. The consistency in residual variance is heavily influenced by anomalous and outlier values, such as those caused by hemispheric climatic oscillations (Wessels et al. 2012), and may also be breached. The Theil-Sen trend is a non-parametric trend estimation technique. Functionally similar to linear least squares regression, it operates on non-parametric statistics and is not dependent upon the assumptions of linear regression. Trends are estimated using the median values and are therefore less susceptible to noise and outliers, with a robust trend estimated with up to *ca.*29% noise across the data (Theil 1992, Sen 1968). The Mann-Kendall test measures the monotonicity or consistency of a trend (Kendall 1938). The test is a cumulative value of the instances of increases or decreases from a pairwise comparison, with values of +1 indicating a continually increasing and -1 a continually decreasing trend. Although robust against the assumption of linear regression, the trend is susceptible to producing low values for time series with a strong overall change but moderate annual fluctuations.

Differences between Trends, Datasets and Sensors

A number of studies have compared the results obtained from applying a variety of trend methods (Fensholt et al. 2012, de Jong, de Bruin, de Wit, Schaepman and Dent 2011). Results indicate that although the trend estimations differ, there is rarely a major difference between results with both direction and magnitude consistent across methods. For global semi-arid regions, Fensholt et al. (2012) compared Mann-Kendall and linear regression models, finding a mean difference of 0.039 and -0.019 for positive and negative trends and maximum differences of 0.285 and 0.158 with standard deviations of 0.037 and 0.029, respectively. A comparison of trend estimation, for a pixel in the Sudanese Sahel, is shown in Figure 2.3.

A majority of studies use NDVI data sets derived from the AVHRR sensor (Table 1). As a meteorological sensor the AVHRR was not designed for terrestrial ecosystem applications (Cracknell 2001), thus a number of issues are inherent. For example, the near-infrared waveband (Channel 2) overlaps with a region of strong atmospheric water vapour absorption, influencing the resulting NDVI values. Unlike modern sensors such as MODIS and SPOT, AVHRR does not possess ancillary bands that allow for the detection of atmospheric conditions. Thus, a range of processing is applied to raw AVHRR imagery in the preparation of NDVI records. The PAL and GIMMS/3 g records do not apply atmospheric correction, instead using maximum value compositing (MVC) of Top of Atmosphere (TOA) values to preserve the original data patterns (Holben 1986, Pinzon and Tucker 2014, Tucker et al. 2005). However, comparison with the LTDR, which possess an atmospheric correction procedure, highlights the residual error that may remain within the GIMMS data due to this omission, particularly in regions with high Aerosol Optical Thickness (AOT) (Nagol et al. 2009). Furthermore, ageing of the AVHRR carrying satellite results in a shift in the equatorial crossing time of the sensor, referred to as orbital drift. Orbital drift can, without reliable correction, influence NDVI values and computed trends, for a location specific quantification of orbital drift effects on AVHRR data see Nagol et al. (2014). Comparisons of the various AVHRR-derived datasets (PAL, GIMMS/3g, LTDR, FASIR) display regionally varying levels of agreement. For the Iberian peninsula, Alcaraz-Segura, Liras, Tabik, Paruelo and Cabello (2010) found good spatial agreement between the PAL, LTDR and FASIR datasets, with the GIMMS-derived trends differing. A similar observation was identified in South America where the GIMMS data failed to identify trend highlighted by PAL and FASIR records (Baldi et al. 2008). In the USA and Mexico, records displayed good correlation, however, trend estimates did vary particularly in dryland areas (Scheftic et al. 2014). In a global-scale analysis, Beck et al. (2011) compared the four AVHRR-derived records with Landsat and MODIS imagery. Consistency in trends was identified for Australia and central Asia, with divergent trend estimates in Africa, South America and the Sahel (Beck et al. 2011).

Comparisons between sensor datasets are a common method of quality assurance for AVHRR-derived NDVI records. The MODIS sensor is considered the most accurately calibrated and atmospherically corrected NDVI record available. Therefore, comparing the MODIS products with overlapping AVHRR-derived data can highlight issues present with the older AVHRR records. A global comparison of MODIS and GIMMS NDVI trends, for dryland regions was, undertaken by Fensholt
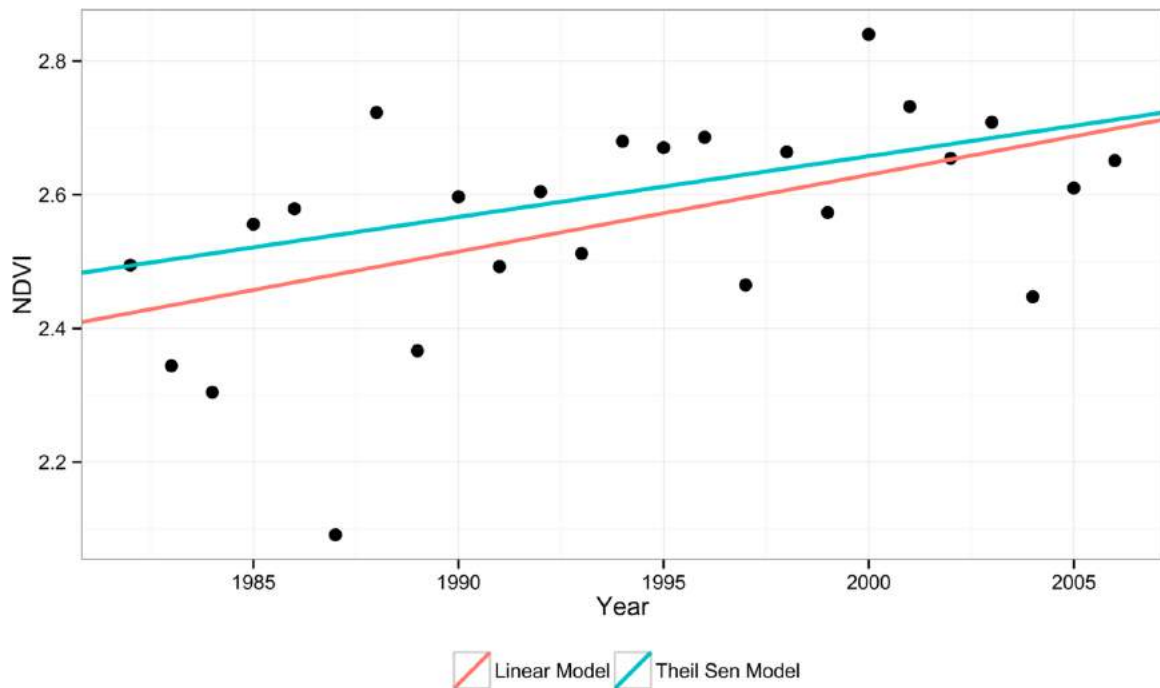
Figure 2.3: Comparison of linear and Theil Sen regression slopes for a pixel in the Sahel.

et al. (2012). Trend values show high correlations (0.8>) for most semi-arid regions; however, areas bordering the arid zone with sparse vegetation were lower indicating spurious NDVI in these localities. This was in agreement with earlier work which identified that MODIS-GIMMS correlations were higher in the humid regions of the Sahel, compared to the arid areas (Fensholt and Rasmussen 2011).

Detecting Structural and Real-Time Change

Trend breaks

All of the methods detailed above establish a trend detailing the change in NDVI over time; this represents a simplification of what may be a highly complex chronology of shorter duration trends (de Jong et al. 2012, Verbesselt, Hyndman, Newnham and Culvenor 2010). Analysing the overall trend, particularly with long time series, may be misleading as contrasting trends can potentially balance out. Verbesselt, Hyndman, Newnham and Culvenor (2010) proposed that NDVI change can be classified in three components: seasonal/cyclic changes, gradual variation, and abrupt or sudden changes. Within this outline, they developed the Breaks for Additive Season and Trend (BFAST) algorithm, which disaggregates an NDVI time-series into three constituents: seasonal variation, trends, and noise (Verbesselt, Hyndman,

Newnham and Culvenor 2010). By allowing the detection of multiple shorter duration trends, a better understanding of the temporal drivers of NDVI can be obtained. de Jong et al. (2012) implemented the BFAST algorithm on the global GIMMS ND-VIg archive. Semi-arid regions were identified as being highly variable in trend direction and magnitude, partly due to the impact of hemispheric climatic oscillations (de Jong et al. 2012, De Jong, Verbesselt, Zeileis and Schaepman 2013). It was highlighted that dryland regions frequently displayed abrupt greening spells followed by periods of gradual browning.

Real-Time Change Detection

The detection of historic trends and shifts in vegetation productivity is very useful to scientific inquiry, and may serve to inform land management policies to mitigate degradation drivers. However, historic trends are of limited value to contemporary management, as considerable reductions must first materialise (see Section 5.2). Thus, real-time or near real-time detection is necessary to inform policy makers at the earliest possible opportunity. This objective, i.e., the identification of real-time environmental disturbance, is shared by a number of environmental applications, such as food security (Verbesselt, Hyndman, Newnham and Culvenor 2010), deforestation Hargrove et al. (2009) and epidemiology (Spruce et al. 2011). The challenge of being able to identify real-time disturbance is in distinguishing a genuine trend from the seasonal trend and noise components. White and Nemani (2006) demonstrated that phenological change could be forecast by comparing a user-defined threshold against the historical variability found within clustered phenoregions. The setting of arbitrary user-defined thresholds encounters difficulty when there are complex land cover transitions or frequent periods of high instability, adding a significant cost to application (Verbesselt et al. 2012). To overcome this issue, Verbesselt et al. (2012) proposed a pixel-level disturbance detection approach, based on the historical time-series of each individual pixel. For each pixel, a stable "history" period is automatically determined and disturbances are compared to this regime (Verbesselt et al. 2012). This approach proved suitable for detecting drought-induced disturbance but was not so successful in removing background noise.

Removing Precipitation Influence

As previously mentioned, Rain Use Efficiency (RUE) is the quotient value of NPP to corresponding precipitation (Le Houerou 1984, Prince et al. 1998). It has been proposed that degradation reduces the precipitation usage of an area, as overland flow and runoff increase with reduced vegetation cover and density. Thus, a reduced RUE can be indicative of land degradation, independent of climatic effects (Prince et al. 1998). This mechanism is based on two key assumptions (Fensholt and Rasmussen 2011):

1. linearity in the response of NDVI/NPP to increased precipitation;

2. independence of RUE to fluctuation in its constituents

The well reported linear relationship between NPP and rainfall in drylands (Nicholson et al. 1990) can potentially be compromised when tail events for both rainfall and NPP occur. At high precipitation amounts, factors other than rainfall become limitations to NPP, and increases in precipitation do not induce further productivity (Nicholson et al. 1990). At very low precipitation there may be no vegetation present resulting in RUE values approaching infinity. This is further exacerbated by the positive intercept caused by soil reflectance (Fensholt and Rasmussen 2011). At low biomass levels the vegetation is unable to prevent runoff and infiltration from occurring, thus subsequently low RUE will be observed. Rainfall increases may potentially drive an increase in both RUE and biomass, rendering RUE irrelevant as a detrending technique (Hein and De Ridder 2006). However, this interpretation has been criticised as being limited to sites with anomalous precipitation regimes (Prince et al. 2007, Kaspersen et al. 2011, Ruppert et al. 2012). RUE values have been demonstrated to correlate with inter-annual precipitation fluxes (Fensholt and Rasmussen 2011, Wessels et al. 2007). However, it is statistically questionable to test for dependence between RUE and rain as they are not independent (Dardel et al. 2014). Fensholt et al. (2013) proposed the use of a seasonality subtracted 'small integral' of NDVI, as opposed to the full growth season integral, which could mitigate against correlations with rainfall, provided linearity assumptions are satisfied.

The Residual Trends (RESTREND) method compares the response of an NDVI time-series to a predicted response. The predicted response is generated by calculating a regression between NDVI values and precipitation (Evans and Geerken 2004, Archer 2004). The residuals from this regression are then subjected to a trend analysis. A positive trend in residuals indicates an increasing NDVI signal

compared to the precipitation trend (land improvement), whereas a negative trend indicates a declining NDVI per precipitation unit (degradation). By implementing a statistical rather than a quotient method, this approach avoids the limitations of RUE with regards to linearity and dependence (Wessels et al. 2007). A comparison of RUE and RESTREND is shown in Figure 2.4, note the negative RUE trend induced by high rainfall at the end of the time series.

2.6 Relating Time-Series Frameworks to Degradation Processes

All trend analysis assessments are based on the foundation that comparable sites, when subjected to degradation, will display reduced photosynthetic production, and thus NDVI (Wessels et al. 2006, Prince et al. 2009). This represents a symptomatic approach, as the mechanism of land degradation is irrelevant, provided a reduction in NPP materialises (Hill et al. 2008). Thus, the two key assumptions of these methods are, firstly, that degradation consistently materialises as a reduction in NPP, and secondly, that NDVI variation is capable of capturing this reduction. These issues are reviewed below.

Does Land Degradation Initiate a Decline in NPP?

The assumption that land degradation reduces the NPP of a site is dependent upon the underlying mechanism. A reduction in vegetation cover, whilst species composition and diversity is maintained, will materialise as a reduction in NPP (Miehe et al. 2010). However, a common degradation mechanism affecting dryland regions is encroachment of woody shrub species into grasslands. This process results in an increase in bare ground coverage coupled with increased runoff and alterations of soil C and N stocks (D'Odorico et al. 2013, Ravi et al. 2010). Nevertheless, shrubland encroachment does not necessitate a reduction in NPP. Thus, the analysis of the seasonal maximum or annual integral of NDVI is unlikely to detect this process successfully. However, shrubs species, and encroachment, do exhibit a number of distinct eco-hydrological responses, which may be exploited by an NDVI-based analysis. Shrubs species are, in general, perennial plants and manage to survive the dry season. Mitchard and Flintrop (2013) mapped woody and shrub biomass in African Savannahs, using the dry season maximum NDVI. The results of this analysis agreed with collated field data of shrub encroachment and forest degradation,
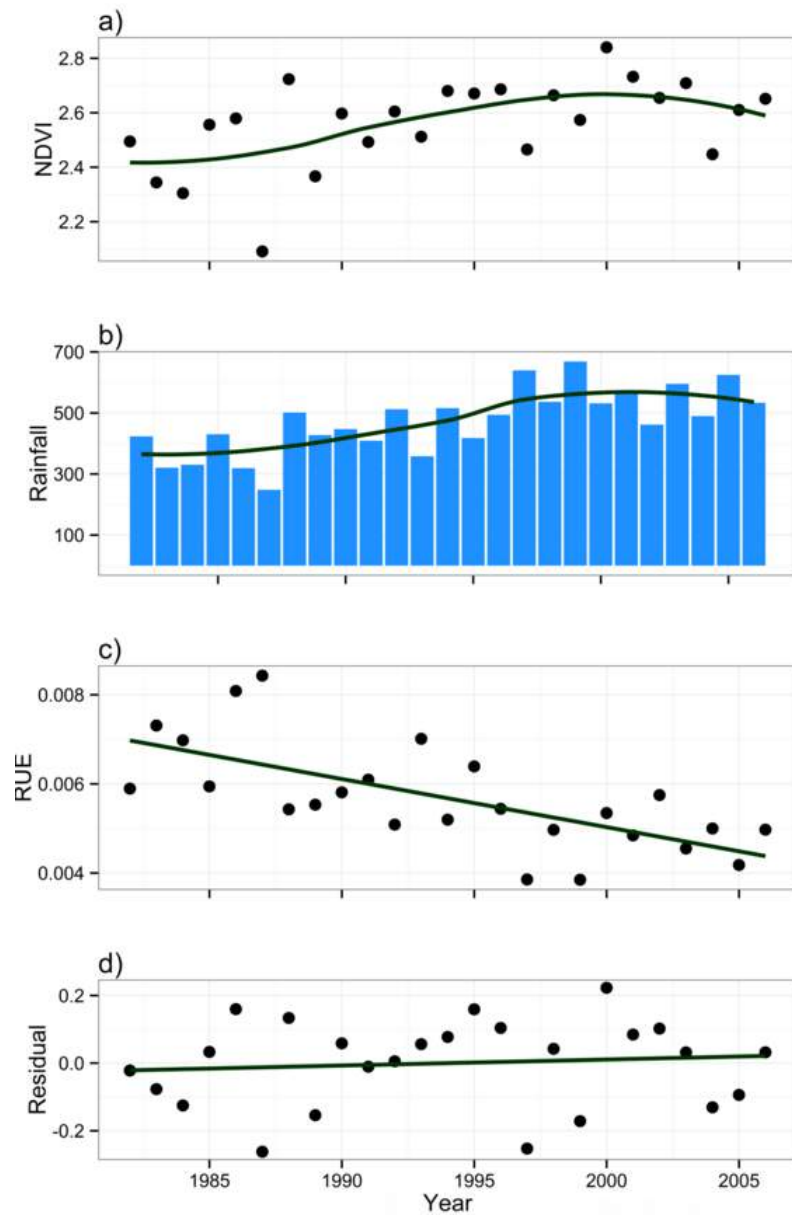
Figure 2.4: Comparison of the Rain Use Efficiency and residual trends for a pixel in the Sahel.

although the authors stipulate that the results should be viewed with caution due to the technical issue with dry season NDVI (Mitchard and Flintrop 2013). The ability of shrub species to support deeper root networks also influences their usage of precipitation. Williamson et al. (2012) investigated the species-specific response of NDVI to preceding precipitation events. Grassland species reported the highest relationships for concurrent precipitations, whereas shrubland relationships were notably improved when the previous years were included (Williamson et al. 2012). Verrôn et al. (2006) highlighted the potential of variation in the rainfall-NDVI coefficient (the precipitation marginal response) as a potential indicator of species composition variation. It should be noted that shrub encroachment is not universally accepted as a component of land degradation (Eldridge et al. 2011). Nevertheless, the associated reduction in pastoral resource that accompanies an increase in shrub coverage makes it a commonly perceived degradation process in many regions, and is thus included herein. In addition to the commonly acknowledge process of shrub encroachment an impoverishment of woody vegetation species has also been reported (Herrmann and Tappan 2013). Herrmann and Tappan (2013) and Herrmann et al. (2014) compared Senegalese vegetation trend maps with archive photography and focus group meetings with local inhabitants. Results indicated that NDVI derived-greening trends did not necessarily correlate with users perceptions of vegetation improvement. In some locations a decrease in tree coverage and a shift to drought tolerant shrub species was reported, irrespective of changes in population and land usage. Interestingly, opposing results were found for an area of the Sahel in Mali, where an increase in cultivation and tree cover was identified (Spiekermann et al. 2015).

In summary, a variety of NDVI-based methods have been designed and tested, but validation of results, and hence the suitability of NDVI-based methods to assess degradation, remains limited

Can NDVI Trends Capture a Reduction in NPP?

The ground truthing and validation of products generated by remote sensing is a critical methodological stage. However, the validation of trend analyses is inherently problematic. It is rarely feasible to validate 30-year trends with a large spatial footprint. In addition, there are few biomass-sampling sites with a spatial scale suitable for validating coarse resolution pixels and even fewer sites with a continuous record dating back to the early 1980s. Here, we summarise the existing literature on

comparisons of long-term biomass data with vegetation index values and trends, and discuss alternative methods of validation, such as qualitative validation and simulation analysis.

Wessels et al. (2006) compared a 533-site, 19-year biomass dataset with an AVHRR-derived NDVI record for the Kruger National Park, South Africa. This comparison produced generally favourable correlations for the NDVI/biomass relationships, with an average R^2 of 0.42 capturing the majority of inter-annual variability. Sites with low correlations were attributed to the heterogeneous land cover resulting in mixed pixels, poorly represented by the biomass samples (Wessels et al. 2006). A number of Sahelian localities have been subjected to long-term observation under the African Monsoon Multidisciplinary Analysis-Coupling the Tropical Atmosphere and the Hydrological Cycle (AMMA-CATCH) programme. Two of these sites, i.e., Gourma, located in northern Mali (data from 1984 - 2011) and Fakara in southern Niger (data from 1994 - 2011), were assessed against long-term GIMMS3g NDVI time-series trends (Dardel et al. 2014). At both sites, field data agreed with the direction and magnitude of the corresponding NDVI trend, with respective correlation co-efficients of 0.74 and 0.41. The co-efficient for Fakara becomes 0.59 when an outlier for 2010 is omitted (Dardel et al. 2014). The lower values obtained for Fakara were attributed to a mixed agro-pastoral land use pattern, when compared to the predominantly pastoral land use identified at the Gourma site (Dardel et al. 2014). The issue of localised land use/cover patterns resulting in mixed pixels was also noted by Brandt, Verger, Diouf, Baret and Samimi (2014). This was partially rectified by utilising a higher-resolution NDVI product (Geoland V1 at 5 km resolution), which revealed patterns obscured by the GIMMS3g data. However, attempts to document localised factors for regional analysis proved problematic due to the large variety of land use/cover conditions present (Brandt, Romankiewicz, Spiekermann and Samimi 2014). In the absence of long-term biomass records, a number of studies have used qualitative comparisons to validate trend outputs. Wessels et al. (2007) compared rainfall-corrected NDVI trends, using RESTREND, to a national land survey output, with an acceptable level of agreement between the two outputs. Further qualitative validation was undertaken by Evans and Geerken (2004), who used field study surveys and visual interpretation of Landsat imagery to validate degradation assessments for Syrian drylands. Both of these studies relied on a generally high level of agreement between outputs and the validation data to assess the reliability of applied methods. Studies that attempt large-scale regional(Huber et al. 2011, Fensholt and Rasmussen 2011) or global (Bai et al. 2008,

Hill et al. 2008) assessments, frequently rely on even less robust validations and focus on the linkages of hot-spots with environmental change narratives postulated by field studies. Although commonplace, studies utilising qualitative validation methods have been highly criticised. Wessels et al. (2012) highlighted that this process does not sufficiently assess the accuracy and sensitivity of methodologies to variable start-dates and intensities of degradation.

A recent alternative to the approaches above is simulation analysis, which tests the sensitivity of methods by artificially altering a dataset prior to analysis, thus a technique is assessed against a known baseline. This approach has been used to test the responsiveness of time-series segmentation methods aiming to decompose noisy data series (Verbesselt, Hyndman, Newnham and Culvenor 2010, Verbesselt et al. 2012, Verbesselt, Hyndman, Zeileis and Culvenor 2010) prior to the application on a global time-series (de Jong et al. 2012, De Jong, Verbesselt, Zeileis and Schaepman 2013). The advantage of the simulation approach is that the intensity and duration of a shift can be determined, and the response of the applied analysis directly compared (Forkel et al. 2013). A land degradation simulation assessment was implemented by Wessels et al. (2012), where a variety of start-date and intensity land degradation simulations were applied to 1 km-NDVI data covering the Kruger National Park, to represent the degradation of a non-degraded baseline. This study revealed that an NDVI reduction of 20%-40% was required to identify a significant negative trend in the region, using either RESTREND or a number of other trend techniques (Wessels et al. 2012). Thus, the majority of trend techniques employed (Fensholt et al. 2012) would be capable of detecting only the most severe of degradation processes, and would therefore not be useful as a degradation early-warning system (Wessels et al. 2012). Comparable simulation experiments were used to test the sensitivity of RUE in the Sahel region (Dardel et al. 2014). Here a degradation of >20% was found to be detectable, provided it did not occur at the start or end period of analysis.

A number of studies have proposed that additional analyses using higher resolution imagery, such as the Landsat and SPOT satellites, would be well suited to provide further localised information on trends observed(Stellmes et al. 2010, Röder et al. 2008, Herrmann et al. 2005). Comparisons of Landsat and AVHRR-based trends have revealed generally similar patterns Stellmes et al. (2010), with further analysis demonstrating that vegetation estimates derived from Landsat imagery all display similar trend patterns (Sonnenschein et al. 2011). Recent progress in applying time-series analysis on Landsat imagery stacks has demonstrated the potential

for observing land use/cover variation at high spatial and temporal resolution (Griffiths et al. 2012, Kennedy et al. 2007, Pflugmacher et al. 2012, Kennedy et al. 2010). In addition, the ability to generate large-area compositing techniques from multiple Landsat scenes (Griffiths et al. 2013, Roy, Ju, Kline, Scaramuzza, Kovalskyy, Hansen, Loveland, Vermote and Zhang 2010), offers new opportunities for multi-scale analyses to improve on the relationships between land use/cover change and NDVI trends on multiple spatial and temporal scales. An important consideration of remote sensing studies is the resolution and scale of imagery used (Woodcock and Strahler 1987). Higher resolution imagery will better identify local issues and trends, particularly in heterogeneous areas (Brandt, Romankiewicz, Spiekermann and Samimi 2014, Stellmes et al. 2010). This advantage must be balanced with the more generalised large-scale view undertaken a large number of studies, where observing local factors is not a primary objective (Fensholt et al. 2012, Bai et al. 2008). NDVI-based studies have historically been limited to the coarse-resolution preprocessed datasets details above (Table 1); this has limited the discussion of the impacts of altering the scale upon trend estimations. Recent developments in the provision of both free and pre-processed Landsat data (Masek et al. 2006, Wulder et al. 2012) may lead to an increased focus on higher-resolution sensor data, therefore the impact of varying pixel size on trend estimation should be a research priority prior to the undertaking analysis.

2.7   Conclusions and Outlook

Land degradation and desertification are important issues to both ecological and social research. The need for a quantitative, repeatable methodology to assess land degradation and desertification reliably is more pressing than ever before. EO data offer the only viable method for large-scale assessments, and despite the continued controversy over the techniques used, considerable progress has been made over the last 30 years. This review has identified two key prerequisites to the establishment of degradation and desertification monitoring and early warning systems. Firstly, methodologies must be subject to a standardised and robust validation in order for policy makers and planners to have confidence in results; secondly, degradation at minor intensities or early stages must be detectable in order for preventive action to be taken before irreversible damage occurs.

The validation of trend analysis would ideally be undertaken by robust comparisons with field biomass data covering a comparable spatial and temporal scale.

However, this is rarely possible. The need for using remotely sensed vegetation data is related to this very issue and a major concern is the requirement for consistency between studies. This could potentially be achieved through a standardised comparison with whatever long-term data exist. The proposed Global Drylands Observing System (GDOS) (Verstraete et al. 2009, 2011) would be a critical precursor to this. Alternatively, the simulation experiments proposed by Wessels et al. (2012) and Verbesselt et al. (2012) offer clear potential for the development of consistent and repeatable methodologies (Dardel et al. 2014), which could be aided by the transition to open-source statistical programs. The availability of packages such as BFAST (Verbesselt, Hyndman, Newnham and Culvenor 2010) and Greenbrown (Forkel et al. 2013) demonstrates the potential for such a transition.

The early detection of land degradation, particularly at low intensities represents a major limitation on the usability of degradation early-warning and monitoring systems. The application of structural and real-time change detection represent the greatest progress on this issue, but further work is still required. Bayesian statistics, whereby model assumptions are based on prior knowledge, may also be beneficial for identifying deviation form expected trajectories.

The land degradation monitoring community may also benefit from the experiences of deforestation observation projects, which have acknowledged the importance of local stakeholders and end-users for efficient development (Asner 2014, Foody and Boyd 2013). The use of volunteered information and photographs for validation of land cover maps could be of value as an additional data source in regions with limited long-term field data. The monitoring of desertification is meaningless if not integrated with local end-users. The traditional top-down approach of researchers developing products leads to a lack of connection between the intended users and the design procedure, and may not be suitable for handling the wide variety of local issues (Asner 2014). Software tailored for land degradation, comparable to the CLASlite (Carnegie Landsat Analysis System-lite) program, which allows end-users to access information and development methodologies to map deforestation and forest cover, would be of advantageous (Asner et al. 2009). However, technological limitations in many developing regions may hamper the uptake of such technology (Roy, Ju, Mbow, Frost and Loveland 2010).

It should be cautioned that NDVI analysis is best suited as one component of a multi-faceted methodology. The multiple symptoms and drivers of land degradation provide a number of opportunities for quantitative assessment using EO (de Jong, de Bruin, Schaepman and Dent 2011, Vrieling 2006). It is through the

combination of these indicators that a holistic assessment of land degradation can be achieved (Symeonakis and Drake 2004, Le et al. 2012). In addition, NDVI-based analyses only consider the biomass of an ecosystem; this falls short of fully appreciating the wide range of ecosystem services and local uses that may be present (Jacob et al. 2014). Degradation assessments cannot be achieved through a biomass or Carbon stock assessment alone, as it is the usage and flow of biomass/Carbon that provide benefit to the biosphere (Janzen 2006). Land degradation and desertification prevention and remediation efforts should also consider local stakeholder usage and ecosystem functions in order to promote poverty alleviation and environmental health objectives in synchrony (Stringer et al. 2012).

Chapter 3

Enhancing NDVI-based biomass models through feature selection and spatio-temporal cross validation

Abstract

The accurate mapping and quantification of above ground biomass (AGB) is required for a number of applications, including carbon accounting, fire and grazing management, amongst others. Accordingly, relating field measurements of AGB to satellite-derived indicators, most prominently the Normalised Difference Vegetation Index (NDVI), has been a feature of the remote sensing literature for over 30 years. Recently, there has been an increase in the use of machine learning methods and the incorporation of auxiliary environmental variables for spatio-temporal modelling. However, there is increasing evidence that these models may be vulnerable to artefacts of data structure, such as spatial autocorrelation and inappropriate auxiliary variables, which may hinder the development of accurate models. In this study, a robust methodology for the creation of moderate-resolution AGB estimates is presented. We obtained AGB data from an 18-year long dataset comprising 533 sites within the Kruger National Park of South Africa. We then generated a 1km-resolution NDVI product by downscaling the GIMMS 3g NDVI using Empirical Orthogonal Teleconnections (EOT) and the MODIS MYD13A2. AGB was then predicted based on a series of NDVI-metrics and auxiliary environmental variables in a Cubist regression model framework. Our analysis consisted of two components: i) a comparison of validation approaches, including a k-fold cross validation (CV) and multiple spatial/temporal CVs; and ii) a variable selection component, incorporating forward feature selections (FFS) on the above validation strategies. Prediction

accuracies differed considerably, with the Root Mean Squared Error ranging from 1310 to 1844 kg ha[1], depending on the variables and validation strategy employed. Errors were consistently higher with spatial or temporal validation strategies. Spatial overfitting was prominent in most models, which we attribute to spatial auto-correlation within the predictor variables. Comparatively, the NDVI-biomass relationship was highly variable between years, with unseen years being very poorly modelled. This potentially results from changing species composition and moisture content on an annual basis. The FFS was effective at correcting these issues, where possible, by constructing models with appropriate variable combinations. For temporal models, the profile of auxiliary variables was increased leading to a more deterministic prediction approach. This study contributes to the growing literature highlighting the potential pitfalls of machine learning for spatio-temporal predictions, and offers strategies for their detection and mitigation.

3.1 Introduction

The Normalised Difference Vegetation Index (NDVI) is one of the most commonly used remotely sensed indicators of vegetation. NDVI quantifies a measure of vegetation vigour by normalising the difference between the wavelengths of light absorbed for photosynthesis (red) and those reflected to prevent plant cellular overheating (near infrared) (Tucker 1979). The resulting value is closely related to the absorbed fraction of photosynthetically available radiation (fPAR), which in turn constrains the maximum threshold of Net Primary Production (NPP) (Monteith and Moss 1977). Accordingly, combining field sampling sites, where above ground biomass (AGB) or NPP are measured *in situ*, with satellite based NDVI imagery to produce spatially explicit predictions of such variables has long been a focus of study (Eisfelder et al. 2012, Tucker 1979, Prince 1991, John et al. 2018).

A common approach for predicting biomass is linear regression using the summed growth season NDVI (Eisfelder et al. 2012, Fensholt et al. 2012). This is both simple and theoretically sound, given the well established linearity between NDVI and low-moderate biomass levels, particularly in semi-arid regions (Prince 1991, Prince and Tucker 1986, Prince and Astle 1986). Additionally, models that incorporate auxiliary variables representing factors known to influence biomass, such as elevation or soil type, generally have higher performances (John et al. 2018, Wessels et al. 2006). Further improvements in accuracy can be obtained through machine

learning algorithms, such as Random Forest or Cubist models, that use iterative re-sampling of the data to quantity non-linear relationships and variable importance. These methods regularly out preform simpler statistical models (Meyer et al. 2016, John et al. 2018). However, both of these options require careful consideration, as spatio-temporal models may be vulnerable to effects that incur overfitting and exaggerate the obtained accuracies (Brenning 2012, Meyer et al. 2016). Brenning (2012) highlighted that the resampling procedures employed by machine learning methods may unwittingly exploit residual spatial autocorrelation among predictor variables, while Meyer et al. (2018) showed the potential for multiple auxiliary variables to combine and act as pseudo-site codes within complex models, due to their duplication in spatio-temporal data. Therefore, special attention should be paid to the choice of modelling approach and validation strategy.

The longest running NDVI dataset is the Global Inventory Monitoring and Modelling System (GIMMS) product, produced from Advanced Very High Resolution Radiometer (AVHRR) imagery since 1981. However, this temporal depth is counterbalanced by a relatively coarse spatial resolution. Raw AVHRR imagery is collected at 1 km^2 pixels, yet the poor calibration and limited cloud detection capabilities mean that most derived products are finalised at the 8 km pixel scale (Brown et al. 2006, Pinzon and Tucker 2014). This is notably lower than the resolution of more recent products such as MODIS (250 m), SPOT (1km), SeaWiFS (4km), and MERIS (1km). Appelhans et al. (2015) and Detsch et al. (2016) propose combining GIMMS data with a temporally overlapping higher resolution dataset, and using Empirical Orthogonal Teleconnections (EOT) to downscale the GIMMS data to a higher resolution. This procedure proved capable of producing a 1 km NDVI product for the Kilimanjaro region, Tanzania (Detsch et al. 2016).

In this study, our aim is to develop a robust methodology for the creation of moderate-resolution biomass estimates. We use a case study in a semi-arid savannah region to address the following research questions: i) to test the ability of EOTs to downscale coarse-resolution GIMMS NDVI, ii) to assess the impact of model validation strategies that account for spatio-temporal overfitting, and iii) to investigate the potential of variable selection procedures, combined with appropriate validation strategies, to improve the accuracy of models.
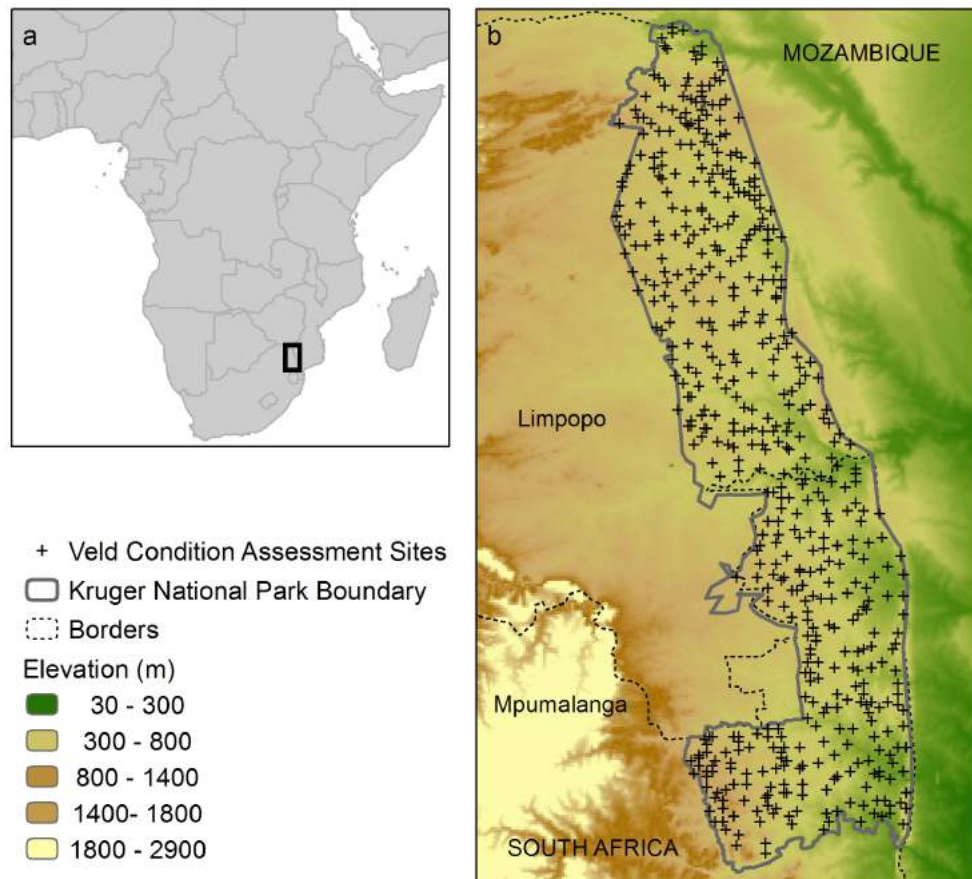
Figure 3.1: (a) Location of the study area, the Kruger National Park, within Africa; (b) a digital elevation model of the study area and the Veld Condition Assessment sites

3.2 Study Area

The Kruger National Park is located in north-east South Africa, within the provinces of Limpopo and Mpumalanga (Figure 3.1). The Kruger National Park is one of the oldest and largest protected areas in Africa, being designated since 1926 and covering roughly 2,000,000 ha. The park consist of typical mixed savannah land cover types, with a mosaic of grasses, shrubs, and trees (Mucina et al. 2006). Average woody cover decreases from 65% in the west to 40% in the east, primarily in line with soil type and geology. There is a broadly south-north rainfall gradient, with mean annual precipitation increasing from 350 to 950 mm (Scholes et al. 2001). Rainfall mainly occurs in the southern hemisphere summer months of October - April.

3.3 Data

AVHRR GIMMS-3g NDVI

We used the GIMMS NDVI dataset - third generation, hereafter $NDVI_{gimms}$. $NDVI_{gimms}$ is produced from the various AVHRR sensors in operation since mid-1981. Following processing, NDVI data are provided at an aggregated 8 km resolution and semi-monthly monthly (15 day) intervals. Bayesian methods are used to ensure compatibility between the AVHRR sensors. Additional processing is undertaken to account for orbital decay, atmospheric affects, and volcanic aerosols (Pinzon and Tucker 2014).

$NDVI_{gimms}$ data,for the 1981 - 2015 period was processed to monthly maximum value composites (Holben 1986), and a Whittaker smoother applied to minimise noise and fill remaining temporal gaps. The Whittaker smoother is a bespoke technique for remotely sensed vegetation time-series. Applying a penalised least squares curve, fitted values are forced towards the upper envelope of the series (Atzberger and Eilers 2011). As cloud and atmospheric artefacts generally incur a negative bias on NDVI, the fitted values are more robust.

MODIS NDVI

NDVI data from MODIS sensors benefit from considerable improvements in sensor calibration and design, relative to the older AVHRR imagery (Huete et al. 2002). Various MODIS-NDVI collections are available. We used the 1 km, 16-day Aqua product (MYD13A2), hereafter $NDVI_{modis}$. We limited ourselves to the MODIS-Aqua product due to the reported calibration issues, and associated induced bias, with the MODIS-Terra sensor (Detsch et al. 2016).

To standardise processing of the NDVI datasets. $NDVI_{modis}$ data for the years 2003 - 2015 were used, clouds and contaminated pixels were masked based on the provided MODIS quality assurance layer, followed by temporal compositing to maximum monthly values and the application of a Whittaker smoother.

Herbaceous Biomass

Herbaceous biomass data were acquired from the South African National Parks Vegetation Condition Assessment (VCA) surveys (Trollope 1990). The VCA covers roughly 533 sites on an annual basis, and has been conducted from 1989 to 2006.

Sites are distributed to account for landscape heterogeneity within the KNP. Each site covers 50 m x 60 m (0.003 km^2) area. Four 50 m transects are used to take 100 grass height estimates over 2 m intervals. Biomass is estimated using a disc pasture meter to record grass height. After accounting for grass moisture content, a regression equation is used to estimates biomass (kg ha^{-1}) from grass height:

$$y = -3019 + 2260\sqrt{x} \qquad (3.1)$$

where y is the estimated herbaceous biomass, and x is the mean disc pasture readings from the 100 samples per site. This model results in an R^2 of 0.895. The 95% confidence interval for the resulting biomass estimates is ± 328 kg ha^{-1} for low values (*ca.* 1500 kg ha^{-1}), ± 285 kg ha^{-1} for the mean (*ca.* 4200 kg ha^{-1}), and ± 526 kg ha^{-1} for higher values (*ca.* 9360 kg ha^{-1}).

3.4   Methods

Empirical Orthogonal Teleconnections

Empirical Orthogonal Teleconnections (EOT) originate in climate science, and are used to decompose spatio-temporal data sets into independent orthogonal (i.e non-correlated) trends (Van den Dool et al. 2000). They are similar to the more common Empirical Orthogonal *Functions* (EOF). However, whereas EOF decompose across both space and time, EOT are purely focused on time. We provide a brief outline of EOT, for a full mathematical overview, see Van den Dool et al. (2000) and Van den Dool (2007).

For our purpose, the aim of using EOT is to identify individual pixels in a predictor gridded time-series (P_p) - in this case NDVI$_{gimms}$, that have strong predictive power over a response gridded time-series (P_r) - NDVI$_{modis}$. This is achieved by a multi-stage, brute force, multiple linear regression procedure. Firstly, linear regressions between all predictor pixels (P_p) and all response pixels (P_r) are calculated. The pixel with the highest predictive power over the response pixels is selected as the base node. Secondly, the response series are reduced by removing the variance explained by the base node. Further, nodes are selected by applying the same process on the reduced series, until a desired number of nodes (EOT) are produced.

EOT functions, calculated from the temporal overlap of NDVI$_{modis}$ and NDVI$_{gimms}$ (2003-2015), can be applied to the non-overlapping (i.e pre-2002) NDVI$_{gimms}$ layers to produce a downscaled product. We produced a downscaled NDVI series at

1 km resolution. To validate the EOT-derived, downscaled NDVI layers, hereafter NDVI$_{eot}$, we compared NDVI$_{eot}$ against the co-occurring NDVI$_{modis}$ layers. This was carried out by removing a three-year segment of both datasets from the EOT calculation, and comparing the derived NDVI$_{eot}$ layers with NDVI$_{modis}$. This process was repeated four times, resulting in four separate three-year blocks over the 12-year overlapping period. To quantify the performance of the EOT downscaling, we calculated the Root Mean Squared Error (RMSE), Mean Absolute Error (MAE), and coefficient of variation (R^2). This resulted in 1 km^2 resolution NVDI dataset for the 1981 - 2015 period.

Modelling of Biomass

Overview

We constructed a series of predictor variables from the NDVI$_{eot}$, for the years 1989 to 2006. From the layers contained within: a) the southern hemisphere hydrological year (30th-April - 30th April), and b) the growth season (1st October - 30th April), we calculated the following statistics: sum, standard deviation, and a range of percentiles (25, 50, 75, 90). We also included the following auxiliary predictors: elevation (from the STRM 30 m DEM); tree cover (from the MODIS MOD44B product); soil taxonomy, geology, and survey year. All additional variables were resampled to 1 km resolution using nearest neighbour resampling.

Our modelling approach is focussed on two key areas, target-based validation strategies (Section 3.4), and variable selection procedures (Section 3.4)

Cubist Models

The machine learning method Cubist was used for all modelling tasks (from Jed Wing et al. 2017). Cubist models are related to regression trees, and generate predictions based on the following procedure: firstly, a regression tree is constructed, whereby the tree branches are a series of nested *'if-else'* statements, based on the predictor variables. Each splitting node calculates a linear regression using the predictors used thus far. The splitting process continues until there are insufficient samples to either split the data or fit a model. The terminal leaf of each branch then generates predictions using a linear regression of the samples retained. This prediction is smoothed using the preceding linear models. The derived tree is then simplified using a pruning procedure. Finally, a series of models, refereed to as a *'committee'*, are generated with the prior model fits being used to adjust the trees, and the

final model being an average of the committee predictions (this is comparable to boosting).

Validation Strategies

The strategy used to validate model performance can have a major effect on the perceived accuracy. The most common approaches are: i) test-set-holdout, whereby the data are divided into separate subsets for training and testing, typically using a 50:50% or 67:33% ratio; and ii) k-fold cross validation (CV), which segments the data into *k* equal folds (normally 5 or 10) with *k-1* folds used for training whilst the withheld subset is used for validation; this process is then repeated until each fold has been withheld. However, these approaches are based on the assumption that each observation is independent, which is violated by both spatial and temporal autocorrelation. Failure to account for the spatio-temporal nature of data, and inherent autocorrelations, may result in model overfitting being missed, if the testing data are drawn from the same (autocorrelated) sample.

Brenning (2012) propose the use of *spatial* CV to overcome autocorrelation. The data are divided into *k* equal folds based on location, according to a k-means clustering of the co-ordinates (Figure 3.2). This acts as a stratified CV with each fold being spatially independent of the others. Similarly, Meyer et al. (2018) demonstrated that spatio-temporal models can be assessed by leave-location-out CV, whereby a single site is used for validation (Figure 3.2). This approach was particularly effective at identifying when models were compromised by inappropriate auxiliary variables, as these values are constant through time, they are replicated within the data and can cause overfitting. Further consideration should also be given to temporal structures in data, therefore, testing on unseen years and on independent sites throughout time, is recommended (Meyer et al. 2018).

Considering these issues, we employ the following validation strategies for all modelling options:

1. k-Fold (K.CV): ten random equally sized blocks, with one block reserved for testing;

2. Leave Location Out (LLO.CV): one location (*site*) is omitted for testing;

3. Leave Time Out (LTO.CV): one time period (*year*) is omitted for testing;

4. Leave Location and Time Out (LLTO.CV): a single site for all time periods is removed for testing.
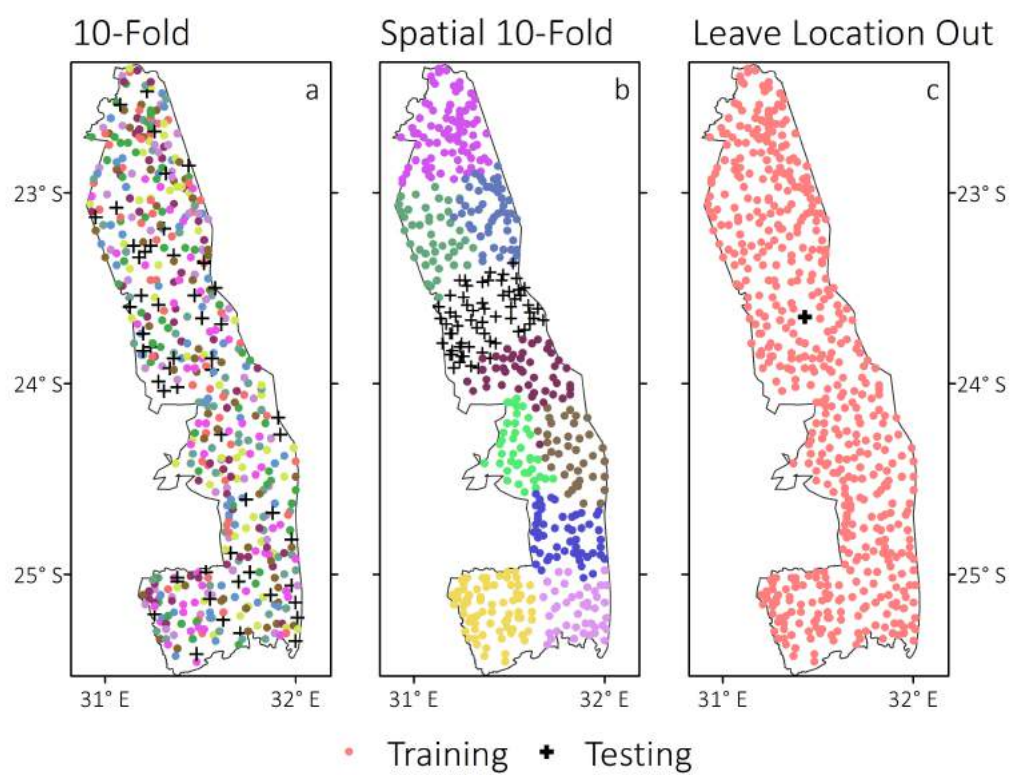
Figure 3.2: Example of the three spatial validation strategies: (a) k-fold; (b) Spatial 10-fold, and (c) Leave Location Out

Forward Feature Selection

Forward Feature Selection (FFS) is a variable reduction technique designed to highlight which predictors are unhelpful or detrimental, and can be removed from models. Firstly, all possible two-variable models are trained and accuracy assessed with the best preforming combination selected. The effect of iteratively adding the remaining variables is then tested. The procedure stops when additional predictors cause a negative impact on the model error. By combining this technique with a target-orientated CV, variables that contribute to spatio-temporal overfitting should be removed. This approach is computationally intensive, requiring the construction and testing of a large number of models, but is more appropriate than other variable section methods (e.g Recursive Feature Elimination) which use errors calculated from the training data alone (Meyer et al. 2018, Gasch et al. 2015).

Software Implementation

All data processing and analysis was undertaken in the R programming language (R Core Team 2015*a*). Downloading the $NDVI_{modis}$ and $NDVI_{gimms}$ was implemented in the *'gimms'* package (Detsch 2018). EOT-downscaling was completed in the *'remote'* package (Appelhans et al. 2015). For the modelling, we used *'caret'* as a wrapper for the *'Cubist'* package (from Jed Wing et al. 2017, Kuhn and Quinlan 2017), with the *'cast'* package providing the target orientated CV and FFS (Meyer 2018).

3.5   Results

NDVI Downscaling

The EOT-based downscaling technique was effective at generating a 1 km^2 resolution NDVI product ($NDVI_{eot}$) from the GIMMS data. Accuracy metrics calculated from the overlapping pixels between $NDVI_{eot}$ and $NDVI_{modis}$ show a high level of agreement (R^2 = 0.86, RMSE = 0.043). Visual examination (Figure 3.3) of the downscaling procedure shows that although residuals ($NDVI_{eot}$ - $NDVI_{modis}$) are generally low, they do exhibit spatial autocorrelation; nevertheless, a majority of the spatial and temporal patterns are captured (Figures 3.3 and 3.4).
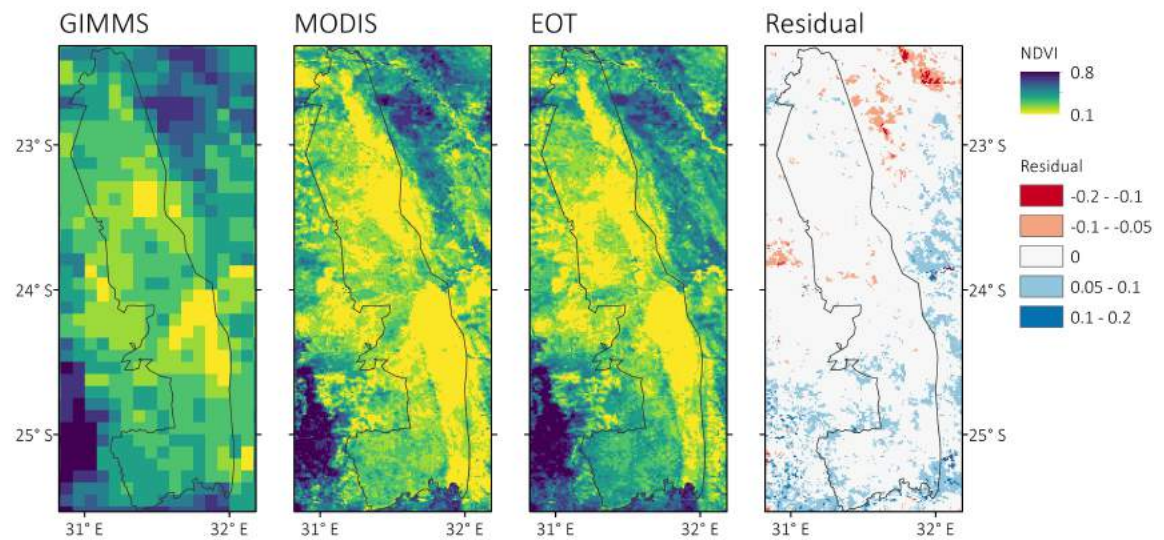
Figure 3.3: Example of the NDVI downscaling process and accompanying residuals, for may 18th 2014
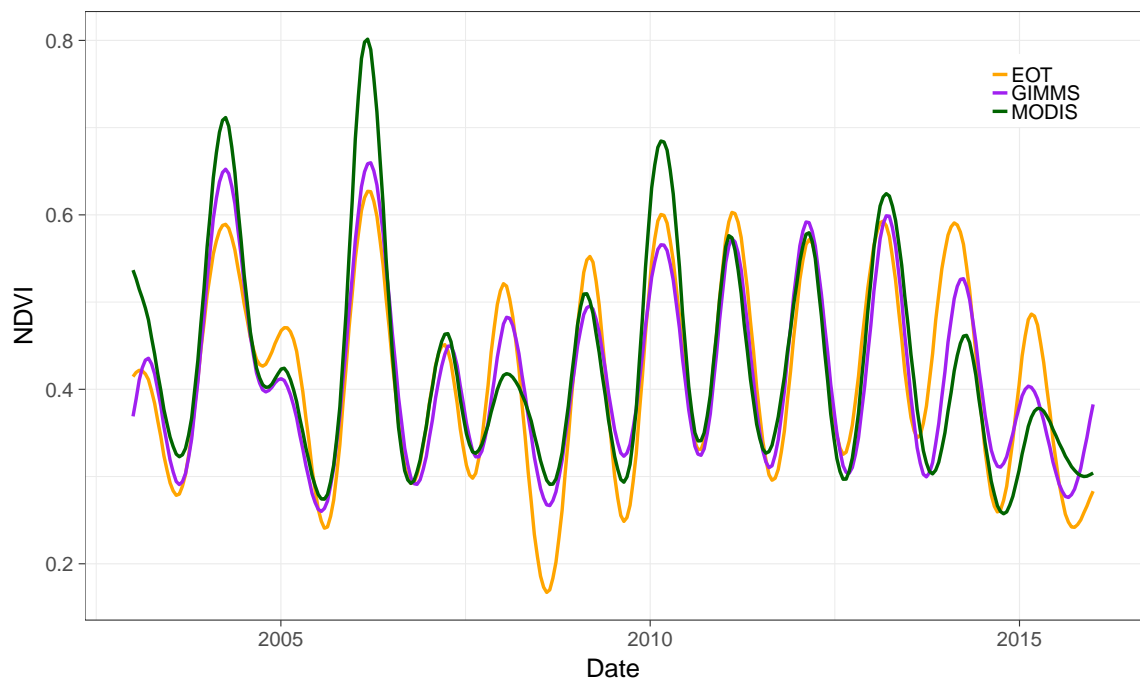
Figure 3.4: NDVI time-series for the three datasets: GIMMS, MODIS, and EOT downscaled

Variable Selection

The variable importance for features selected by the FFS are shown in Figure 3.5. The use of FFS consistently reduced the number of variables in the modelling process. The spatial-orientated approaches, LLO and spatial CV, selected 12 and 10 features, respectively (Figure 3.5.b and 3.5.b). Both temporal methods, LTO and LLTO, retained five variables (Figure 3.5.d and 3.5.e).

As expected, the models generated by FFS removed a large proportion of the candidate variables. In addition to discarding a majority of the NDVI-derived layers, at least one auxiliary variable was discarded. Of the auxiliary variables, geology and elevation were consistency retained, year and mean tree cover were used by the spatial-orientated methods (LLO and spatial CV), with soil taxonomy kept by LLO and LTO.

For the NDVI-derived layers, there was a clear divide between the 'all variables' model (Figure 3.5.a) and the target-orientated approaches (Figures 3.5.b-e). In the 'all variables' model, a large number of NDVI metrics were highly ranked. Many of these were subsequently dropped following feature selection. In the spatially-selected models, a number of features were consistently retained. These included the annual 75th percentiles; and from the growth season, the standard deviation and the 50th and 25th percentiles.

The models derived by the FFS have a number of similarities, with a number of variables featuring prominently: the NDVI 75th and 90th percentiles of annual NDVI, elevation, and geology. However, the specific variables selected by the differing CV strategies is indicative of spatio-temporal modelling constraints that require further analysis.
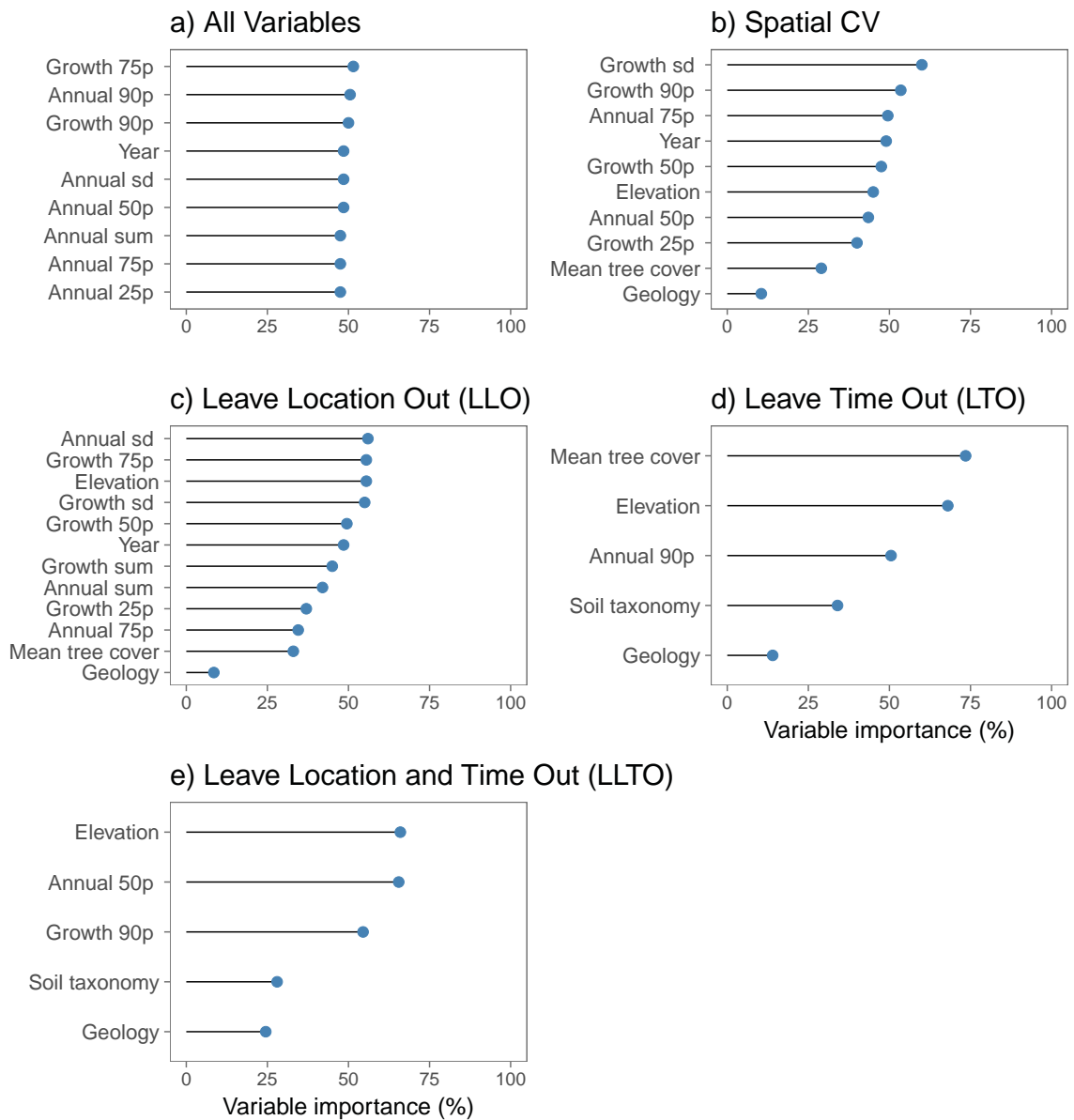
Figure 3.5: Variable importance scores derived from the forward feature selections for the different cross validation strategies. For 'All variables' model (a) only the top 8 features are shown. NDVI-derived layers are referenced by the period of calculation (growth season or annual cycle), and the associated statistic (p: percentile, sd: standard deviation)

Model Validation

For the five variable combinations and validation strategies, Figure 3.6 shows density scatter plots of predicted values compared to the observed measurements, and associated linear regressions lines. Shaded density histograms for the predictions and training values are shown in Figure 3.8. Corresponding accuracy statistics (RMSE, MAE, and R^2) are shown in Table 3.1. The different validation strategies resulted in a wide range of reported accuracies. For the 'all variables' model, RMSE increased from 1310 when using k-fold CV to 1860 when LTO CV was applied, a difference of 550. Both spatial and temporal approaches incurred an increase in RMSE, relative to k-fold CV, yet the rise was most pronounced when a time-omitting CV strategy was used. RMSE increased by 110 when spatial CV was used (against k-fold CV). This compares to increases of 550 and 531 for LTO and LLTO, respectively. This pattern was consistent for the spatially-tuned models, whereas temporally orientated combinations demonstrated the lowest accuracies using spatial CV. This variability and the large differences between the k-fold CV and target-orientated approaches, indicates the presence of spatio-temporal overfitting in the initial '(all variables') model. This overfitting can be seen in Figure 3.6, with the predictions based on k-fold showing the closest fit to the 1:1 line, whereas the other methods show more spread and deviation. Further evidence of potential overfitting is shown in the predictions of three individual sites in Figure 3.7; with the temporally-selected models showing less reflexivity relative to the spatial variables. A comparison of two mapped predictions (Spatial CV and LTO) for the years 1997 - 2000 are shown in Figure 3.9.
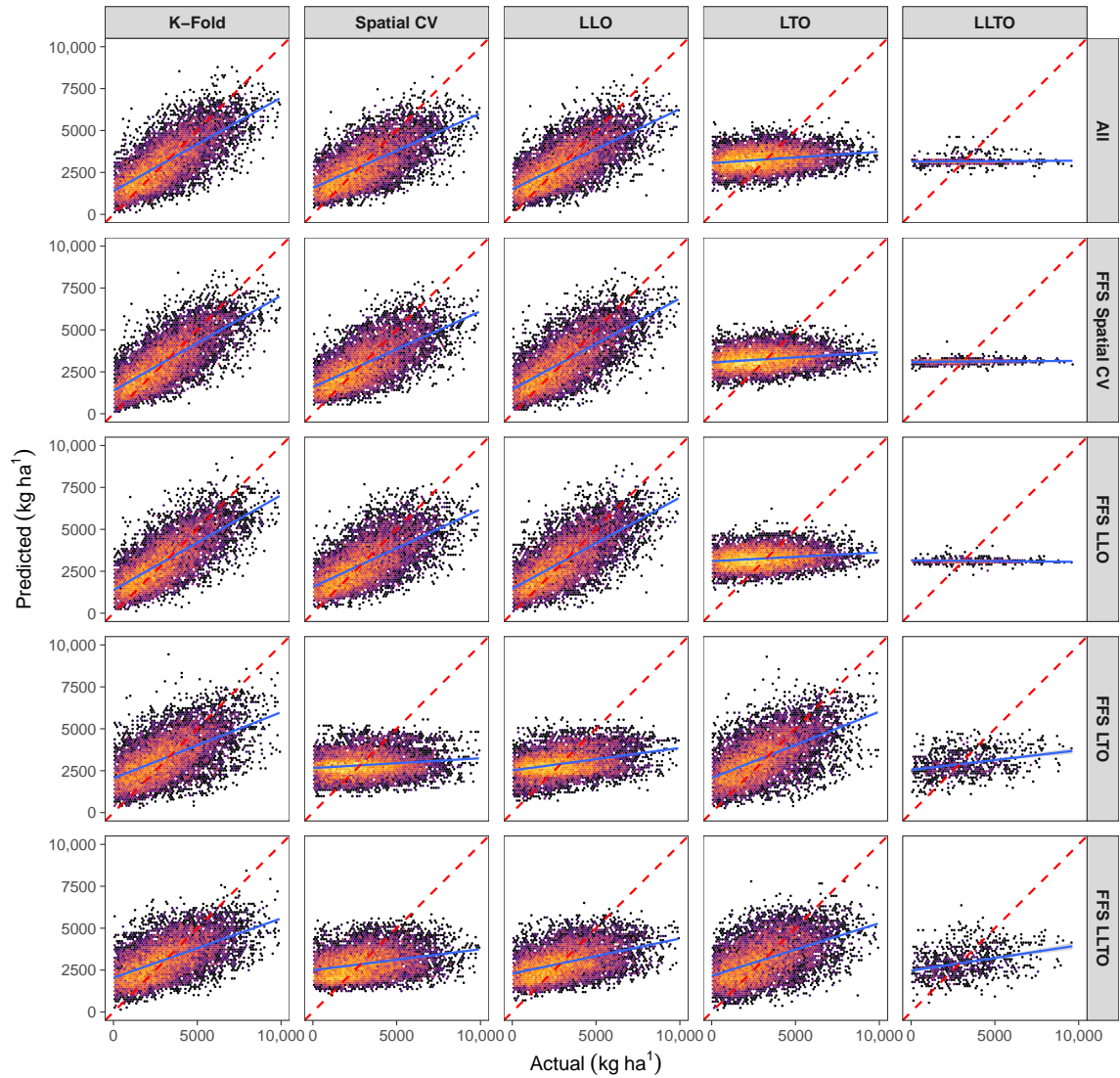
Figure 3.6: Density plots of predicted and observed biomass for the different validation strategies (columns) and variable combinations (rows). The red dashed line is a 1:1 relationship, the blue is the actual linear model. CV: Cross Validation, FFS: Forward Feature Selection, LLO: Leave Location Out, LTO: Leave Time Out, LLTO: Leave Location and Time Out.
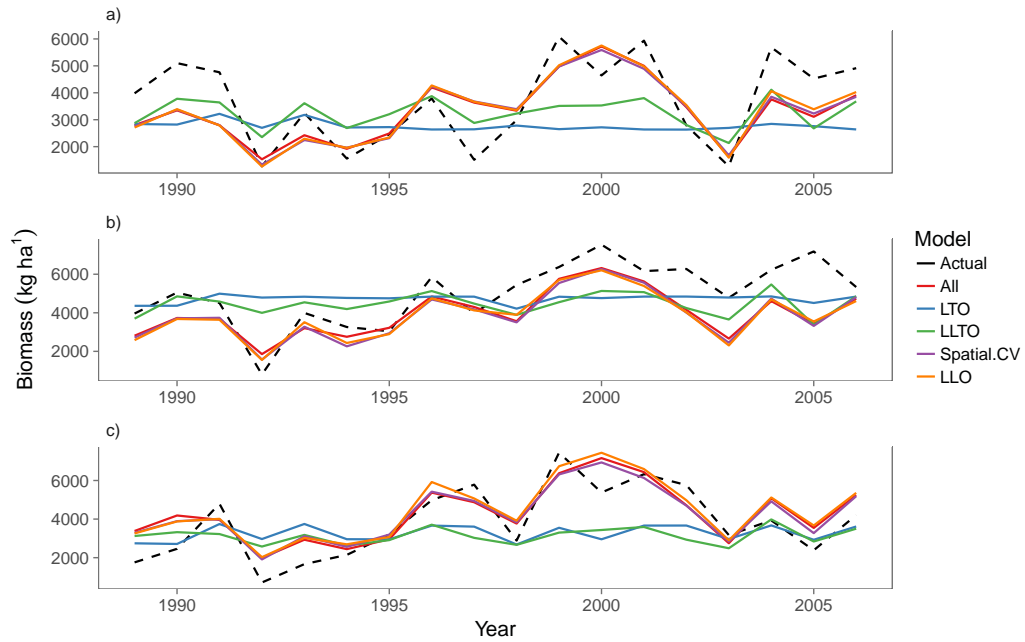
Figure 3.7: Predictions and observed biomass using the five model combinations, for three sampling plots. LLO: Leave Location Out, LTO: Leave Time Out, LLTO: Leave Location and Time Out
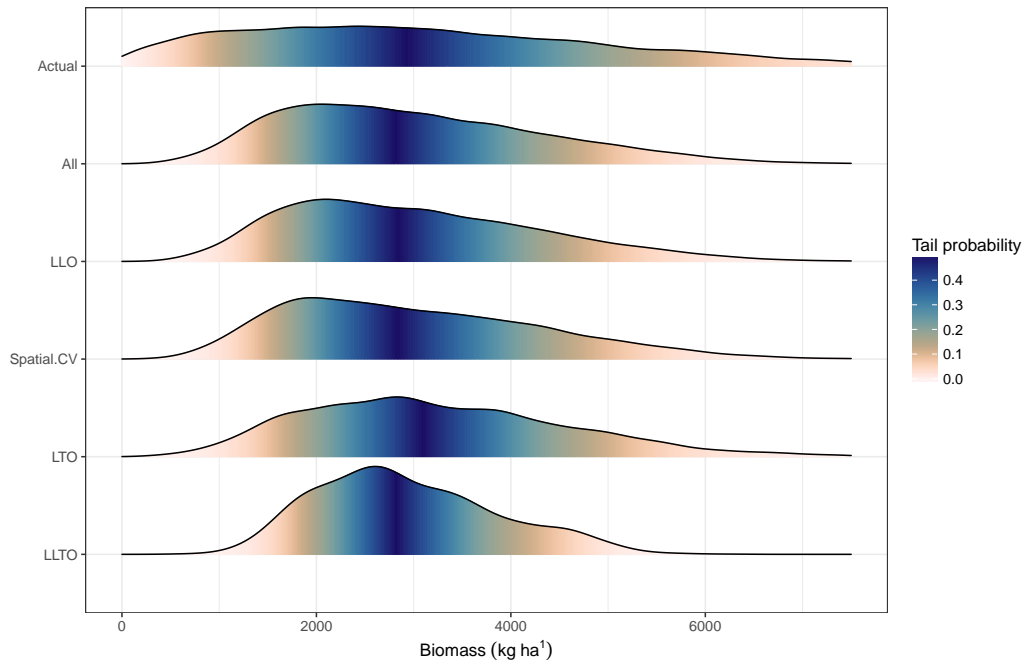
Figure 3.8: Density plots for the final predictions from the five models and field data. Tail probabilities are calculated from the group level empirical cumulative distribution function (ECDF). LLO: Leave Location Out, LTO: Leave Time Out, LLTO: Leave Location and Time Out
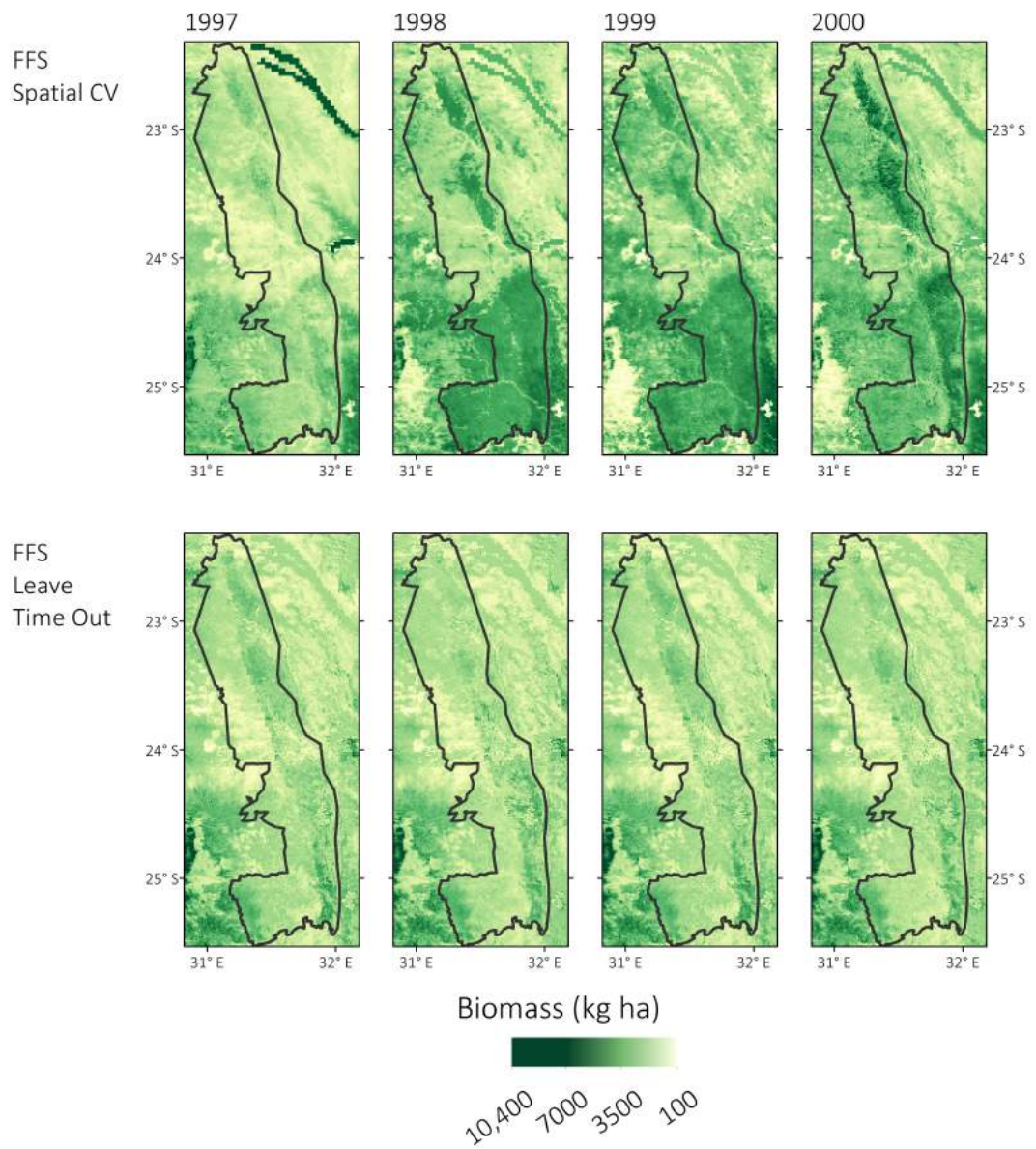
Figure 3.9: Maps of predicted biomass for two model combinations.

Variables	Validation	RMSE	R^2	MAE
All	k-Fold	1310	0.53	1026
	Spatial CV	1420	0.41	1116
	LLO	1311	0.51	1087
	LTO	1860	0.11	1547
	LLTO	1841	0.02	1523
Spatial CV	k-Fold	1295	0.54	1014
	Spatial CV	1409	0.42	1111
	LLO	1293	0.51	1072
	LTO	1868	0.11	1547
	LLTO	1835	0.07	1511
FFS LLO	k-Fold	1302	0.54	1020
	Spatial CV	1420	0.41	1117
	LLO	1299	0.51	1078
	LTO	1878	0.08	1557
	LLTO	1858	0.01	1533
FFS LTO	k-Fold	1578	0.34	1243
	Spatial CV	1925	0.03	1542
	LLO	1718	0.12	1434
	LTO	1563	0.39	1286
	LLTO	1770	0.13	1439
FFS LLTO	k-Fold	1556	0.34	1227
	Spatial CV	1840	0.08	1454
	LLO	1623	0.22	1351
	LTO	1656	0.22	1331
	LLTO	1758	0.15	1401

Table 3.1: Model accuracies derived from the four variable sets using the four validation strategies. RMSE: Root Mean Square Error, MAE: Mean Absolute Error CV: Cross Validation, FFS: Forward Feature Selection, LLO: Leave Location Out, LTO: Leave Time Out, LLTO: Leave Location and Time Out

3.6   Discussion

Mapping the spatio-temporal dynamics of biomass is important for a range of applications, such as fire prediction, understanding climate change impacts, and livestock management. Although relating satellite-derived metrics, such as NDVI, to biomass has been a staple of the literature of over 30 years, there has been limited application of modern statistical methods to this task. To address this gap, we analysed a long-term, spatially concentrated grass biomass dataset in a machine learning framework, to identify the benefits and limitations of variable selection and validation methods. Our study provides a number of insights for the prediction of

aboveground biomass using NDVI time-series.

Firstly, Empirical Orthogonal Teleconnections (EOT) provide an effective means of generating moderate resolution NDVI data sets. Our accuracy statistics, calculated from the overlapping $NDVI_{eot}$ and $NDVI_{modis}$ layers are high (R^2 - 0.86, RMSE - 0.043) and similar to those reported by Detsch et al. (2016) for the Kilimanjaro region, Tanzania (R^2 - 0.96, RMSE - 0.043). This is an encouraging finding, as the ability to generate robust, long-term, moderate-resolution datasets may be of particular benefit in similar semi-arid regions where other satellite archives, such as Landsat or SPOT, are problematic or lacking. The global coverage of AVHRR and MODIS data would enable applications in many locations.

Secondly, spatial overfitting was evident in the biomass models, as demonstrated by comparing the k-fold and spatial CV accuracies (Table 3.1), and the fit of predicted against observed values (Figure 3.6). Meyer et al. (2016, 2018) demonstrate that spatial overfitting can be caused by an over-representation of auxiliary variables in temporal models, resulting in features combining to form pseudo-ID codes for each site. The spatially-selected models (FFS.CV and FFS.LLO) do drop one auxiliary feature each; however, a far greater proportion of the NDVI layers are discarded. Of the twelve NDVI metrics, six and eight were discarded by the spatial models, respectively. Comparing the spatially-selected models, it is noteworthy that the FFS-spatial CV model retained less variables than the FFS-LLO, and that spatial CV consistently returned lower accuracies. This would indicate that the observed overfitting is driven by spatial autocorrelation among the predictor variables, particularly the NDVI metrics. It is plausible that autocorreltation is more of an issue in this situation due to the relatively dense field sites. This will reduce the likelihood of unintended feature combinations forming as unique values. Similarly, sites are more likely to exhibit autocorrelation in both NDVI and auxiliary layers.

Our third and most significant observation is the severity of temporal overfitting in the models. The 'all variables' and spatially-selected models had low performance on unseen years (Table 3.1), and exhibited regression towards the mean in their predictions (Figure 3.6). This was somewhat expected, as these models had the year variable ranked highly in variable importance (Figure 3.5). We theorise that including year as a parameter in the models allows flexibility in the NDVI-biomass relationships, by acting as a bias correction for inter-annual fluctuations. This would concur with Mbow et al. (2013) who found the NDVI-biomass relationship in savannah grasslands varied depending on species composition, particularly during years with anomalous rainfall. Similarly, Wessels et al. (2006) obtained

higher accuracies when modelling individual years, relative to using a multi-annual dataset, attributing this to a miss-match in scale between the NDVI and field sites. Our study uses the same datasets as Wessels et al. (2006), so the influence of scale differential should not be discounted here; rather, we offer additional explanations for the observed patterns. The temporally-selected models dealt with the temporal overfitting by optimising the use of the auxiliary variables, using only one or two NDVI layers (Figure 3.5). These environmental variables are known to influence the structure of savannahs, making the predictions more akin to deterministic ecological models (Staver et al. 2017, Sankaran et al. 2005). This results in the predictions being less responsive (Figure 3.7), as the role of the NDVI is reduced, with particular difficulty in estimating years with suddenly high or low values. This process is visible in Figure 3.9, where the LTO model results in a less variable output that the spatial CV.

All predictions were poor for the tails of the training data, particularly values greater than 5500 kg ha^{-1} and around zero. (Figures 3.6 and 3.8). These errors were expected for a number of reasons. Firstly, the biomass data used as training data are not precise measures of biomass, such as those obtained by destructive sampling, but are estimated based on grass height and moisture content. For values between 4200-9360 kg ha^{-1}, there is an increasing confidence interval from 328 to 526 kg ha^{-1} (Wessels et al. 2006). This relatively high uncertainty will be propagated on to the NDVI-biomass models, making a close fit for high values unlikely. Secondly, the NDVI-biomass relationship has been shown to saturate at moderate levels, as NPP becomes constrained by factors other than fPAR (Tucker 1979). Finally, machine learning methods, in general, tend towards poor prediction in the tails. Given the long tails of the training data, especially rightwards, errors are to be expected. Accurate predictive mapping of extreme values is an area that merits further study.

The overarching observation of this study is that spatio-temporal models require a robust validation strategy that accounts for these structures. However, although we caution against the use of non-structured approaches, such as k-fold or test-set-holdout, selecting a suitable alternative method is still somewhat specific to the particular condition or situation. If models are being developed with the aim of making predictions within the temporal coverage of the training data, then a spatial CV method will suffice. As unseen years will not be applied for predictions, any temporal overfitting is inconsequential. Between the spatial methods, spatial CV was consistently more conservative than LLO. This is likely due to the higher

density of our field sites and we would recommend that if possible both methods are applied. If the aim is to generate predictions outside the period of training data then a temporal approach is required. This will allow identification of any overfitting or bias correcting variables, such as using year here. These methods are likely to reduce the reported accuracies in many cases, compared to using non-target CV. However, this is necessary to obtain an accurate understanding of the limitations and uncertainties of models and predictions.

3.7   Conclusion

This study adds to recent research in highlighting that machine learning methods, including those based on bootstrapping or boosting, are not immune to overfitting, as has commonly been assumed. Accuracy assessment methods that fail to account for spatio-temporal structures in the data (e.g. reporting training errors, k-fold CV, etc.), are particularly vulnerable, yet these are the most ubiquitous methods used in the literature. With regards to the prediction of grass biomass from NDVI, we emphasise that the inter-annual fluctuation of rainfall and species may be particularly pertinent to temporal overfitting. These findings combined suggest that generating reliable biomass maps from NDVI may be more challenging than has been assumed. However, the usefulness of any final product to is dependent upon the level of uncertainly that is acceptable.

Chapter 4

Mapping Woody Cover in Semi-arid Savannahs using Multi-seasonal Composites from Landsat Data

This chapter has been published in the following journal article:

Abstract

Increasing attention is being directed at mapping the fractional woody cover of savannahs using Earth-observation data. In this study, we test the utility of Landsat TM/ ETM+ based spectral-temporal variability metrics for mapping regional-scale woody cover in the Limpopo Province of South Africa, for 2010. We employ a machine learning framework to compare the accuracies of Random Forest models derived using metrics calculated from different seasons. We compare these results to those from fused Landsat-PALSAR data to establish if seasonal metrics can compensate for structural information from the PALSAR signal. Furthermore, we test the applicability of a statistical variable selection method, the recursive feature elimination (RFE), in the automation of the model building process in order to reduce model complexity and processing time. All of our tests were repeated at four scales (30, 60, 90, and 120 m - pixels) to investigate the role of spatial resolution on

modelled accuracies. Our results show that multi-seasonal composites combining imagery from both the dry and wet seasons produced the highest accuracies (R^2= 0.77, RMSE= 9.4, at the 120 m scale). When using a single season of observations, dry season imagery performed best (R^2= 0.74, RMSE= 9.9, at the 120 m resolution). Combining Landsat and radar imagery was only marginally beneficial, offering a mean relative improvement of 1% in accuracy at the 120 m scale. However, this improvement was concentrated in areas with lower densities of woody coverage (<30%), which are areas of concern for environmental monitoring. At finer spatial resolutions, the inclusion of SAR data actually reduced accuracies. Overall, the RFE was able to produce the most accurate model (R^2= 0.8, RMSE= 8.9, at the 120 m pixel scale). For mapping savannah woody cover at the 30 m pixel scale, we suggest that monitoring methodologies continue to exploit the Landsat archive, but should aim to use multi-seasonal derived information. When the coarser 120 m pixel scale is adequate, integration of Landsat and SAR data should be considered, especially in areas with lower woody cover densities. The use of multiple seasonal compositing periods offers promise for large-area mapping of savannahs, even in regions with a limited historical Landsat coverage.

4.1   Introduction

Savannah ecosystems are characterised by a dynamic mosaic of tree, shrub and grass species. Variations in these components can result in widely divergent ecological functions (Sankaran et al. 2005). There is growing concern over the health and sustainability of savannahs across the world. Increases in shrub cover at the expense of grasslands (i.e. shrub encroachment) have been reported in semi-arid environments globally (Naito and Cairns 2011, Stevens et al. 2017, Tian et al. 2017, Skowno et al. 2017). In contrast, overexploitation of woody shrubs and trees for fuelwood may be depleting woody cover in other regions (Wessels et al. 2013, Brandt et al. 2017).

Monitoring savannahs is a challenging endeavour, and due to the discontinuous nature of land cover in such environments, categorical maps are of limited value (Xian et al. 2013). Alternatively, representing the 2-dimension horizontal woody cover component as a continuous fractional layer is more ecologically relevant, and recent advances in the field have focused their attention to this characteristic (Armston et al. 2009, Bucini et al. 2010, Naidoo et al. 2016). However, the spatial heterogeneity of savannahs makes fractional cover modelling vulnerable to scale

effects, as areas of very high or low coverage will be lost by aggregation to coarser scales (Guerschman et al. 2009). Therefore, it is necessary to consider analyses over a range of resolutions, enabling an optimum balance between model accuracy and spatial detail to be established (Urbazaev et al. 2015).

Passive optical Earth observation (EO) data, such as Landsat, have commonly been employed to map savannah vegetation in the past (Prince and Astle 1986). Such data discriminate vegetation type by exploiting the full spectral range of reflected solar radiation. Passive optical data also allow for vegetation indices, such as the Normalized Difference Vegetation Index (NDVI), to be used as proxies of various biogeophysical parameters, such as net primary productivity (NPP), fraction of photosynthetically active radiation (fPAR), and leaf area index (LAI) (Higginbottom and Symeonakis 2014, Zhu et al. 2013, Carlson and Ripley 1997). Yet single date optical imagery can be inappropriate for discriminating woody and grass coverage, as photosynthetic activity is detected indiscriminately (Olsson et al. 2011). In savannahs, the woody cover component decreases temporal variation within the NDVI signal, as bushes and shrubs maintain leaves throughout the dry season (Bucini et al. 2010, Naidoo et al. 2016). Information derived from a pixel-level time series can therefore contain valuable information for land cover mapping. If sufficient observations are available, phenological metrics detailing the start and end points of seasons can be calculated (Brandt et al. 2016, Zhang et al. 2014). Alternatively, spectral-temporal variability metrics from single spectral bands or indices (e.g. minimum, maximum, mean, median, etc.) can quantify variability even in regions with lower observation densities (Müller et al. 2015, Zhong et al. 2014).

Irrespective of processing method, optical data possesses fundamental limitations for mapping woody environments, because it does not directly correlate to surface structure (Naidoo et al. 2016, Cutler et al. 2012). Active EO sensors such as Synthetic Aperture Radar (SAR) provide information on the 3-dimensional structure of the land surface, by emitting microwaves and measuring the intensity of energy reflected back to the sensor after interactions with ground objects i.e. the backscatter (σ) of the signal. The use of SAR data in fractional woody cover mapping, particularly L-band, operating with wavelengths of 0-15 cm , has been well demonstrated (Naidoo et al. 2015, 2016, Bucini et al. 2010, Mathieu et al. 2013). Mitchard et al. (2009) identified a consistent relationship between cross-polarised L-band backscatter and aboveground biomass (AGB) across four pan-African tropical savannahs, regardless of vegetation composition. Advanced Land Observing

Satellite (ALOS) Phased Array type L-band Synthetic Aperture Radar (PALSAR) imagery has been highlighted as the most reliable satellite-based indicator of both AGB and canopy coverage for woody cover in semi-arid savannahs (Naidoo et al. 2015, 2016). However, the use of L-band imagery for mapping long-term land cover change is affected by a number of data continuity issues, sensor failures (JERS-1, ALOS PALSAR), high data costs, and the short lifespan of radar systems, resulting in a limited temporal archive compared to Landsat. There are less limitations when using C-band radar, such as Radarsat or Sentinel-1, due to more consistent coverage (Reiche et al. 2015). However, C-band radar is not as sensitive to woody cover, compared to L-band (Mathieu et al. 2013).

More recently, the fusion of optical and radar imagery has been shown to provide an improvement upon single-sensor fractional cover accuracies (Bucini et al. 2010, Naidoo et al. 2016). Bucini et al. (2010), Naidoo et al. (2016) combined L-band radar data with Landsat to map woody canopy coverage in the Kruger National Park, South Africa: the fusion approach improved the accuracy over single sensor predictions, particularly when combining SAR with multi-season imagery. Lucas et al. (2006) used PALSAR thresholds in conjunction with Landsat-derived Foliage Projected Cover maps to successfully discriminate regrowth stages in open Eucalyptus forests. Merging various SAR wavebands, such as C, X, or L, have also been shown to provide benefits for woody cover mapping, although these improvements were found to be smaller (around 3%) when compared with L-band alone (Naidoo et al. 2015). Choosing the appropriate sensor, or combination of sensors, for woody cover mapping, is therefore an increasingly complex decision with further study required.

The increasing number and variety of EO systems in operation, coupled with open-data policies, presents a wide range of pathways for land cover mapping. Compared to earlier investigations, it is now routine for studies to use high-dimensional data. However, this approach comes with statistical limitations. Predictive models trained using high-dimensional data are prone to overfitting, thus transferring poorly to unseen validation data. This issue is important, potentially incurring a high degree of variance into classifications, whilst reducing bias (i.e. the bias-variance dilemma) (James et al. 2013, Kuhn and Johnson 2013). A number of techniques exist to process high-dimensional data and extract the most relevant variables, aiming to reduce model complexity whilst retaining predictive accuracy (Guyon et al. 2002, Guyon and Elisseeff 2003). To date the implementation of these methods

in remote sensing analyses has been limited (Meyer et al. 2016), but may be increasingly beneficial in the near future as the number of data sources continues to increase.

Within this context, the overarching aim of this study is to develop a framework for accurately mapping the fractional woody cover of semi-arid savannahs at large spatial scales, using freely and widely available data sources. We address this overarching aim by carrying out a multi-scale comparative exercise that provides answers to the following questions:

1. Can annual time series of Landsat metrics be used to accurately map fractional woody cover, and to what extent does seasonality of the compositing period influence results?

2. How do Landsat-based estimates compare to multi-sensor fusion approaches combining L-band SAR data?

3. Can automated variable selection methods, such as Recursive Feature Elimination, assist in reducing the number of variables used without compromising accuracy?

4.2 Study Area

Our study area is the Limpopo Province, South Africa (Figure 4.1). The province is 125,000 km^2 and intersects 14 Landsat WRS-2 scenes. This region is predominantly open deciduous savannah and grassland, with discontinuous woody cover ranging from 0-60% coverage (Mucina et al. 2006). The climate is mainly semi-arid with small humid subtropical areas (Kottek et al. 2006). Mean annual temperatures range from 21-23 °C and winters are mild and frost-free (Scholes et al. 2001). Rainfall increases along a north-south gradient, with mean annual precipitation of 450 mm/year in the north, rising to 700 mm/year in the south (Scholes et al. 2001). The majority of rainfall occurs in the winter months (October to March; Figure 4.2).

There are pronounced contrasts in land use intensity across the region. In the east, the Kruger National Park is the largest protected area in South Africa featuring minimal human usage beyond fire experiments and animal enclosures. This contrasts with the communally governed areas originating from apartheid-era homelands (Worden 2012). These areas generally feature very high population densities ranging from 200-300 people per km^2, resulting from forced resettlement in the
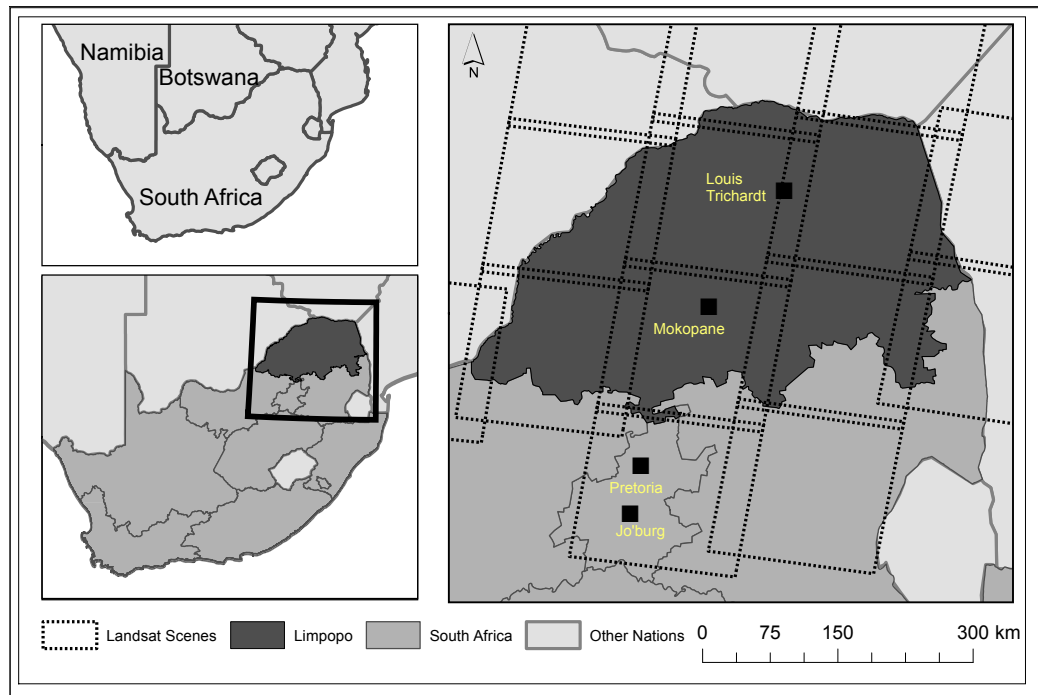
Figure 4.1: Location of the study area, the Limpopo Province of South Africa

1960-1990 apartheid period (Pollard et al. 2003). Consequently, overgrazing and unsustainable wood harvesting are widespread with many areas classified as degraded (Wessels et al. 2007)

4.3   Data

Training and Validation Data

We aimed to develop a transferable method for woody cover mapping. Accordingly, we used training and validation data from aerial imagery, so that our methodological framework would be applicable in study areas where such imagery is available but other data may not be or are costly, e.g. field surveys, Lidar. In South Africa, the National Geospatial Information (NGI) agency of the Department of Rural Development and Land Reform have been providing 0.5 m colour aerial photography since 2008 , with an orthoreftification accuracy of ± 3 m (NGI 2017) . Six 5x5 km images were selected according to a stratified approach based on mean annual precipitation, with acquisition dates between the 19th April and 7th August of the years 2008 and 2009 (Table 4.2).
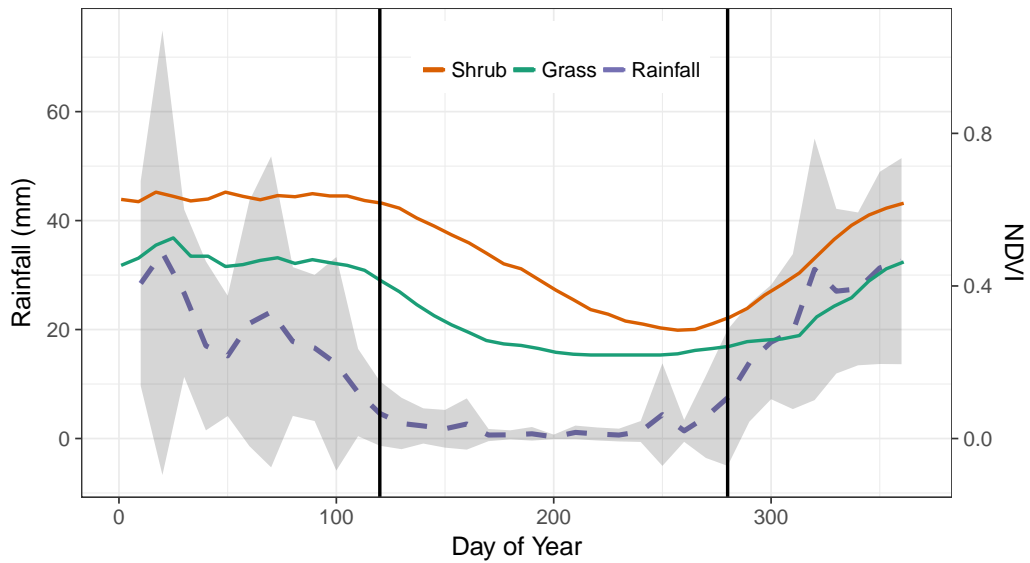
Figure 4.2: Annual seasonality of NDVI for a dense shrub and grassland pixel, and regional rainfall for the Limpopo Province. NDVI is the mean value from 15 year of MODIS-MCD43A4 16 day observations, rainfall data is the mean and standard deviations from FEWS-NET (https://www.fews.net/). The vertical lines indicate the start and the end of the dry season.

Satellite Imagery

Landsat

Spectral-temporal variability metrics are a method of capturing information on the temporal evolution of spectral values within a pixel (Müller et al. 2015). We hypothesised that metrics capturing this variability would be effective for woody cover monitoring. To generate metrics, all available Landsat 5 and 7 images that intersected the Limpopo Province for 2009-2010 were used (Table 4.1); for the wet season, additional images from the two neighbouring hydrological years were also used (scene footprints shown in Figure 4.1). Top-of-atmosphere (TOA) reflectance was calculated using standard bias-gain equations. Pixels affected by clouds or cloud shadow were removed based on the F-mask algorithm (Zhu and Woodcock 2012). No correction was applied for the Scan Line Corrector (SLC-off) errors and these pixels were omitted. For each pixel, all available co-located observations were used to calculate the following statistics: mean, median, minimum, maximum, and standard deviation. These metrics were calculated over three time-periods: annual, dry season and wet season (Figure 4.2), resulting in a total of 90 Landsat-derived layers. The number of images used within each observation period is given in Table

Period	Start Date	End Date	Landsat 5	Landsat 7	Total Images
Annual Cycle	1st January	31st December	86	259	345
Wet	1st November	30th April	52	186	238
Dry	1st May	1st October	27	102	129
Total			88	324	412

Table 4.1: Number of Landsat images used in each period for variability metric calculations. Wet season metrics are calculated over three hydrological years: 2009-2010, 2010-2011, and 2011-2012. Total does not equal the sum of rows as images can be included in both a single season and the annual period.

4.1. Due to persistent high cloud cover, wet season metrics were calculated over three southern hemisphere hydrological years. Processing was undertaken in the Google Earth Engine cloud computing environment (Gorelick et al. 2017, Moore and Hansen 2011).

ALOS PALSAR

ALOS PALSAR, and its successor ALOS-2 PALSAR-2, are fully polarimetric L-band Synthetic Aperture Radar systems (Rosenqvist et al. 2007). These sensors operate at a wavelength of 23.6 cm. We used the 2010 data from the ALOS PALSAR global mosaic, a science-ready product generated annually for 2007 to 2010 (ALOS), and 2015 (ALOS-2). The images for this mosaic were from the dry season, with acquisition dates between 1st July - 3rd October and two images from 2009. Dual polarization HH (horizontal-horizontal) and HV (horizontal-vertical) backscatter data were used. Pre-processing of the input raw imagery includes orthorectification using the Shuttle Radar Topography Mission (SRTM) Digital Elevation Model (DEM), calibration, speckle reduction, and a destriping procedure (Shimada and Ohtaki 2010, Shimada et al. 2014). The raw digital number format was converted to backscatter (σ^0) using the calibration equation:

$$\sigma^0 = 10 * log10(DN + 0.001)2 + CF$$

where DN is the raw digital number and CF is a calibration factor (=-83). The 25 m mosaic was resampled to match the Landsat resolution using bilinear resampling.
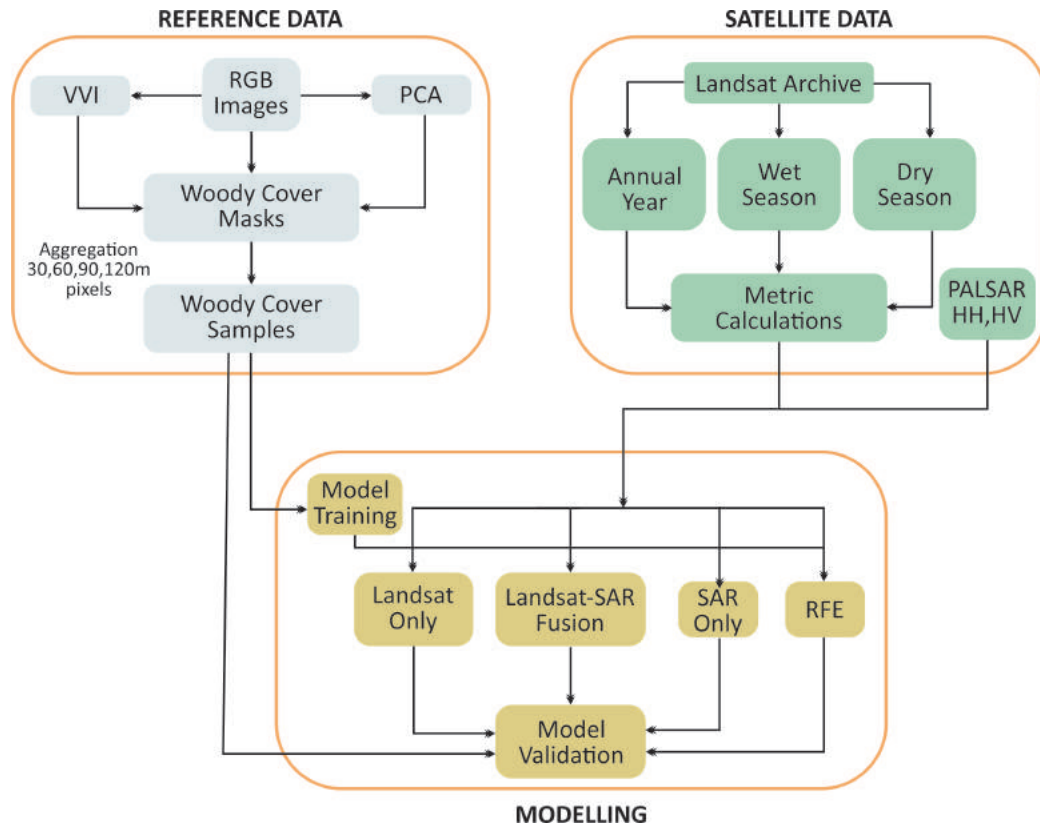
Figure 4.3: Flow chart of methodological framework. VVI: Visible Vegetation Index; PCA: Principle Components Analysis; RFE: Recursive Feature Elimination.

4.4 Methods

The methodological framework is shown in Figure 4.3. To establish the optimum approach for fractional woody cover mapping, we ran a series of random forest regressions to compare the accuracies achieved from single season Landsat metrics, multi-season data, or multi-sensor combining Landsat and SAR data. These models were repeated at four resolutions: 30, 60, 90 and 120 m, to ascertain the ideal scale for large-area monitoring. Processing was undertaken in the R Statistical Software Environment, using the raster, caret, and randomForest packages (Hijmans et al. 2015, Kuhn and Johnson 2013, Liaw and Wiener 2002, R Core Team 2015*b*). Fractional cover sampling code was adapted from Leutner and Horning (2016).

Creation of Reference Data

To create training data the six aerial imagery subsets were classified into woody/non woody masks. We opted for aerial image classification to enable methods to be transferable to other locations, due to the generally satisfactory availability of aerial imagery at appropriate scales (Staben et al. 2016). Firstly, a principal components analysis (PCA) was applied to the three RGB layers and the first two components were extracted. Secondly, we calculated the visible vegetation index (Joseph and Devadas 2015) which uses visible light spectra to estimate photosynthetic activity and is defined as:

$$VVI = \left[\left(1 - \left| \frac{R - R_0}{R + R_0} \right| \right) \left(1 - \left| \frac{G - G_0}{G + G_0} \right| \right) \left(1 - \left| \frac{B - B_0}{B + B_0} \right| \right) \right]^{\frac{1}{w}}$$

where VVI is the visible vegetation index, R, G and B are the red, green, and blue intensities in the image, R_0, G_0 and B_0 are values of red, green, blue used to reference green colour (30, 50, and 1, respectively), determined by the image bit rate (Joseph and Devadas 2015).

A Random Forest classifier was used to create the binary woody-non woody layers from the original RGB layers, principle components, and VVI. Individual models were generated for each image using 400 manually selected points per image (75/25% training-validation split). The mean classification accuracy was 85%. Full accuracy statistics are given in Table 4.2. An example classified mask is shown in Figure 4.4.

To generate training and validation data for the satellite imagery, Landsat pixel-sized squares (i.e. 30x30 m) were extracted from the woody/non-woody masks and the percentage woody coverage calculated. From each image, $7000/\alpha$ samples were extracted, where α takes the values of 1, 2, 3 or 4, depending on the aggregation level used to test the effect of scale in the accuracy of the woody cover estimates (Figure 4.3). For example, for a pixel size of 30m, α= 1 and the samples extracted from each image are 7000, whereas for an aggregation level of α= 2 or a pixel size of 60 m, the number of samples extracted are 7000/2= 3500. These samples were merged and split into equal training and validation subsets with equal probability distributions of woody cover (Figure 4.5). The spatial aggregation process may incur central tendency in training values, with the reduction in high or low samples making the subsequent regression task easier. To quantify this, we tested for any significant difference between the sample distributions using Pairwise-Wilcoxon tests. These highlighted a significant ($p < 0.05$) difference
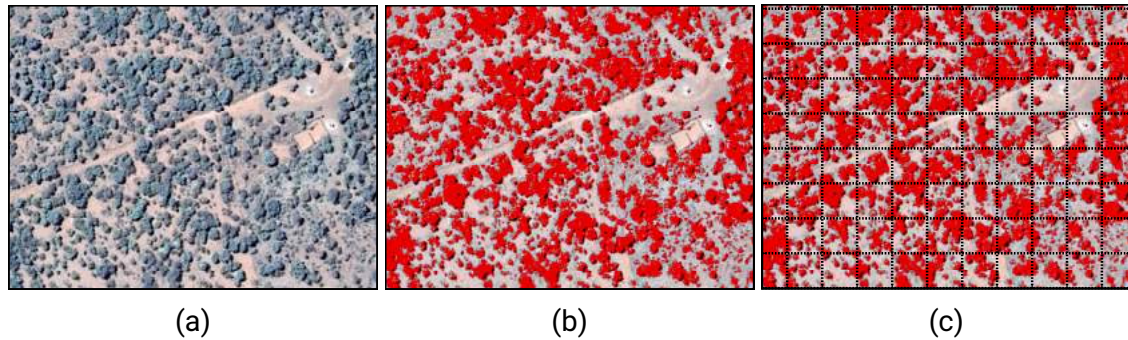
Figure 4.4: Example of the RGB woody classification.a) raw RGB image, b) classified woody cover shown in red, and c) 30 m grid for fractional cover sampling.

Mask Number	Date	Accuracy	Sensitivity	Specificity
1	19/04/2009	0.74	0.73	0.75
2	30/04/2009	0.85	0.88	0.8
3	01/05/2009	0.85	0.88	0.8
4	07/08/2008	0.87	0.87	0.88
5	23/06/2008	0.85	0.86	0.85
6	01/06/2008	0.92	0.88	0.95

Table 4.2: Woody cover mask classification accuracies. Positive Class: Woody Cover

between the data at 30 m and all other scales which can also be visualised in the relatively reduced number of high (>75%) and low (<10%) values in the respective aggregated pixel histograms (Figure 5).

Random Forest Regression

Predictive models were generated using the Random Forest algorithm. Random Forest is an ensemble machine learning procedure that combines bootstrapping and aggregation (bagging) with decision trees (Breiman 2001). All models were individually tuned using 10 repeats of 10-fold cross validation to identify the ideal parameter specification. This covered the number of variables considered at each tree node and the number of trees constructed. As a further measure, we tested the effect of varying the sample size; we tested: i) using all available samples, and ii) using an equal sample size for each resolution. The differences between these were insignificant, and therefore only the all sample results are shown.
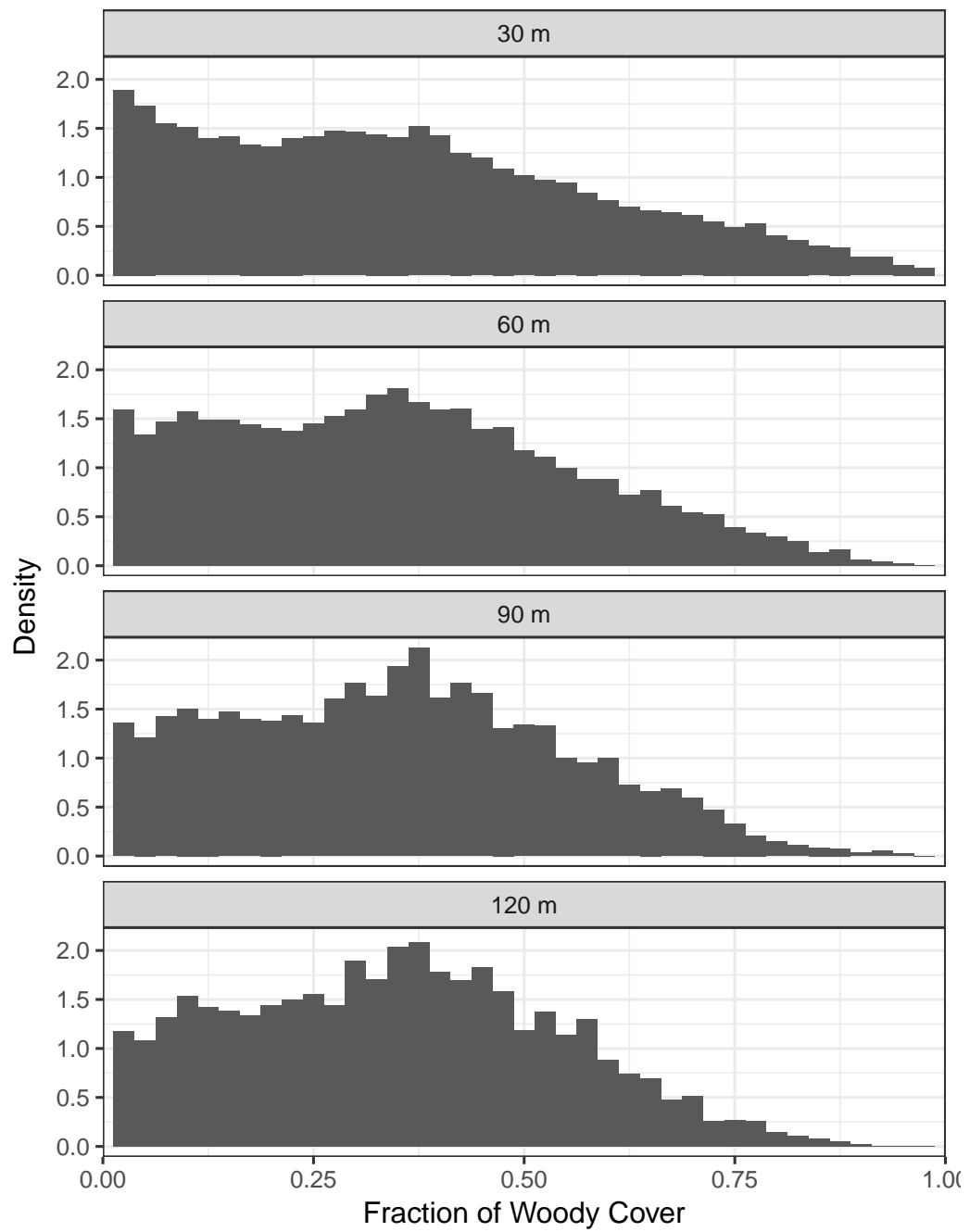
Figure 4.5: Density histograms of model training values at the four scales tested

Variable Selection

To identify optimum predictive models, we incorporated all potential variables into a variable selection process. According to statistical learning theory, a model containing fewer predictors that is comparably accurate is preferential to a more complex model (James et al. 2013, Kuhn and Johnson 2013). Backwards selection methods are effective in identifying the ideal number of variables for prediction, allowing the selection of the most parsimonious model that offers comparable accuracy (Guyon and Elisseeff 2003, James et al. 2013, Kuhn and Johnson 2013). The combination of Landsat metrics and PALSAR data resulted in 92 predictors (90 Landsat metrics + 2 PALSAR backscatter), a number of which are correlated. To identify the most important predictors, we implemented the backwards selection method of recursive feature elimination (RFE). RFE is a parameter selection process that incorporates the estimation of test (validation) errors and variable importance (Guyon et al., 2002). Firstly, a model is constructed using all available predictors (Mp). The test error of this model (i.e. adjusted R^2 and RMSE) is then estimated using 10-fold cross validation, and variable importance scores are calculated. A second model is then established which excludes the lowest contributing variable from Mp, and test error and variable importance are recalculated. This process is repeated until a one-variable model remains. A full iteration of this procedure is repeated 10 times to account for variations in the cross validation sampling, providing a robust estimate of test errors. An ideal model that offers the best performance whilst using the least variables can then be selected.

4.5 Results

Woody Cover Mapping

A fractional woody cover map derived from the most accurate model tested, is shown in Figure 4.6. Subsets comparing the mapped woody cover estimates from a number of models and the NGI aerial imagery are shown in Figure 4.7.

Seasonal Landsat Models

The performance of Landsat-based models is shown in Figure 4.8 and Table 4.4. When using metrics derived from a single season, the highest accuracies were obtained by using the dry season metrics, followed by the full annual cycle, with the
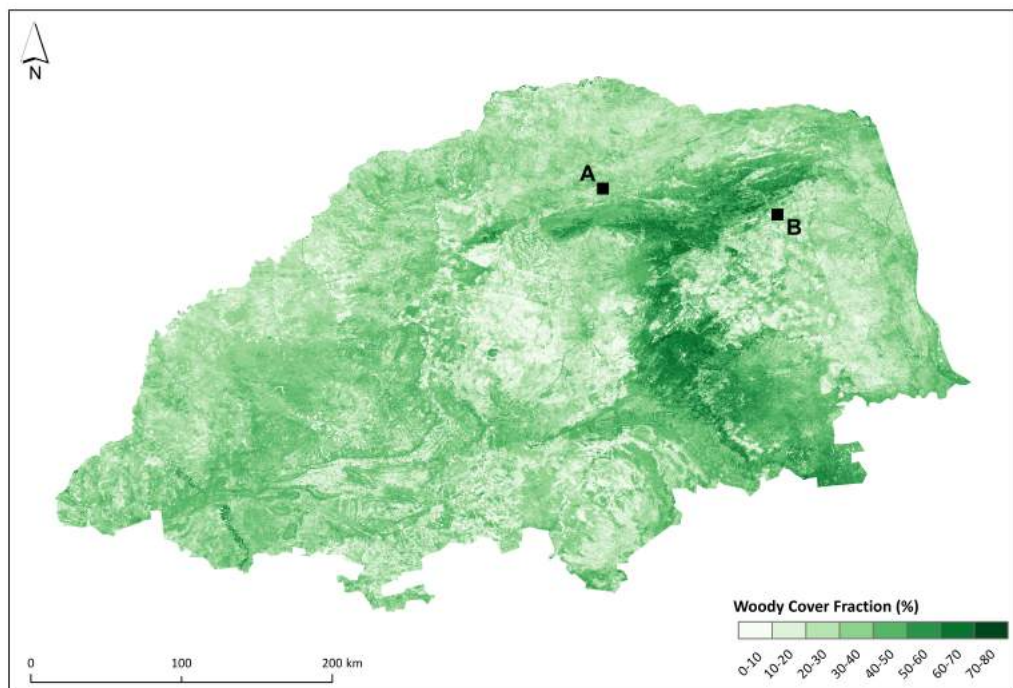
Figure 4.6: Fractional woody cover results for the Limpopo Province based on the Recursive Feature Elimination model at the 120 m pixel scale. Black squares A and B are the locations of the subsets in Figure 4.7.
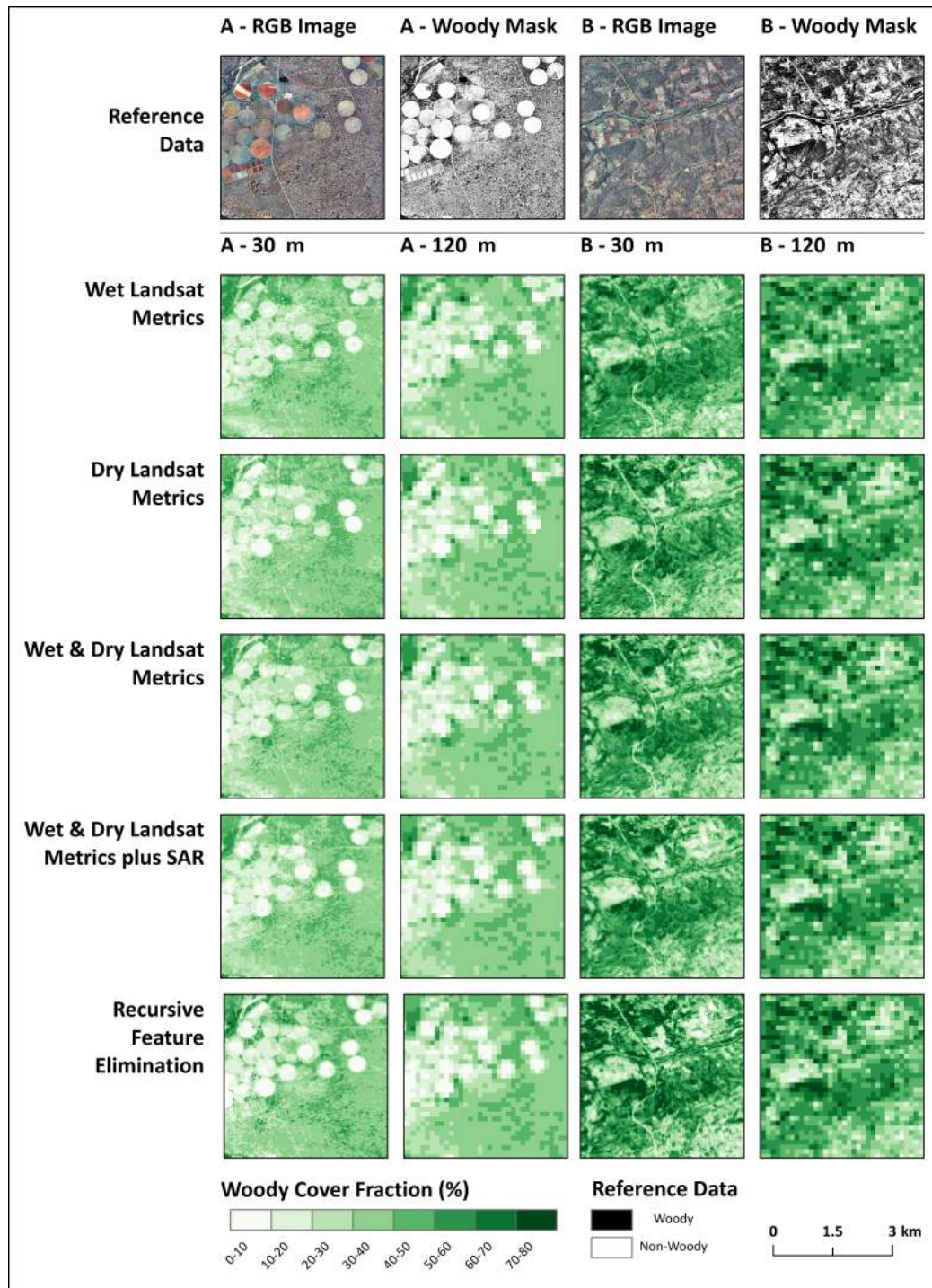
Figure 4.7: Spatial patterns of woody cover for subsets A and B of Figure 4.6 at 30 and 120 m pixel scales. Five model predictions and the respective reference aerial imagery from the NGI are shown. Aerial imagery acquisition dates: A: 19th April 2009, B: 30th April 2009.
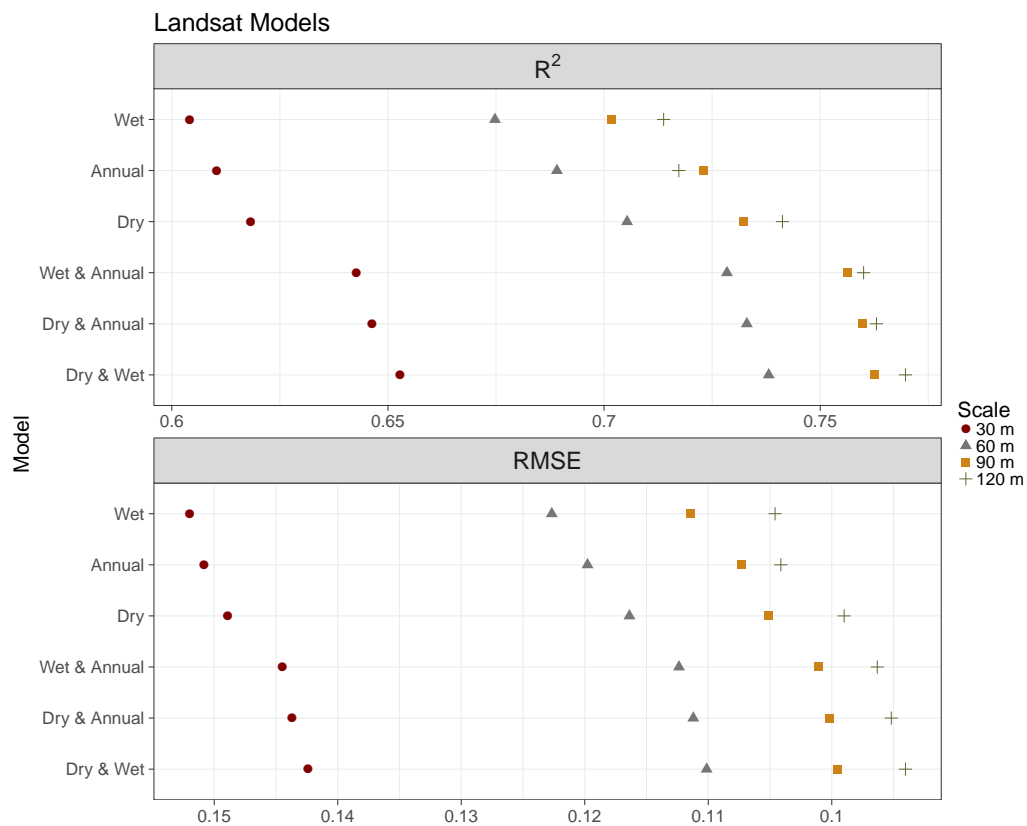
Figure 4.8: Model accuracy results for Landsat metrics-based models RMSE units are percentage woody cover (0-100%)

wet season performing the worst. This pattern was consistent across all scales (Figure 4.8). Using a combination of metrics derived from two seasons, the highest accuracies came from models incorporating both dry and wet season data, followed by dry and annual, and finally wet and annual (Figure 4.8). Reducing the pixel resolutions (i.e. increasing the aggregation factor), consistently raised the model performances, with the largest improvement occurring in the initial aggregation from 30 m to 60 m.

Fused Models

Accuracy statistics from models combining Landsat metrics with ALOS PALSAR backscatter are shown in Figure 4.9 and Table 4.4. Overall, the same ranking of seasonal performance as Landsat-only models was observed. For a single season, accuracy decreased from dry to annual to wet, whilst multi-season models were ranked: dry and wet, dry and annual, and wet and annual. The only exception to

	120 m R^2	RMSE	90 m R^2	RMSE	60 m R^2	RMSE	30 m R^2	RMSE
Landsat Dry and Wet	0.003	-0.1	-0.5	0	-0.9	0.2	-0.005	0.1
Landsat Dry and Annual	0.006	-0.1	-0.2	0	-0.4	0.1	-0.004	0
Landsat Wet and Annual	0.003	-0.1	-0.3	0	-0.7	0.1	-0.002	0.1
Landsat Dry	0.014	-0.3	-0.1	0	-0.2	0.1	-0.004	0.1
Landsat Annual	0.025	-0.5	1.4	-0.3	0.9	-0.2	0.001	-0.1
Landsat Wet	0.009	-0.2	0.4	-0.1	-0.7	0	-0.003	0

Table 4.3: Difference between the Landsat only and Landsat-PALSAR fusion models.

this order was at the 90 m pixel scale, where the single season annual metrics and dry-annual multi-season models performed best (Figure 4.9).

The fusion of PALSAR backscatter with Landsat metrics had contrasting impacts on model accuracy (Table 4.3). At the 120 m scale, all models were improved. Conversely, at the 30 m scale, performances were negatively affected. At mid-range scales (60 and 90 m), the single season annual models were improved, as did the 90 m 'wet' model. All other mid-scale models responded negatively to the SAR fusion or were unaffected. At the 120 m scale, the fusion was generally more effective for single season models over multi-temporal combinations. Finally, at all scales, the annual models performed better when used together with the SAR data. PALSAR only model were consistently the lower preforming model, with the following accuracy statistics: 30 m: R^2- 0.37, RMSE- 15.5; 60 m: R^2- 0.313, RMSE- 16.9; 90 m: R^2- 0.25, RMSE- 18.7; R^2- 0.18, RMSE- 22.2.

Recursive Feature Elimination

The accuracy results from the RFE automated variable selection approach is shown in Figure 4.10. At all scales, model accuracies were higher when more than 25 variables where included in the model and performance declined rapidly when fewer than that were considered. The optimal number of variables to balance predictive accuracy and model simplicity was established as 57 for the 120 m-pixel scale, 54 for the 90 m, 70 for the 60 m, and 85 for the 30 m, the top five variable for each model are shown in Table 4.5. Applying a threshold of two standard errors, based on the cross validations samples for the best model, allows similarly performing models to be compared (James et al. 2013). These models ranged from the one that includes all 92 layers to a minimum of 14 variables for the 120 m scale, 20
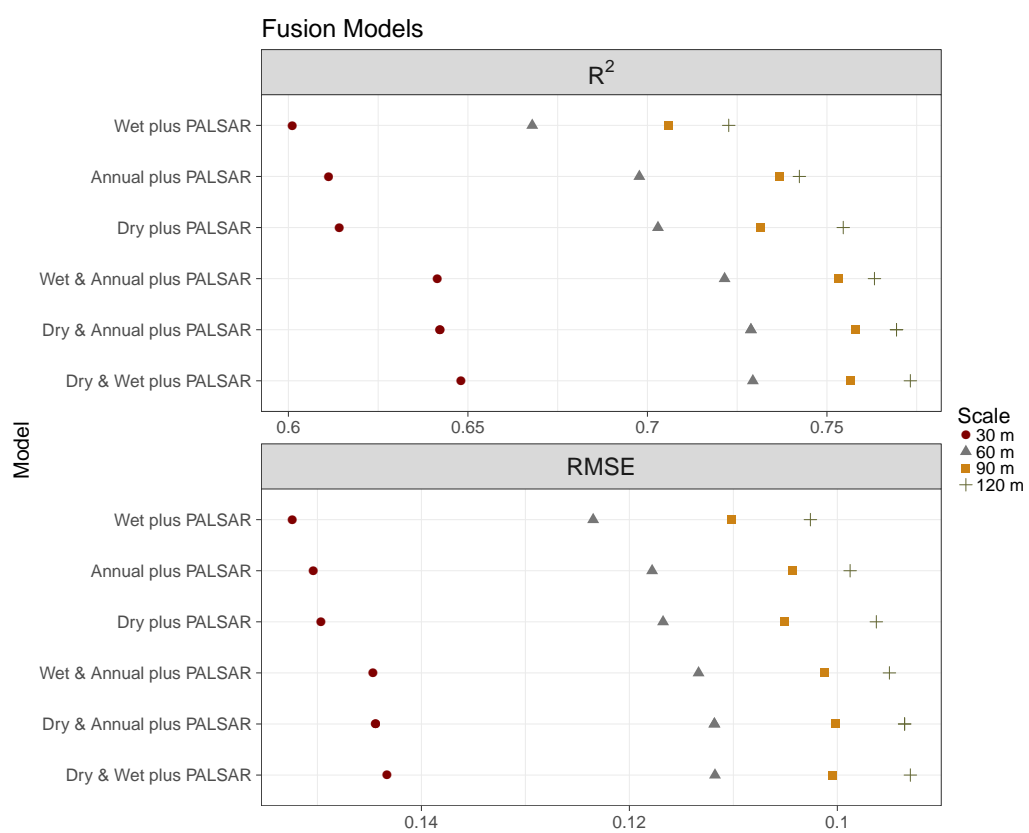
Figure 4.9: Model accuracies (R^2 and RMSE) for Landsat-PALSAR fusion models

	120 m n-3,848		90 m n-6,826		60 m n-10,499		30 m n-21,000	
	R^2	RMSE	R^2	RMSE	R^2	RMSE	R^2	RMSE
Landsat Dry and Wet	0.77	9.4	0.76	10	0.74	11	0.65	14.2
Landsat Dry and Annual	0.76	9.5	0.76	10	0.73	11.1	0.6	14.4
Landsat Wet and Annual	0.76	9.6	0.76	10.1	0.73	11.2	0.64	14.4
Landsat Dry	0.74	9.9	0.73	10.5	0.71	11.6	0.62	14.9
Landsat Annual	0.72	10.4	0.72	10.7	0.69	12	0.61	15.1
Landsat Wet	0.71	10.5	0.70	11.1	0.67	12.3	0.60	15.2
Landsat Dry and Wet+	0.77	9.3	0.76	10	0.73	11.2	0.65	14.3
Landsat Dry and Annual+	0.77	9.4	0.76	10	0.73	11.2	0.64	14.4
Landsat Wet and Annual+	0.76	9.5	0.753	10.1	0.72	11.3	0.64	14.5
Landsat Dry+	0.76	9.6	0.73	10.5	0.70	11.7	0.61	15
Landsat Annual+	0.74	9.9	0.74	10.4	0.70	11.8	0.61	15
Landsat Wet+	0.72	10.3	0.71	11	0.67	12.3	0.60	15.2
PALSAR Only	0.37	15.5	0.313	16.9	0.25	18.7	0.18	22.2
Recursive Feature Elimination	0.79	8.9	0.78	9.7	0.75	11	0.66	14.2
All 92 Variables	0.78	9.2	0.77	9.8	0.74	11	0.66	14.2

Table 4.4: Accuracy statistics for all modes, + indicates Landsat-PALSAR fusion models

for the 90 m scale, 29 for the 60 m, and 39 for the 30 m scale. At all scales, the model constructed by the RFE was the best preforming (Figure 4.11), providing an improvement in the achieved R^2 of at least 0.012. The 120m scale RFE model was the overall most accurate (Figure 4.6). To compare the within model variation in accuracy, Figure 12 shows class accuracy statistics for 10% intervals of woody cover

	30 m	60 m	90 m	120 m
1	HH	HH	HV	HV
2	B1 SD Dry	B1 SD Dry	HH	HH
3	B2 SD Dry	B4 SD Dry	B4 Median Annual	B3 Median Annual
4	B4 Median Wet	HV	B3 Median Dry	B5 Median Dry
5	B4 SD Dry	B1 Min Wet	B3 Median Annual	B3 Median Dry

Table 4.5: Top five variables from the Recursive Feature Elimination model, at each scale (30m, 60m, 90m and 120m). SD: standard deviation.
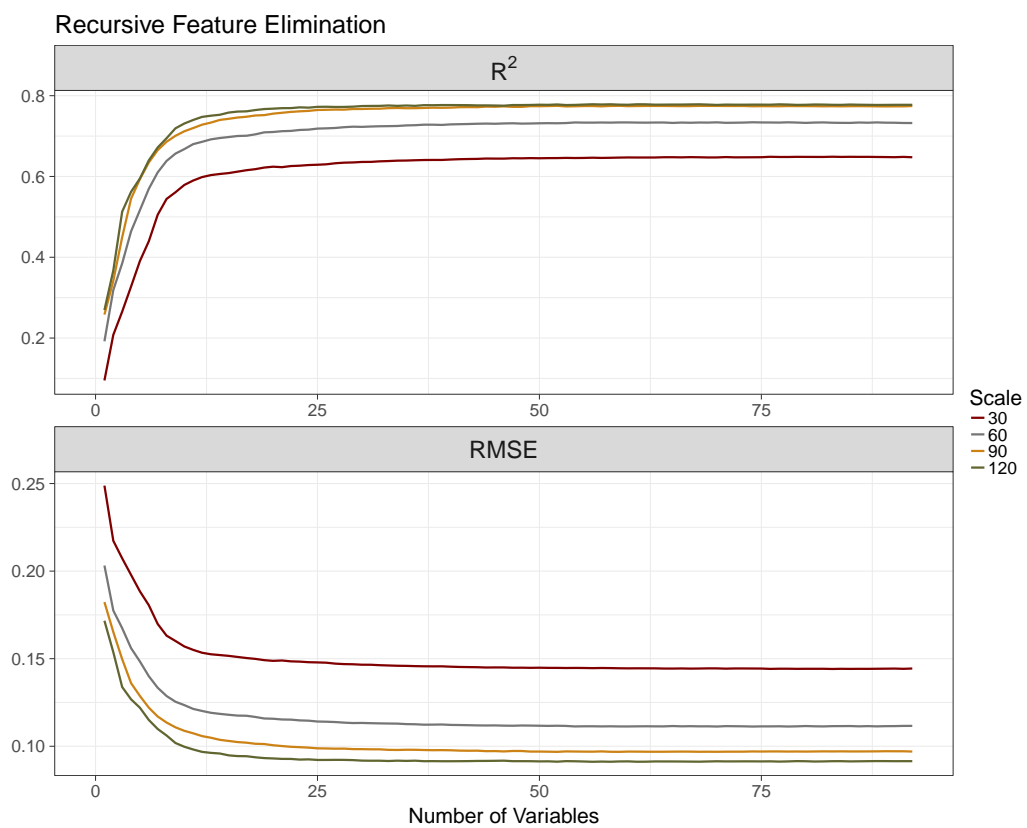
Figure 4.10: Cross-validated R^2 and RMSE results from the recursive feature elimination (RFE) process
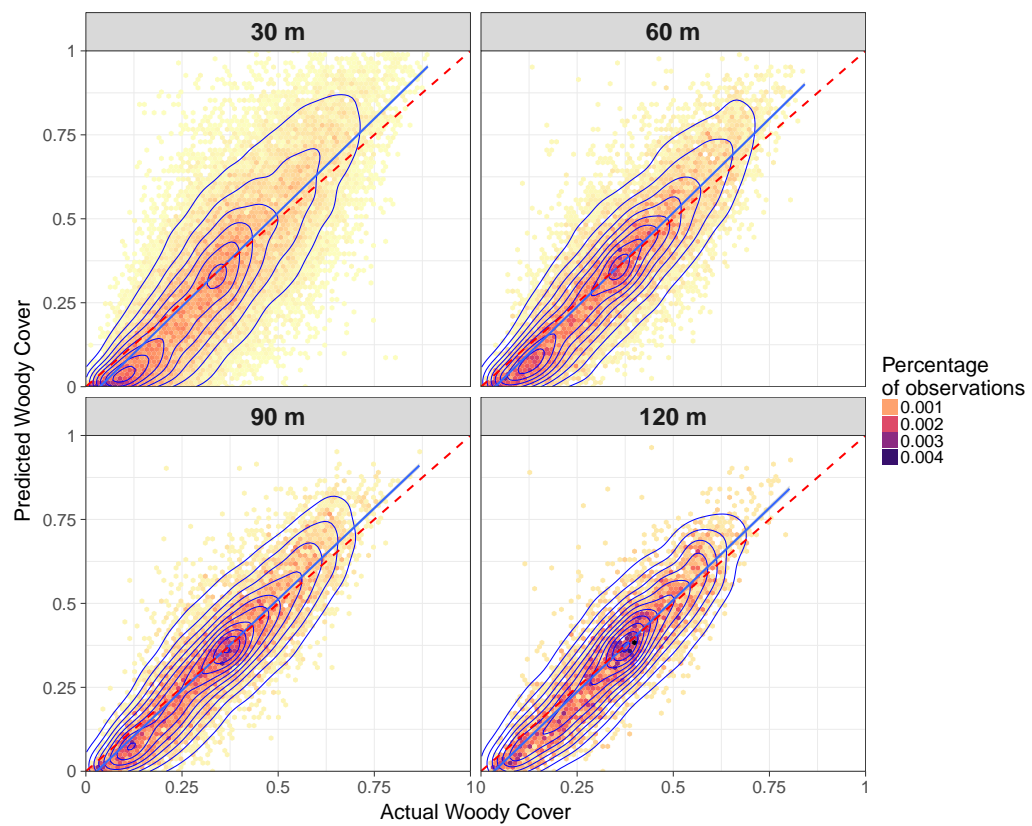
Figure 4.11: Density scatter plot of the Recursive Feature Elimination models at the four resolutions
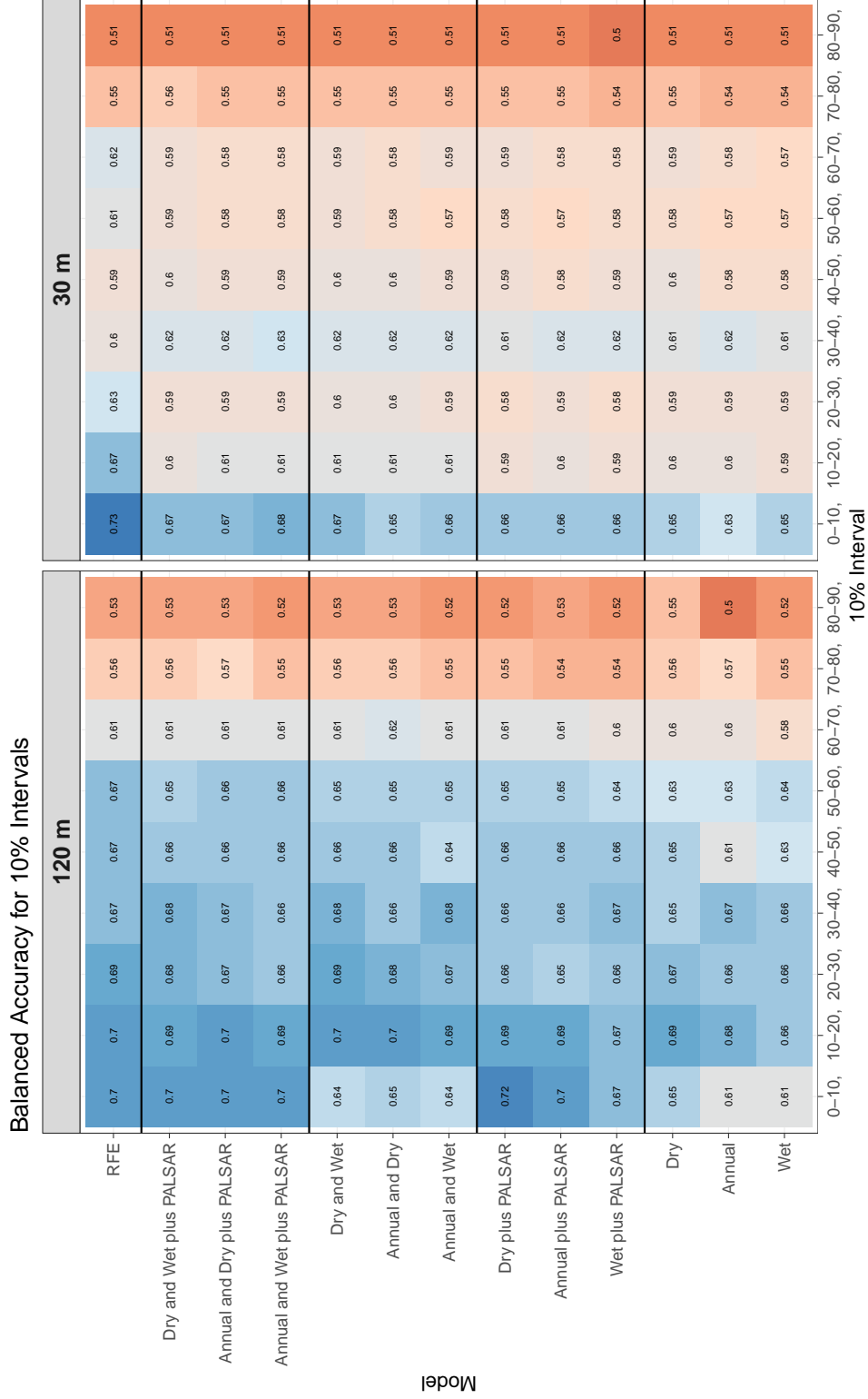
Figure 4.12: Balanced accuracy figures for the different 120 and 30 m-scale models and woody cover density classes, the original continuous woody cover values were binned into 10% intervals. RFE-Recursive Feature Elimination model.

4.6 Discussion

Landsat metrics, seasonality and scale

The accuracies obtained from the Landsat-derived woody cover maps varied according to the temporal window for which metrics were calculated. For single season data, the dry period metrics were the most useful. This result was anticipated due to the persistence of green shrubs into the dry season, compared with the grass layer (Figure 4.2; (Naidoo et al. 2016, Tsalyuk et al. 2017)). This makes woody cover easier to discriminate, compared to other periods where differences are less pronounced (Brandt et al., 2016). This can also explain the overestimation of wet season models in Figure 4.7, as the grass and wood layers are more difficult to separate and identify.

The distribution of errors also varied with seasonality. Dry season metrics performed better in areas of sparse woody cover (0-30% cover), whereas wet metrics offered marginal improvements in the 30-40% and 50-60% percentiles (Figure 4.12). This can be attributed to the dry season metrics having relatively greater discriminatory power at sparse coverage where woody canopies are more distinct. Furthermore, some areas of moderate woody coverage were under-predicted by dry season only metrics. This can be attributed to the fact that some woody species are less persistent in dry conditions (Subset B in Figure 4.7).

The best result from the multi-seasonal Landsat comparisons was the combination of dry and wet season metrics. Although wet season metrics were the least effective mono-temporal models, when combined with the contrasting dry season, the information covering the peak biomass period was beneficial. This improvement was mainly limited to coverage between 10 and 70% where each percentile produced greater class accuracies than either single-season case, at both fine (30 m) and coarse (120 m scales). In general, the multi-seasonal combinations improved prediction across the full range of woody cover densities, with the 10-40% percentiles, at 120 m resolution, achieving the highest-class accuracies. The ability to extract multiple sets of metrics from a time-series of images is noteworthy, reducing to a certain extent the drawback of a temporally limited Landsat archive in many savannah regions. As fractional woody cover approaches the highest values (>70%), all models perform poorly with no model achieving a percentile class accuracy of more than 56% (Figure 4.12). This is partly due to the rare occurrence of this class, which affects the regression analysis. The poor accuracy for dense woody savannahs has been noted by numerous other studies (Naidoo et al. 2016,

Bucini et al. 2010), and should be a priority for future studies. We tested models at four scales: 30, 60, 90, and 120 m pixels. As pixel size increased, model accuracies consistently improved (Figs 8 and 9). The largest improvement occurred with the initial aggregation from 30 to 60 m, with a mean R^2 increase of 13.09%$\pm$0.9, across the 13 models tested. However, this change must be considered with the distribution of the input training values. At 30 m, there is a relativity larger spread of values and a higher proportion of dense and sparse woody coverage (Figure 4.5). Accordingly, this distribution is a more complicated endeavour for the regression analysis, as indicated by the low class accuracies for high cover percentiles (Figure 4.12). Concurrently, the greater proportion, and pixel purity, of sparsely (0-10%) wooded areas at 30 m result in comparably high class accuracies for the first percentile class (Figure 4.12). Resampling to a coarser resolution reduces the occurrence of dense woody coverage, due to central tendency, making the regression exercise easier. This simplification is restricted to the 30 to 60 m aggregation with no visual or statistical evidence that additional resampling improves the outcome of the regression. Further reductions in the pixel resolution result in more modest but consistent improvements of 4.20%$\pm$0.74 and 1.30%$\pm$0.99 in the R^2 when re-scaling from 60 to 90 m and from 90 to 120 m, respectively. At coarser scales, artefacts from the Landsat processing are likely to be smoothed, as errors resulting from the Scan Line Corrector failure and undetected clouds are minimised (Figure 4.7). Furthermore, despite the high georeferencing accuracy of the datasets, errors from potential misalignment of the training imagery and Landsat data may be more prevalent at 30 m and averaged at coarser scales. For many regional-scale applications, land cover maps at 90 or 120 m may be sufficient, and an accuracy vs. precision trade-off might be appropriate. Maps at 120 m may be more accurate, but have less fidelity for detecting the clumps and canopies of dryland vegetation. This trade off may become more pertinent with the availability of 10-20 m imagery from Sentinel-2 (Bastin et al. 2017).

Overall, the accuracies achieved by the Landsat-based models are comparable to those of radar-based studies at similar scales. Urbazaev et al. (2015) achieved R^2 values of 0.71 and 0.66 using multiple and single season PALSAR images at 50 m resolution, respectively, whilst Naidoo et al. (2016) obtained R^2 of 0.8 and 0.81 using single-season PALSAR data at 105 m. Given our considerably larger study area, our results are promising for regional-scale analysis, as the spatial breadth, temporal depth, and rapid processing potential of the Landsat archive is unmatched by any radar system (Roy et al. 2014, Kennedy et al. 2014). Our metrics-based approach

outperforms the various single date Landsat scenarios across multiple seasons achieved by Naidoo et al. (2016) who reported R^2 values of 0.32-0.65 at 105 m resolution. There are clear benefits to quantifying seasonal variability using metrics, as demonstrated by the high ranking of standard deviation layers (Table 4.5). Furthermore, multi-seasonal metrics further improved results over multi-seasonal image combinations. We attributed this refinement to two factors: firstly, metrics are more resistant to bias incurred by rainfall and moisture variation; secondly, metrics such as standard deviation can represent the temporal profile of the land cover, imitating time-series approaches. This is in agreement with Müller et al. (2015), who found that annual metrics outperform best available pixel composites for tropical savannahs in Brazil.

Large-area mapping of savannah systems remains a challenge due to high heterogeneity and subjective biome classifications (Herold et al. 2008, Hüttich et al. 2011). Current approaches for regional-scale mapping generally focus on best-available pixel composites for classification (Frantz et al. 2017, Griffiths et al. 2013, White et al. 2014). Due to the high temporal variation in savannahs, this method is particularly vulnerable to bias effects caused by pixels being selected in different phenological stages (Hüttich et al. 2011, Müller et al. 2015). We demonstrate that Landsat-based spectral variability metrics offer a robust alternative for land cover mapping at large spatial scales, applicable to epochal or annual analyses. South Africa possesses good availability of Landsat imagery in the USGS archive, owing to the successful transfer of data from the Johannesburg receiving station, active since 1980 (Wulder et al. 2016). However, in many savannah regions, such as the Sahel and east Africa, the historical Landsat archive is sparse. By combining multiple years of observations, wall-to-wall mapping should be possible even with low annual image availability. Furthermore, segmenting a time-series into multiple temporal windows allows additional value to be extracted from a single series of observations, potentially compensating for a relatively limited archive. The high image acquisition rate of Landsat 8 relative to the historic Landsat archive, combined with comparable imagery from the Sentinel-2 satellites, will result in improved temporal resolution for optical imagery (Roy et al. 2014, Drusch et al. 2012). Increased observations should enable our multi-seasonal metrics approach to be expanded by using more or smaller temporal windows, for example the beginning or ending of the dry season. Evidence from MODIS-based studies suggests that this refinement may allow increased discrimination of subtle land covers, such as densely wooded savannahs, which are currently poorly mapped (Hüttich et al. 2009).

Landsat-PALSAR Fusion

Integrating the Landsat metrics with L-band PALSAR backscatter had divergent impacts. Finer-scale maps (30 to 90 m) were negatively affected by the inclusion of radar, with the Landsat-only models outperforming their fused counterparts (Figure 4.9). Comparably, the PALSAR-only models performed poorly, especially at fine-scales (Table 4.3). We attribute the detrimental effect of radar at fine resolutions to the high-level of noise in radar imagery at this scale, as illustrated in Figure 4.13. Errors caused by factors such as speckle, moisture content and geolocation accuracy are far more prevalent in finer-scale radar data. Therefore, at 30 to 90 m pixel scales, the PALSAR imagery contains a weak signal-to-noise ratio, incurring a negative impact on the regression model. Accordingly, SAR-fusion reduced class accuracy by 1% for area 20-60% coverage, at 30 m scales (Figure 4.12). Conversely, the coarse scale models (120 m) were consistently improved by the addition of PALSAR backscatter to the Landsat metrics, with the single-season combinations undergoing the greatest improvement. The lower improvements for the multi-seasonal scenarios indicates that some of the information contained in radar backscatter can be obtained from multi-seasonal metrics. The inclusion of L-band radar had the highest impact on sparse woody cover classes (0-30%). Within these classes, inclusion of the SAR variables increased balanced accuracies by 1-9% and 1-2%, at 120 and 30 m scales, respectively (Figure 4.12). Visual examination of the prediction subset maps indicates that this improvement is due to the SAR fusion correcting for overestimations when there is 0 - 20 % woody cover (e.g. the central pivot irrigation fields in Subset A of Figure 4.7). The high-ranking of radar variables by the RFE variable importance scores (Table 4.5), indicates that compared to individual Landsat metric layers PALSAR performs well. This may seem contradictory against the low accuracy of the radar only models. However, it is well documented that radar backscatter is a correlates strongly with woody cover, and the superiority of the Landsat models is most likely due to the large number of variables deployed. This affect is further amplified when multi-seasonal Landsat models are considered.

Multi-sensor fusion approaches are becoming more popular, due to an increase in the number of operational sensors and the open-access data policies. The improvements at coarse scales are in line with those found in other studies employing SAR and Landsat data together (Bucini et al. 2010, Naidoo et al. 2016). However, this study is the first to quantify the effect and mechanism of this fusion across multiple seasons and scales. The accuracies of our PALSAR-only models are lower than

other South African studies (e.g. (Naidoo et al. 2016, Urbazaev et al. 2015)). We attribute this to the following issues; firstly, our study area is larger and more heterogeneous, encompassing human modified landscapes, whereas the other two studies were confined to the Kruger National Park. Secondly, the source of training data could also have affected the accuracy of our PALSAR-based estimates: we employ aerial photographs while Naidoo et al. (2016) and Urbazaev et al. (2015) use characterisations that are more accurate from the field or from LiDAR sources (Naidoo et al. 2016). Finally, it should also be noted that our study used a mosaicked ALOS PALSAR layer produced from images acquired across a three month window (1st July - 3rd October), including two images acquired in the previous year. Seasonal effects, such as canopy density and moisture content, may prevent the mosaicked images from being artefact-free. Alternatively, the global-scale processing undertaken in the creation of the mosaicked PALSAR layer, such as speckle reduction and topographic normalisation, may reduce the fidelity of backscatter measurements when compared to scene-specific methods applied elsewhere (e.g.(Naidoo et al. 2016, Urbazaev et al. 2015)). Furthermore, multi-sensor fusion has a potential for image miss-registration errors between the imagery (Lehmann et al. 2015).

Although overall model accuracies are only moderately changed by the inclusion of L-band SAR data, the consistent allocation of improvements at low densities of woody cover may be highly relevant to semi-arid savannah case studies. The process of shrub encroachment into grasslands is a major threat to the livelihoods of many pastoralists in the developing world. For prevention and remediation to be successful, action must be taken as early as possible. The periodic monitoring of sparsely wooded savannahs, which are vulnerable to shrub encroachment, is therefore a pressing requirement. For this purpose, the fusion of PALSAR and Landsat imagery is beneficial, offering a higher likelihood of timely change detection than single-sensor approaches. In the coming years, fusion techniques based C-band radar from Sentinel-1 may offer good promise, owing to the 12 day revisit time.

Merit of variable reduction methods

To ascertain the value of variable reduction methods we applied a Recursive Feature Elimination (RFE) on out 92 variable dataset. The RFE produced the best preforming model at all scales, compared to all Landsat and Landsat-PALSAR fusion cases (Figure 4.11). In general, the number of variables used in the RFE models decreased with aggregation: we attribute the requirement of less variables at coarser
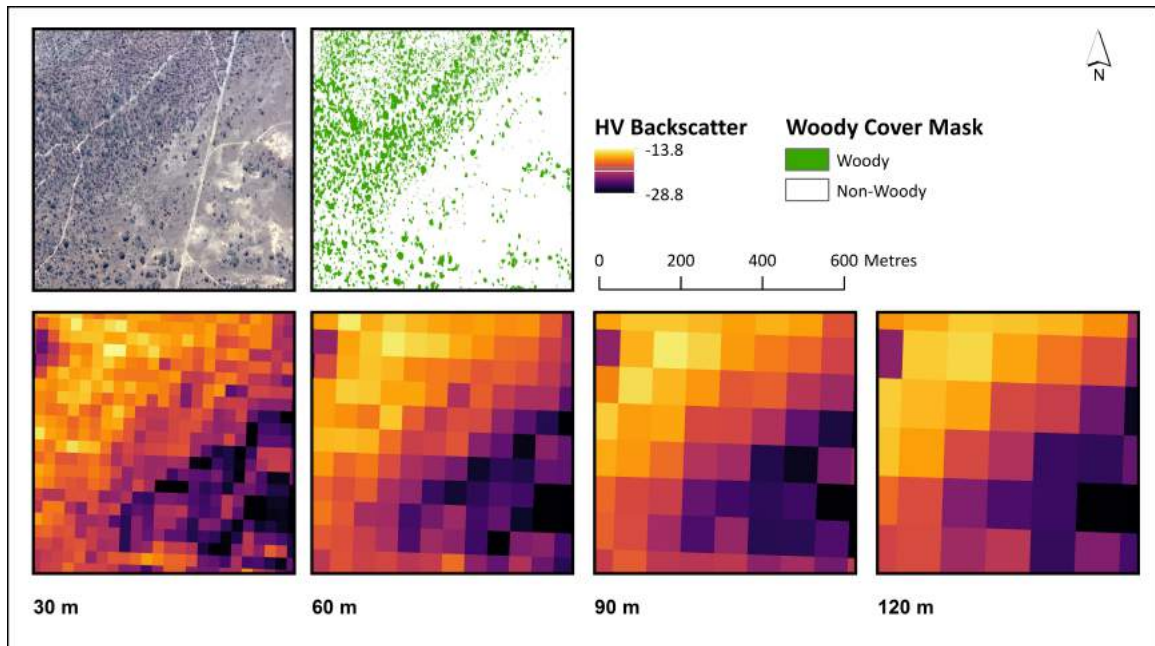
Figure 4.13: Subsets of HV polarized PALSAR backscatter across a grassland-shrub transition at different resolutions

resolutions due to improvements in signal-to-noise ratios as noisier layers are smoothed. Dimension reduction methods are also useful for highlighting the type of variables that contain useful information for the model building. The high ranking of standard deviation - a proxy for seasonal variability highlights the importance of temporal information for woody cover mapping.

As both the number of active sensors and the availability of open data archives increase, remote sensing analyses are using high-dimensional datasets. The utility of variable selection or dimension reduction methods will inevitably increase in order to deal with the increasing data volume. Currently, these tools are primarily used in hyperspectral analyses, but are underutilised in other areas (Pal and Foody 2010). The fact that the RFE was able to automate the process of selecting a superior model highlights the potential of automating model construction using machine learning methods that may currently be underused (Meyer et al. 2016). At large-scales, mapping land cover with fewer variables can drastically reduce processing time, leaving unnecessary variables out can therefore be useful for computing and statistical purposes.

4.7 Conclusions

We tested the potential of Landsat-derived spectral variability metrics and PALSAR composites for mapping woody coverage, in southern African savannahs. We compared the role of seasonal compositing period, and the effect of multi-sensor fusion through the addition of ALOS PALSAR backscatter to the Landsat layers. Furthermore, we investigated the role of pixel scale on map accuracy, and the potential of variable selection methods for automating the model building process.

We draw a number of conclusions from our modelling scenarios. Firstly, Landsat metrics can produce highly accurate maps of fractional cover in savannahs, with dry season imagery being the preferred temporal window. Further improvements can be made by combining multi-seasonal metrics, derived from two contrasting seasons. In particular, integrating dry and wet season layers produced good improvements in map accuracy. Secondly, the fusion of Landsat and PALSAR layers is not always beneficial. At fine scales (30-60 m), L-band SAR integration reduced model performance consistently, potentially due to the high level of noise inherent to radar data, particularly in savannahs. Conversely, at the 120 m scale, the addition of PALSAR was beneficial, particularly for areas with less than 30% coverage, and for some models at 90 m scales as well. Finally, the use of a recursive feature elimination automated variable selection process was very efficient in constructing an accurate parsimonious model, producing the most effective model at every scale examined whilst reducing the number of variables used to of 57 out of 90.

In summary, Landsat metrics offer a suitable option for regional-scale mapping of savannah woody cover, and should allow decadal scale analysis of land cover changes. The use of multi-seasonal composites are particularly promising for accurate fractional woody cover mapping. For contemporary monitoring, the fusion of Landsat metrics with L-band radar is recommended for areas with lower woody cover densities, and particularly for the rapid detection of shrub encroachment into grass-dominated savannahs. Future studies will benefit from automated variable reduction approaches and the increased image acquisition rates from the Sentinel constellation, which feature both radar (C-Band) and optical satellites.

Chapter 5

Carbon Fertilisation is the Primary Driver of Shrub Enchroachment in South African Savannahs

5.1   Introduction

Savannahs and grasslands throughout the world are experiencing an increase in the coverage and density of woody plants, relative to historical levels (Stevens et al. 2017). The rate and nature of this change varies over spatial and temporal scales, and has resulted in a range of ecosystem conversions (Naito and Cairns 2011). In many grasslands, indigenous shrubs have increased in densities sufficient to initiate conversion to shrubland, particularly in North America (Van Auken 2009). Concurrently, the occurrence and size of trees within savannah systems has risen, especially in Africa and South America (O'Connor et al. 2014, Naito and Cairns 2011). While in humid-savannah, many forest boundaries are expanding (Cuni-Sanchez et al. 2016). Regardless of the process by which woody encroachment occurs, many ecosystem function properties are altered, making it a major, yet poorly understood, global change mechanism (Eldridge et al. 2011, Ward 2005). Woody encroachment is also more than a purely environmental concern: reductions in grass biomass are highly detrimental to pastoralists who depend on rangelands for their livelihoods (Anadón et al. 2014). Savannah systems are predicted to be hotspots of global change in the coming decades, with increasing variation in both rainfall and temperature (Diffenbaugh and Giorgi 2012). In addition, African savannahs are projected to host a rapidly growing, human population (Bradshaw and Brook 2014). Understanding the drivers of ecosystem change in these systems is, therefore, a pressing social and environmental concern.

The traditional ecological narrative dictates that shrub encroachment is a localised phenomenon, resulting from poor land management regimes (Scholes and Archer 1997, Archer 1994). The most frequently proposed mechanisms are overgrazing and suppression of fire, both of which are common management techniques in rangelands. Herbivory reduces grassy biomass, increasing the competitiveness of woody plants through water, light, and space availability, whilst simultaneously reducing fuel-loads for potential fires (Roques et al. 2001, Sankaran et al. 2008). Reductions in fire frequency prevent the destruction of saplings and small shrubs, allowing them to reach maturity and sizes sufficient to survive fire events (Bond and Keeley 2005). Field studies comparing grazed and ungrazed plots have frequently observed higher rates of woody encroachment in the presence of herbivory. While, in intensely stocked commercial areas woody plants will often be removed to facilitate the creation of grazing lawns, reducing woody coverage.

More recently, increased focus has been directed at the role of global factors in woody cover dynamics. As savannah woody cover is constrained by both total and wet season rainfall (Good and Caylor 2011, Sankaran et al. 2005), changes in precipitation regime have been proposed as drivers of shrub encroachment. This theory has been supported by small-scale field experiments showing shrubs disproportionally benefiting from increases in rainfall frequency, amount, and variability (Gherardi and Sala 2015, Ward 2005). Yet there is little consensus over what effect, if any, rainfall variation has on large-scale woody cover changes. Furthermore, shrub encroachment is a near-global phenomenon, and rainfall changes are predominantly regional and exhibit little intra-regional consistency.

A further potential global factor is the ongoing rise in atmospheric CO_2 concentrations since the industrial revolution. The efficiency of plants in converting CO_2 to biomass is governed by Water Use Efficiency (WUE). As CO_2 concentrations rise, stomartal conductance is lowered facilitating greater primary production at lower levels of water availability, theoretically aiding woody plants in rainfall limited systems. Chamber experiments have demonstrated that increasing CO_2 concentrations from pre-industrial to contemporary and higher levels resulted in a 300% increase in stem biomass and below-ground starch reserves for African savannah woody species (Kgope et al. 2010). Furthermore, the potential and speed of regrowth following fire events increased. Quantifying the role of CO_2 in the field is difficult due to the absence of Free-Air Concentration Enrichment (FACE) experiments in savannahs. However, a theoretical understanding of water limitations

to woody cover in savannahs makes it reasonable to assume that CO_2-driven increases would be concentrated in water limited environments (Stevens et al. 2016, Sankaran et al. 2005). This has been observed across South Africa using aerial photography and globally using satellite-derived Rain Use Efficiency (RUE) (Stevens et al. 2016, Buitenwerf et al. 2012, Donohue et al. 2013).

Unravelling the cause of woody encroachment is complicated by the potential for field studies to lack regional representativeness. An alternative approach is aerial imagery or EO data. In this study, we combine satellite-derived woody cover maps with an ensemble of predictive variables in a spatial modelling framework question the validity of the candidate theories. Specifically, we aim to conduct a holistic analysis enabling regional-scale inference on the drivers of woody encroachment for South African savannahs.

5.2   Study Area

The study area consists of the Limpopo and North West Provinces in northern South Africa. These municipalities cover a plurality of the savannah biome within South Africa (193,200 km^2, 49% of the total savannah area), in addition to containing 33,830 km^2 of grassland (Mucina et al. 2006). There is an increasing west-east rainfall gradient, with Mean Annual Precipitation (MAP) rising from 300mm/year in the west to a maximum of 1500 mm/year in the Drakensberg Escarpment in the east (Scholes et al. 2001). The majority of rainfall occurs in the October-March rainy season. Overall, annual rainfall levels are low considering savannahs globally. Mean annual temperatures are generally between 21-23°C, with winters being mild and frost-free (Scholes et al. 2001). The study area is covered by a heterogeneous woody cover layer, consisting of shrubs and isolated trees that rarely reach canopy closure (Mucina et al. 2006). To further refine the study area, we used the 30 m Landsat-derived, South African National Land-Cover -2014 map to exclude extensively modified areas, including urban, mine, and intensive cropland or plantation related classes

5.3 Methods

Woody Cover Change Mapping

Woody cover changes were mapped using Landsat-derived woody cover layers, based on the methodology developed in Higginbottom et al. (2018). In summary, two five-year epochs (1984-1988 and 2008-2012) of Landsat imagery were used to generate pixel-level seasonal spectral variability metrics, at 120 m resolution. Reducing the pixel resolutions improves the classification accuracies, and is more suited for observing overall trends. High-resolution imagery were classified into woody/non woody masks, and used as training data for a Random Forest regression for the fractional cover of each 120 m pixel. The Random Forest model was applied to the Landsat metric stacks to generate the two epochal maps. We then calculated both the absolute percentage change, and the relative percentage change in woody cover between the two maps using the following equations:

$$AbsoluteChange = WoodyCover_{2010} - WoodyCover_{1986} \qquad (5.1)$$

$$RelativeChange = \frac{WoodyCover_{2010} - WoodyCover_{1986}}{WoodyCover_{1986}} \times 100 \qquad (5.2)$$

where the subscript year is the central point of the classification temporal window.

Statistical Analysis

Generalised Additive Models

Our modelling framework was developed using Generalised Additive Models (GAM). As *generalised* models, GAMs incorporate the dependent variable (y) using a link function ($g(.)$) to a distribution family, establishing the expected mean (μ) and variance (σ^2), e.g. the Gaussian (normal) distribution ($\mathcal{N}(\mu, \sigma^2)$). As *additive* models, linear covariant coefficients (βx) may be replaced with smoother functions ($f(x)$), allowing for non-linear responses enabling the data to 'speak for itself' (Wood 2006). GAMs can therefore be expressed as:

$$g(\mu) = \beta_0 + f(x_1) + f(x_2)...f(x_p) \qquad (5.3)$$

where:

$$\mu \equiv \mathbb{E}(y_i) \qquad (5.4)$$

and:

$$y \sim \mathcal{N}(\mu, \sigma^2) \qquad (5.5)$$

Models were constructed using the *mgcv* package within the R statistical environment (R Core Team 2015*b*). Thin plate splines were used as smoothers, and were estimated using Residual Maximum Likelihood (REML) (Wood 2003, 2011).

Theoretical Framework

We collated a series of 11 variables that have a hypothetical basis for explaining woody cover changes (Table 5.1) . These variables can be grouped into three categories: rainfall-derived, human, and natural factors. The rainfall variables were calculated using the TAMSAT database, grazing data was extracted from the FAO global livestock layers, population density was acquired from the Global Human Settlement Layers, soil data came from the International Soil Reference and Information Centre's (ISRIC) soil grid dataset.

Based on the underlying explanatory theories for woody encroachment, it is possible to develop a series of expected responses that would support each hypothesis. Accordingly, we examined our modelling results based on the following *a priori* hypotheses:

- The *Land Use* theory holds that grazing and human pressures alter the grass-shrub equilibrium, leading to an increase in woody cover. This would be confirmed by a strong positive effect from population and grazing density

- The *Rainfall Variation* hypothesis states that increases in the amount and variability of rainfall lead to a preferential environment for woody plants, this would be supported by a strong positive effect at high levels of rainfall (annual and wet season) and increasing trends

- The *Carbon Fertilisation* argument postulates that increasing atmospheric CO_2 concentrations allow woody plants to be more productive at lower levels of rainfall (i.e improved Water Use Efficiency) than the previously. Under this theory, increases would be expected in areas of low woody cover (<60%) and which are rainfall limited (<650 mm/year).

92

Type	Variable	Source
Rainfall	Mean Annual Precipitation Mean Wet Season Precipitation Mean Annual Rainy Days Mean Wet Season Rainy Days Mean Annual Rainy Days Trend Mean Wet Season Precipitation Trend	TAMSAT
Anthropogenic	Livestock Density Population Density	FAO
Environmental	Sand Content Initial Woody Cover	ISRIC Soil Grids This Study

Table 5.1: Explanatory variables that may influence woody cover encroachment

5.4   Results and Discussion

The mean woody cover change across our study area was a gain of 1 percentage point (standard deviation: 14%) or a relative change gain of 28% (standard deviation: 16%). Both measures showed a slight rightwards skew, with woody cover increases more prevalent than decreases. The woody cover maps have an overall accuracy of 65%. This must be considered, as the errors within these map propagate into the statistical analysis. However, the largest prediction errors are in the tails, mainly at higher values, with the more typical values of 0-30% woody cover having smaller residuals and greater accuracy. Errors of this magnitude in individual maps would be greatly problematic for inferring land cover change using a *categorical* land cover map.

To quantify the drivers of woody cover change of both increases and decreases, we analysed the absolute and relative rates of change (Figure 5.1) against a suite of explanatory variables. This statistical framework allowed multiple hypotheses to be interrogated. Accordingly, the three predominant explanations for woody cover change could be analysed at once. These theories are: 1) carbon fertilisation; 2) rainfall trends and variability; and 3) land-use management. The fitted models had R^2 values of 0.39 for absolute change and 0.41 for relative change. The model-derived variable response curves are shown in Figures 5.2 and 5.3.
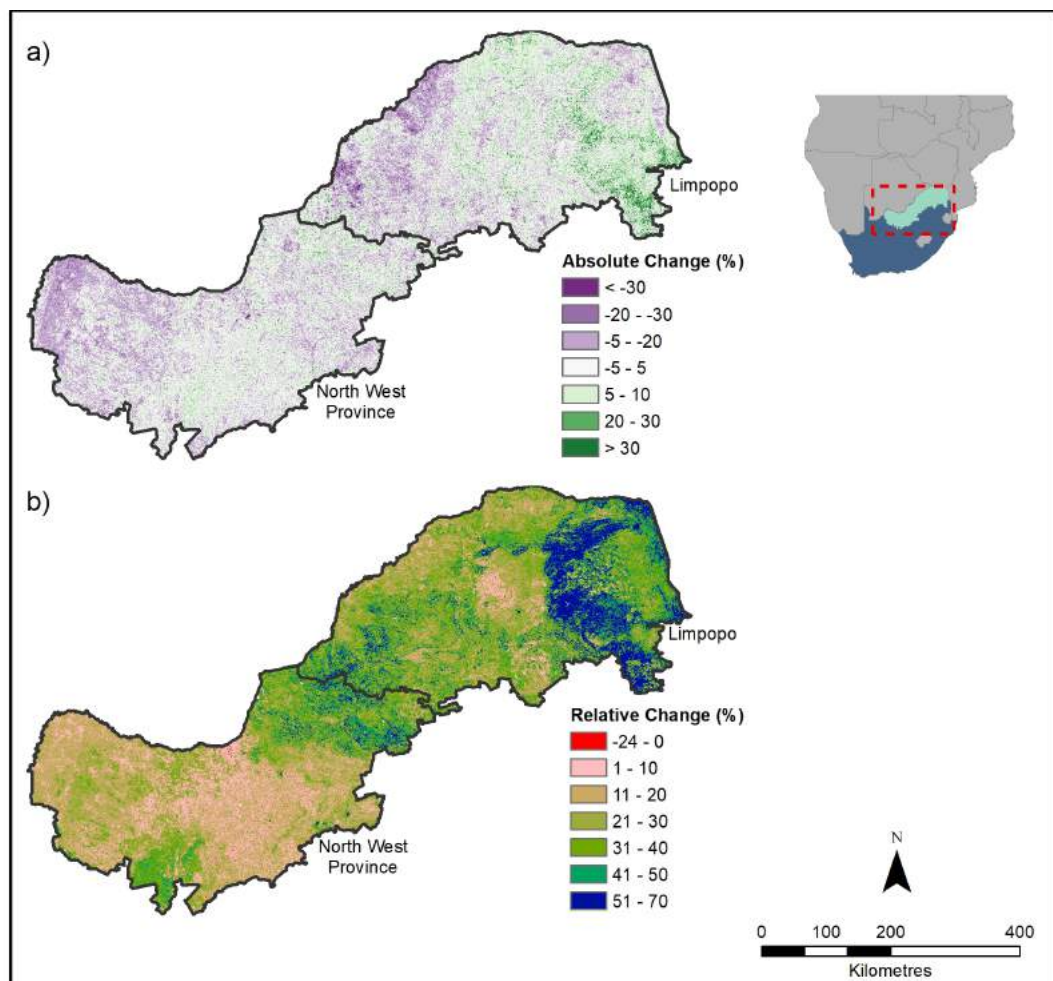
Figure 5.1: a) Absolute woody cover change from 1986-2010. b) Relative woody cover change. Inset shows the study area within sub-Saharan Africa.
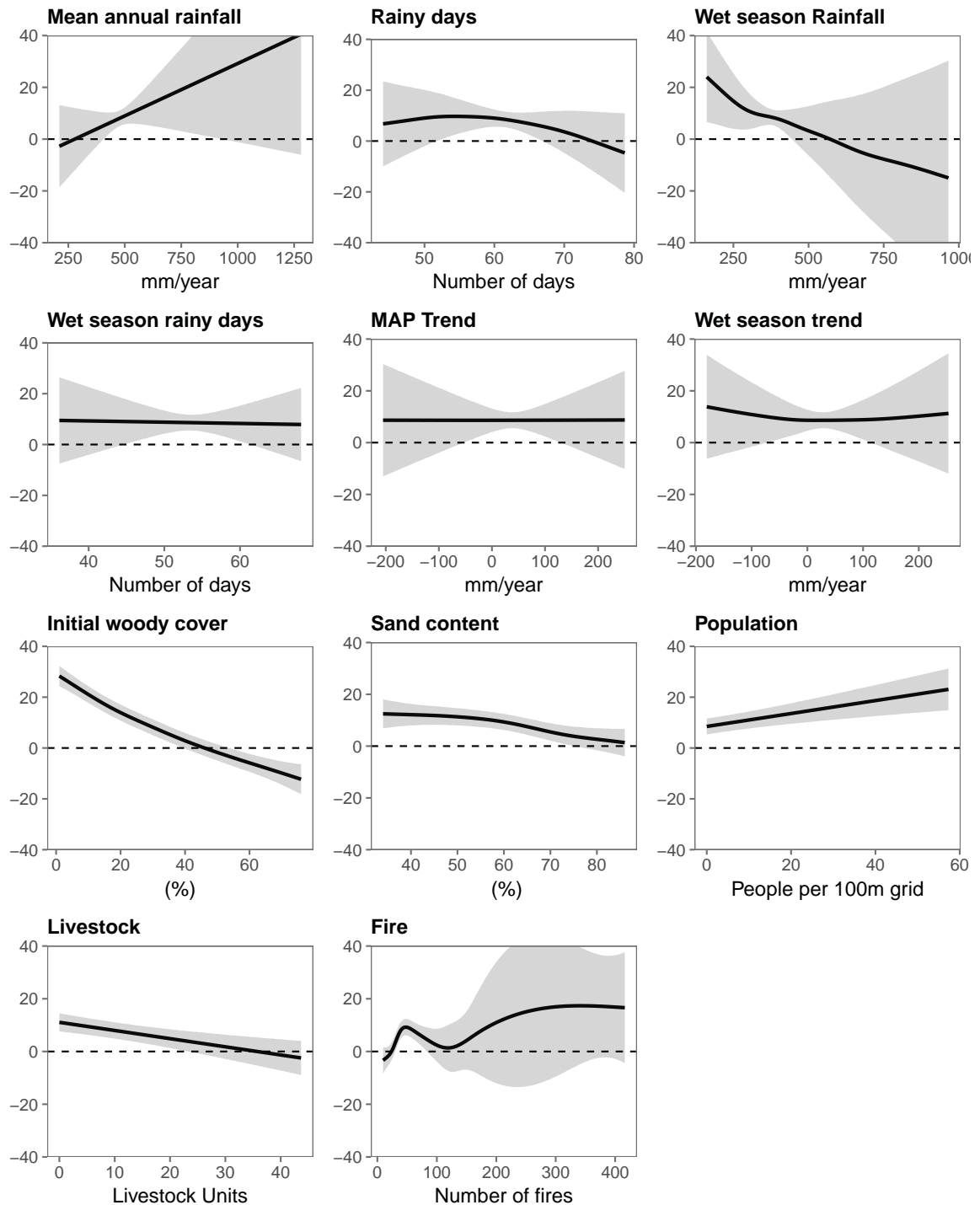
Figure 5.2: Smooth variable functions for absolute woody cover change derived from the GAM
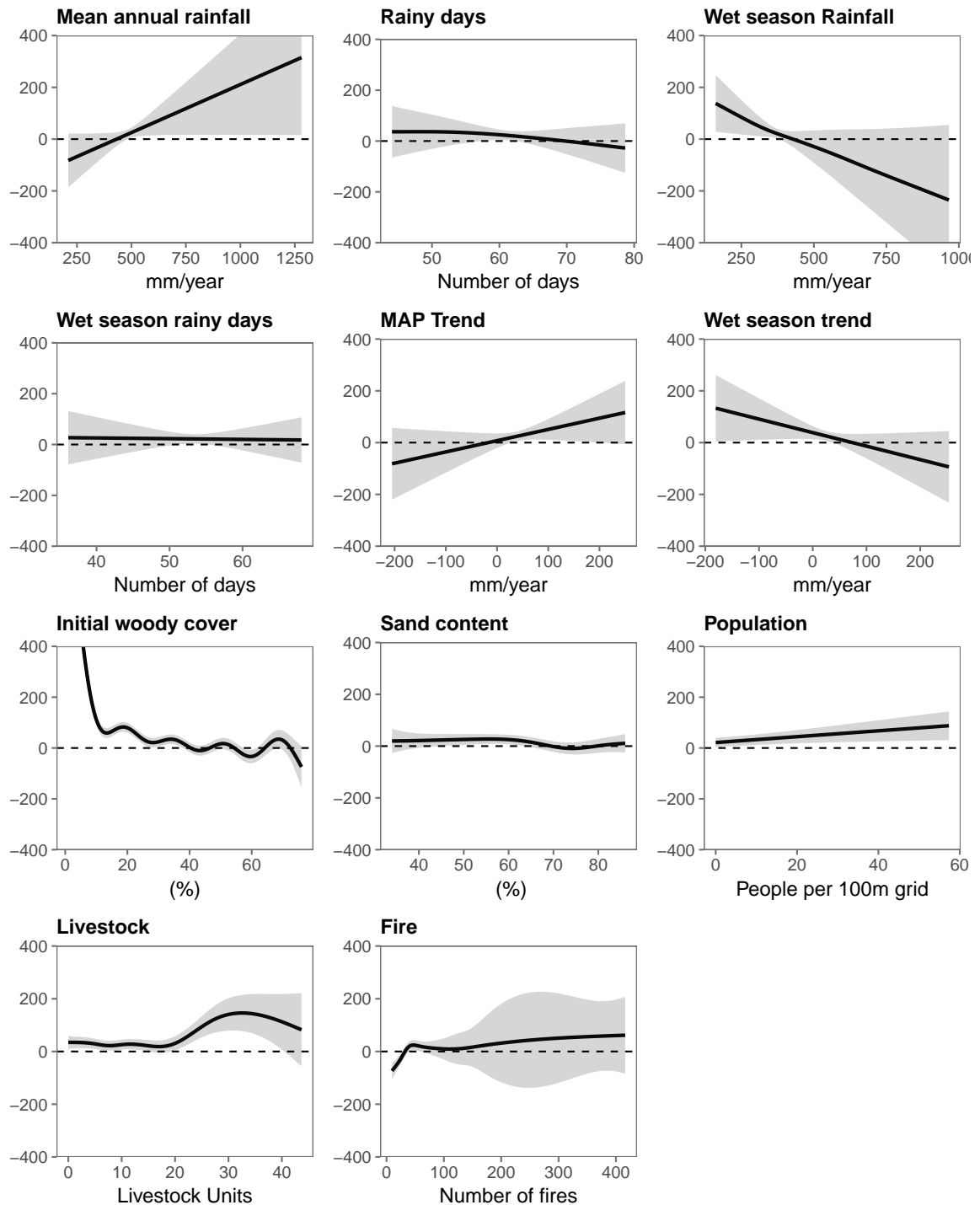
Figure 5.3: Smooth variable functions for relative woody cover change derived from the GAM

Poor land-use management and high grazing densities have long been casti-gated as drivers of shrub encroachment (Archer 1994). This argument originates in the two-layer savannah model of Walter (1939); who theorised that grazing re-moves the grass layer of the savannah, allowing the competing tree layer access to increased moisture- thus facilitating *en masse* recruitment. Support for this the-ory comes from a range of case studies where shrub encroachment was identi-fied on heavily grazed rangelands, particularly in North America and Africa. How-ever, this reflects both a classic case of confusing correlation and causation, and of site selection bias. The existence of encroachment on grazed lands does not affirm a causal driver, particularly when many non-grazed areas also demonstrate increasing woody cover. Furthermore, a disproportionate number of studies have been conducted at a limited number of sites: particularly, the Jornada Experimen-tal Range in New Mexico and the Kruger National Park in South Africa (Laliberte et al. 2004, O'Connor et al. 2014). The Kruger National Park is notably and unrepre-sentative choice due to an extreme juxtaposition of heavily grazed communal land and protected semi-natural savannah (Wessels et al. 2007). This contrast reflects extremes of land-use intensity in southern Africa and is not a typical contrast.

Our analysis revealed a limited effect of livestock density. Relative change rates were unaffected, until densities of 20 LSU per pixel were reached after which a positive trend emerged. This is a high stocking density, which is not typical for ei-ther South Africa or the wider southern Africa. For absolute change, a slight, near-linear, negative relationship was identified; woody cover change was predicted to decrease from around 15% to -2% as livestock density increased from 0 to 40 units per tile. That increasing livestock would reduce encroachment rates may seem counter intuitive when set against the prevailing literature of grazing-facilitated en-croachment. However, this is most likely due to the most intensively grazed areas (i.e intensive commercial grazing lawns) being completely cleared of woody plants, inducing a negative trend at high values. Otherwise, livestock densities appear to have a minor effect on woody cover increases, which is an interesting finding when compared to the number of studies that have identified grazing as a primary driver. This omission of an affect may be influenced by the coarse resolution of the live-stock data (0.5°); however, as this is the only consistent regional-scale data avail-able, it remains the most appropriate source. The availability of high-resolution land-use data, including grazing type and density, would be of benefit for future studies.

Carbon fertilisation-driven shrub encroachment would, theoretically, improve the Water Use Efficiency (WUE) of woody plants, increasing woody cover by improving root development and seedling survival rates (Bond and Keeley 2005, Stevens et al. 2016). Therefore, cover increases would be concentrated in water-limited areas, which receive $\lesssim$ 600-650 mm/year in African savannahs (Sankaran et al. 2005). Neither of our models predicted this pattern when using MAP. However, high rates of increasing cover were identified for areas with low mean *wet season* rainfall. Given the correlation between the wet season and mean annual precipitation totals, this may imply a stronger affect of seasonal rainfall patterns. As woody plants in savannahs have evolved to maximise growth during the seasonally limited growth season, our results would be consistent with proposed ecological mechanisms of increased WUE under elevated CO_2. The variable affect with the tightest confidence interval, for both models, was the initial woody cover, with increases more prominent at proportions below 40%. Low cover areas typically occur in low rainfall areas, so some variable duplication is expected. However, the strength and direction of the modelled trend is further support for the elevated CO_2 theory. These findings are in agreement with a number of studies that have linked a carbon fertilisation mechanism with shrub encroachment based on Earth-observation (Donohue et al. 2013), aerial photography (Stevens et al. 2016), and field surveys (Bond and Midgley 2012).

Savannah woody cover is determined by both annual and wet season precipitation (Sankaran et al. 2008, 2005, Good and Caylor 2011). It is, therefore, plausible that changes in rainfall dynamics may incur a shift in woody cover levels (Gherardi and Sala 2015). For absolute change, trends in rainfall were an insignificant variable for the models. For relative change, MAP and wet season rainfall had divergent effects, with *increasing* MAP predicting woody cover increases, whilst *declining* wet season rainfall also having a positive affect. However, the model considered these variables to be weak predictors. This was expected, as there have been only minor trends in rainfall for South Africa over the 1960-2010 period (MacKellar et al. 2014). Further work on the interactions between rainfall dynamics and woody cover is advised; a simple linear trend in rainfall total, as used here, is not a sophisticated enough method for quantifying changes in rainfall regime and does not account for potentially relevant factors, such as the frequency, intensity and regularity of precipitation events. Furthermore, this is one regional case study; pan-dryland or global studies may be more successful in comparing divergent changes in rainfall regime.

5.5 Conclusion

The phenomena of woody plant encroachment have been documented for savannahs and grasslands in nearly all continents (Stevens et al. 2017). Yet the drivers of this process remain unclear, with a range of local and global factors postulated (Stevens et al. 2016, Archer 1994, O'Connor et al. 2014). Here, we combine satellite-derived woody cover maps with a suite of potentially explanatory variables, to elucidate on the potential drivers and mechanisms of woody cover change, in South African savannahs. The change maps derived from the 1986 and 2010 woody cover classifications are shown in Figure 5.1.

In this study, we aimed to test three competing hypotheses on the drivers of woody encroachment for South African savannahs. The modelled variables most closely matched the *a priori* responses of the carbon fertilisation hypothesis. In recent years, this explanation has been postulated by studies using a variety of methods to account for the observed woody encroachment. Further work in this arena is still necessary, particularly where the data sources are sub-optimal. Land-use history and rainfall dynamics are especially difficult to quantify and would require further investigation. Furthermore, additional factors, such as reactive nitrogen deposition and mega-fauna extinctions, are likely to be relevent but where not included in our models. If Carbon fertilisation is the key driver of shrub encroachment in savannahs, it would raise concerns for future environmental change: as CO_2 levels continue to rise more savannahs and grassland are likely to experience an increase in woody cover levels, which has been linked to savannah land degradation.

Chapter 6

Pervasive greening of African Savannahs from 1982 - 2016

6.1   Introduction

Trends in vegetation greenness, measured using the Normalised Difference Vegetation Index (NDVI), are one of the most ubiquitous tools for inferring ecological change at large spatial scales. The NDVI has long been a favoured metric, owing to its simple calculation, correlation with various ecological attributes, and transferability between sensors (Brown et al. 2006, Pettorelli 2013). In particular, the Advanced Very High Resolution Radiometer (AVHRR) - derived Global Inventory Monitoring and Modelling System (GIMMS) dataset has been used extensively for environmental change purposes (Higginbottom and Symeonakis 2014). Compared to other data records, such as the Landsat collections, AVHRR-derived datasets may appear somewhat basic; with broad spectral channels, coarse resolution pixels, and limited options for atmospheric correction (Cracknell 2001). However, for regional to continental scale studies, AVHRR offers unparalleled temporal and spatial coverage, providing a globally consistent record since 1981.

The regions most studied using GIMMS-NDVI data are the drylands of Africa. These areas are particularly well suited for this form of analysis, due to the limited historical coverage of other Earth-observation archives in the region, with the exception of South Africa (Wulder et al. 2016). Furthermore, NDVI becomes less sensitive to vegetation in dense canopies (NDVI > 0.7), but is relatively responsive to the low biomass levels found in savannahs and grasslands (Eisfelder et al. 2012, Prince and Tucker 1986). Accordingly, a considerable amount of earlier work on the use of NDVI for monitoring environmental change focussed on the Sahel region .

In the 1970s and 1980s, the Sahel experienced one of the most prolonged and intense droughts of the 20th century, with annual rainfall decreasing by 50% (Nicholson 2000, Hulme 2001). The ecological changes caused by this drought fuelled a narrative of anthropogenic-driven desertification, focussed on the southwards expansion of the Sahara desert as a consequence of poor land management (Charney 1975). When the dry period began to abate, satellite observations of vegetation greening provided regional-scale evidence of the close coupling between climate and vegetation; refuting the anthropogenic desertification theory (Nicholson et al. 1998, Tucker et al. 1991). AVHRR-based NDVI estimates revealed that greening occurred through two distinct mechanisms: an increase in the seasonal maximum NDVI, and an expansion of the growing season (Heumann et al. 2007, Herrmann et al. 2005). Further regional-scale analysis highlighted the influence of climatic oscillations, such as El Niño Southern Oscillation (ENSO) and the Pacific Decadal Oscillation (PDO) on African vegetation (Brown et al. 2010). On a more local scale, NDVI trends have shown changes in cropland and increases in woody cover (Brandt et al. 2015, Brandt, Verger, Diouf, Baret and Samimi 2014).

The most common statistical method for detecting change is linear regression against time, using either seasonally or annually summed NDVI (Herrmann et al. 2005). However, linear regression has a number of assumptions, such as the inputs being independent on the y-axis and conforming to a normal distribution, that are rarely fulfilled by an NDVI time-series (De Beurs and Henebry 2005, Wessels et al. 2012). Alternatively, the use of non-parametric approaches has been proposed, such as the Mann-Kendall and Theil Sen regressions (Higginbottom and Symeonakis 2014). These techniques have fewer assumptions than parametric models, and are more suited for noisy time-series (Theil 1992, Sen 1968, Kendall 1938). All of these operations result in a monotonic trend co-efficient, indicating the modelled change over time, which when positive (i.e. an increase over time), indicates vegetation *greening*, and when negative, purports *browning* (de Jong, de Bruin, de Wit, Schaepman and Dent 2011). However, reducing a 30-year plus time series to a single trend is often overly simplistic, as the direction of change may reverse multiple times within this period (de Jong et al. 2012, Verbesselt, Hyndman, Newnham and Culvenor 2010). Detecting breakpoints in time-series requires more complex models, with a variety of techniques capable of determining when a change has occurred (Forkel et al. 2013). However, quantifying the change points in vegetation dynamics can be informative of both human and anthropogenic drivers, providing a

more insightful picture of ecological function and changes that are occurring (Horion et al. 2016).

Long time-series can be analysed in various ways, Fensholt et al. (2012) compared monotonic NDVI trends for global drylands against potential climatic constraints, to critique land degradation claims. Similarly, De Jong, Schaepman, Furrer, Bruin and Verburg (2013) modelled changes in NDVI and climatic variables, highlighting that although climate (especially precipitation) could explain a large proportion of NDVI change, large areas of browning in Africa were not attributable to it. Fensholt et al. (2015) compared NDVI trends calculated using two different aggregation methods (annual mean and growth season sum), with divergences indicating land-cover changes, such as shrub encroachment in southern Africa. Using a Breaks For Additive Season and Trend (BFAST) breakpoint analysis, Horion et al. (2016) were able to map the vegetation changes resulting from the collapse of the Soviet Union and associated agricultural abandonment in central Asia. At finer scales, the combination of Landsat imagery with breakpoint methods, especially LandTrendR (Landsat-based detection of Trends in Disturbance and Recovery) and CCDC (Continuous Change Detection and Classification), has been highly effective for forest monitoring (Kennedy et al. 2010, Zhu et al. 2012).

This study investigates the NDVI dynamics of African savannahs using a variety of time-series analysis techniques and NDVI-derived metrics. The overarching aim is to understand how vegetation dynamics have occurred and evolved during the 1982-2016 period and the ecological implications of these changes. Towards this aim, we generate two NDVI time-series from the GIMMS dataset: the annual maximum and aggregate sum values, hereafter $NDVI_{max}$ and $NDVI_{sum}$, respectively . These series are used as inputs into monotonic linear and breakpoint regression models. The slopes and any associated breakpoints of these models are classified and examined as indicators of large-scale ecological change.

6.2 Data and Methods

GIMMS 3g NDVI

We used the GIMMS 3g NDVI dataset, derived from the AVHRR sensors carried onboard the seven National Oceanic and Atmospheric Administration satellites since June 1981. NDVI is calculated using the standard equation:

$$NDVI = \frac{(\rho NIR - \rho Red)}{(\rho NIR + \rho Red)} \qquad (6.1)$$

where, ρNIR is reflectance in the near infra-red range, and ρRed is reflectance in the visible red part of the electromagnetic spectrum.

The GIMMS dataset is generated from AVHRR imagery. The raw daily 1 km pixels are binned into optimum 15-day, 8 km composites. The pre-processing routines include empirical mode decomposition and Bayesian methods, to remove non-vegetation related artefacts, such as orbital drift, solar zenith angle effects, and sensor transitions. A radiative transfer model is used to correct for the volcanic aerosol loading caused by El Chichón and Mount Pinatubo eruptions (Pinzon and Tucker 2014)

We further processed the GIMMS data to maximum monthly composites and discarded the months for the incomplete 1981 year, resulting in a 34-year (408 months) time-series. When gaps remained after compositing, values were estimated by linear interpolation across months. Our analysis focus was on savannahs, therefore we masked out areas that are likely to be dominated by forests or marginal vegetation. This was achieved by calculating the median NDVI using the monthly time-series, and discarded pixels with a value of less than 0.15 or greater than 0.8 from further analysis. This removed areas with very low vegetation cover (e.g the Sahara and Namib deserts) and dense forests (e.g. the Congo and Guinean forests).

The monthly time-series was aggregated into two annual metrics: $NDVI_{max}$ and $NDVI_{sum}$. This resulted in two 34-year annual time series, to be used as inputs for the trend analyses.

Trend Analyses

A standard linear regression is expressed as:

$$y_i = x_i^\top \beta + u_i \qquad (6.2)$$

where at time i, the dependent variable (y) is estimated based on the predictor variable(s) (x) and the associated co-efficient (β), plus an error term u (i.e. the residual). In our case, NDVI is modelled as a function of time, with the co-efficient quantifying the change. This model assumes that the co-efficient remains constant. To incorporate the potential for one or more change in the co-efficient, Equation 6.2 can be modified as follows:

$$y_i = x_i^\top \beta_j + u_i \qquad (i = i_{j-1} + 1, ...,, i_j, \quad j = 1, ..., m+1) \qquad (6.3)$$

where, the j parameter indicates a segment index, and $I_{m,n} = i_1...i_m$ is a series of breakpoints, thus allowing a different co-efficient to be applied to the predictor variable at different periods. Breakpoints are determined first by an ordinary-least squares moving sum (MOSUM) test. When breaks are detected, the number is estimated by the Bayesian Information Criterion (BIC), and timings are set based on the residual sum of squares (RSS). For a full mathematical overview of the stages in this procedure, see Zeileis et al. (2003), Bai and Perron (2003) and Mann (1945). For details on the application to NDVI time-series see Forkel et al. (2013).

We applied these models on both annual NDVI time-series. Firstly, a standard linear model was implemented with no breaks quantified. Secondly, a model allowing for two structural changes was applied. All analysis was conducted in the R statistical environment (R Core Team 2017). The *raster* and *rgdal* packages provided data handling functionality (Bivand et al. 2018, Hijmans et al. 2015). The GIMMS data were downloaded and processed using the *gimms* package (Detsch 2018). Finally, trends were calculated in the *greenbrown* package (Forkel et al. 2013).

Trend Classification

The slopes resulting from the linear models were grouped into three categories: greening, no change, or browning, after removing pixels with insignificant trends. By comparing the trend classifications from the NDVI$_{max}$ and NDVI$_{sum}$ models, six combinations are possible.

To classify the breakpoint outputs the following procedures were applied. Firstly, all segments with a length less than seven years or resulting from an insignificant break were discounted. This was to ensure that the analysis was focused on long-term trends, and not influenced by short-term shocks, such as drought years, which may induce fleeting breaks. Secondly, the remaining components were classified into greening, browning or no change based on the slope value. Finally, as two breaks were allowed, a maximum of three segments is possible, these classes were conditionally grouped into six categories as follows:

1. Only Greening: pixels where only greening and no-change trends occurred (e.g. Gr-Gr-Gr, Gr-Nc-Nc, Nc-Gr-Nc)

2. Only Browning: pixels where only browning and no-change trends occurred (e.g. Br-Br-Br, Br-Nc-Nc, Nc-Br-Nc)

3. Greening to Browning: pixels where a greening trends was followed by a browning trends (e.g. Gr-Br-Nc, Gr-Nc-Br, Gr-Gr-Br)

4. Browning to Greening: pixels where a browning trends was followed by a greening trends (e.g. Br-Gr-Nc, Br-Nc-Gr, Br-Br-Gr)

5. Multiple Changes: pixels featuring more than one shift from the different change trends (e.g. Br-Gr-Br, Gr-Br-Gr)

6. No Trends: pixels with no directional trend component

6.3   Results

Linear Trend

Changes in NDVI, modelled by linear trends in the annual maximum and sum values, are shown in Figure 6.1. Both metrics show that the dominant trajectory across the study area is of increasing NDVI and greening. Greening pixels comprised 75% of the $NDVI_{sum}$ slopes, and 80% of the $NDVI_{max}$, whereas browning was identified in 25% and 20% of pixels, respectively. Removing trends that did not meet a $P < 0.05$ significance threshold eliminated some of these pixels. Proportionally, more browning was masked for both metrics than greening (Figure 6.3a-b). Pronounced increases in NDVI were observed in the Sahel and southern Africa. Browning was concentrated in east Africa, Angola, Zambia, and Mozambique, with dispersed and isolated patches in the northern Sahel. Non-trending areas, displaying no change, were found in the west of South Africa and in Namibia and sparingly in Western Africa.

Differences between the trend layers, after aggregation into three categories (greening, browning, and no-change), are shown in Figure 6.2. There is a broad agreement between trends, with 68% of pixels showing the same direction or no change at a $P < 0.05$ threshold (Figure 6.3c). However, areas of divergence do occur, whilst changes from no-change to a change category are considerably more common that trend direction reversals (Figure 6.3.c). The main areas of divergence are dispersed across the Sahel and South Africa ($NDVI_{max}$: no change and $NDVI_{sum}$:

Greening), Angola, Zambia, and Mozambique (NDVI$_{max}$: no change and NDVI$_{sum}$: browning), and west Africa (various).

Trend Breaks

The number and dates of trend changes identified by the breakpoint analysis are shown in Figure 6.4, figure 6.6 show the number of breakpoints as an annually aggregated time-series . A large number of pixels are shown to be highly dynamic, featuring one or two trend changes. The NDVI$_{sum}$ time-series shows more variability than the maximum value, where a majority of pixels are monotonic. Using NDVI$_{sum}$, 48% of pixels were monotonic, with 38% and 14% undergoing one or two breaks, respectively ($P < 0.05$). For the NDVI$_{max}$ trends, a greater proportion of pixels had no breaks (55%), whilst 35% had one and 10% had two ($P < 0.05$).

A classification of the multiple trend constituents from the breakpoint analysis is shown in Figure 6.5. Only segments occurring after a significant break ($P < 0.05$) and lasting a minimum of seven years are considered. Figure 6.5 shows that regardless of NDVI metric, a large majority of African drylands, across all regions, have experienced only greening trends in the 1982-2015 period: a minimum of seven-years' increase and no seven-year decrease in the NDVI metrics. Conversely, few areas displayed only browning trends (a minimum of seven years' decrease with no increase). These pixels were geographically clustered in the central Sahel, Angola-Zambia-Mozambique, and Tanzania. Patches of trend reversals (e.g. browning to greening) were present, although not geographically extensive. Using NDVI$_{max}$, reversals were identified in: Angola, Zambia, and southern Somalia (browning - greening), and in Tanzania, Kenya, and the western Sahel (greening - browning). Multiple changes of more than one reversal occurred in Botswana and Kenya. When the NDVI$_{sum}$ is considered, trend changes were more widespread, typically bordering areas of browning such as in Tanzania, Angola, and the Sahel.

6.4   Discussion

Linear Trends

The linear analyses revealed a prevalent trend of greening for African savannahs (Figure 6.1) This is in agreement with other studies at regional, continental, and global scales (de Jong, de Bruin, de Wit, Schaepman and Dent 2011, Fensholt et al.
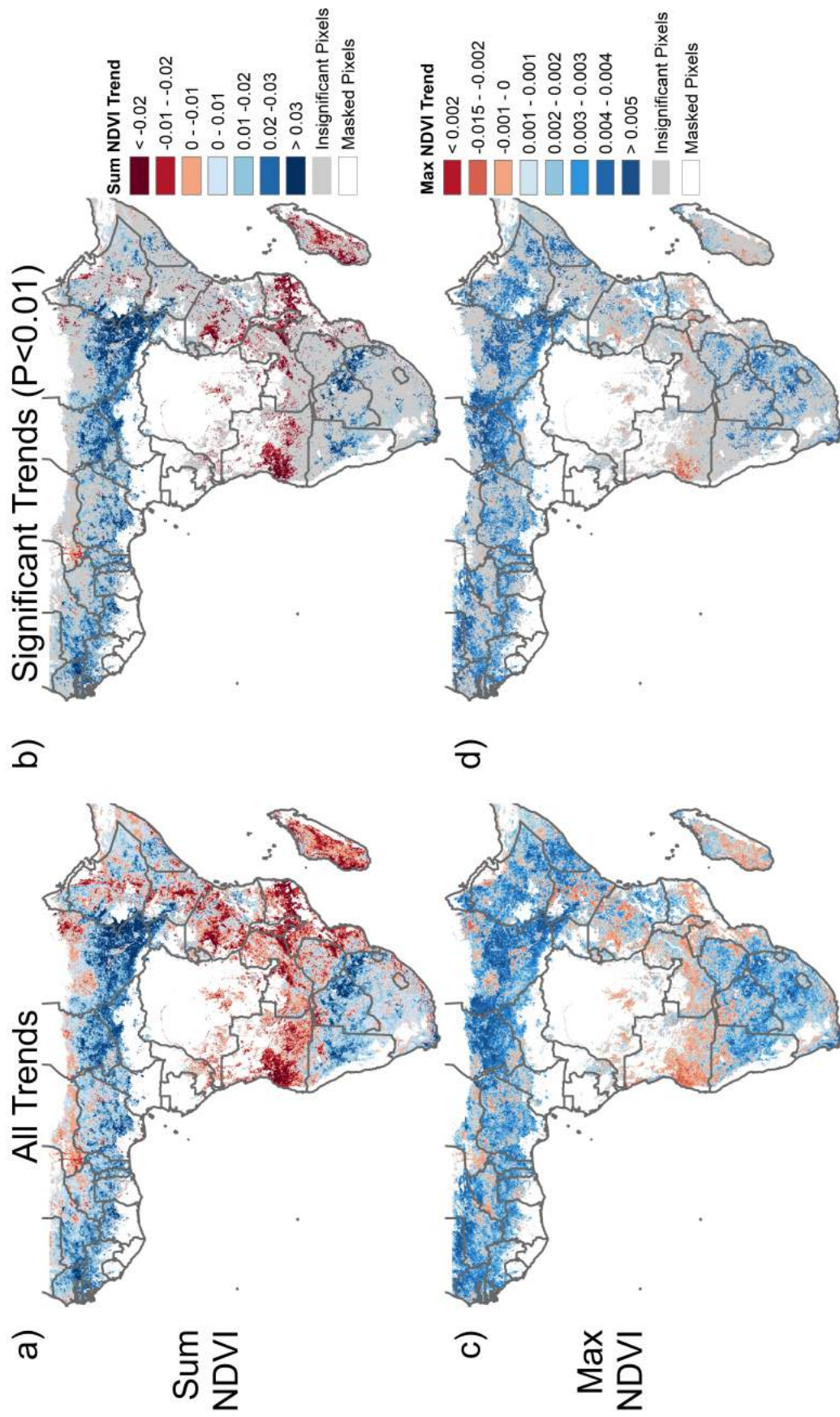
Figure 6.1: Slopes from linear models of the two NDVI metrics (max and sum) against time.
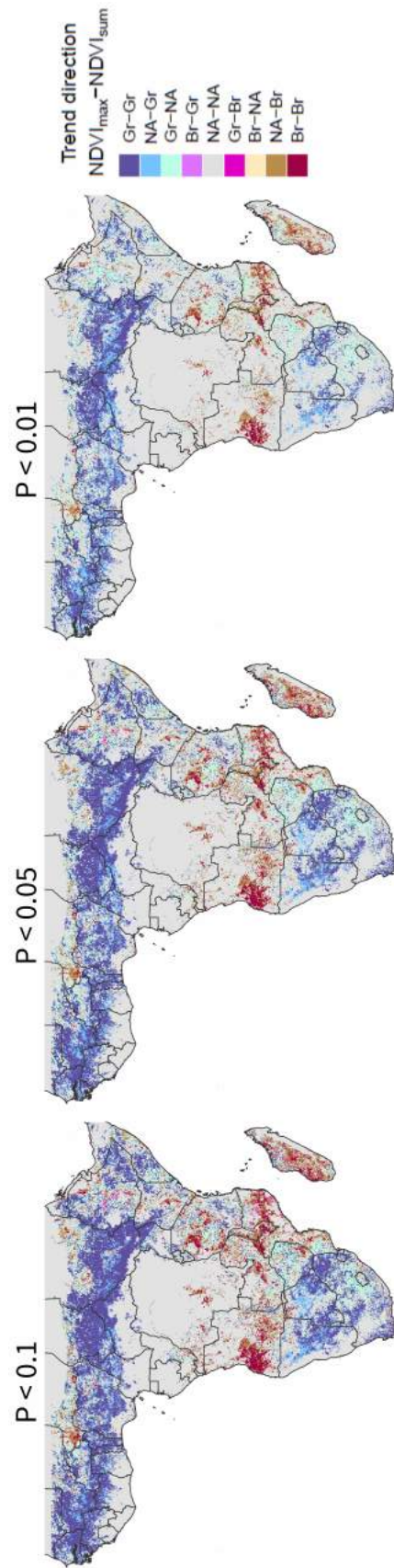
Figure 6.2: Comparison of vegetation trends, from both NDVI metrics, at three significance levels.
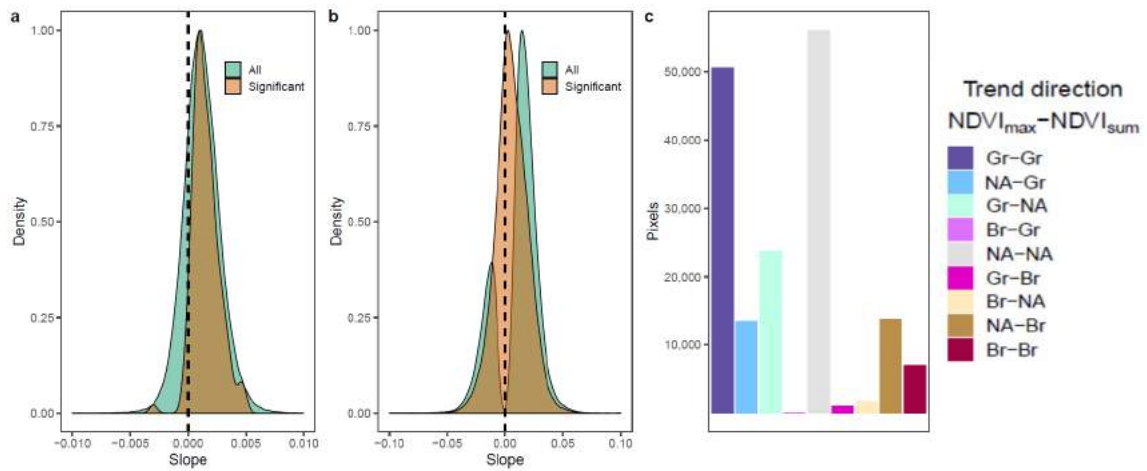
Figure 6.3: a-b) Density plots of slopes for the NDVI$_{max}$ and NDVI$_{sum}$ slopes, respectively, showing all pixels and only those that are significant at the $P < 0.05$ levels. c) Counts of pixels from the trend classification comparisons at the $P < 0.05$ level. Gr: Greening, Br: Browning, NA: No change

2012, Herrmann et al. 2005), and is consistent with observations of increasing vegetation turnover worldwide since the 1980s (Bai et al. 2008). The most pronounced greening has occurred in the Sahel, where long-term increases in vegetation ('regreening') have cocoincided with increasing rainfall, in contrast to earlier narratives of anthropogenic-driven land degradation and desertification (UNCCD 1994, Higginbottom and Symeonakis 2014). However, a relatively limited number of areas in the northernmost parts of the Sahel have experienced browning: more so according to the NDVI$_{sum}$ and the NDVI$_{max}$ this potentially indicates limits to the increases in rainfall and a shortening fo the growing season (de Jong, de Bruin, de Wit, Schaepman and Dent 2011). The NDVI$_{sum}$ model, and to a lesser extend the NDVI$_{max}$, revealed expansive browning across sub-tropical, southern Africa (Figure 6.1.a and c). However, when the insignificant trends were omitted, much of this browning was discarded (Figure 6.1.b and d). Implying that this region has a less consistent NDVI trajectory than other areas, potentially featuring trend changes over the period of analysis (de Jong et al. 2012).

Fensholt et al. (2015) proposed that divergences in the trends of different NDVI metrics may be indicative of changes in ecosystem function. We identified three types of trend divergence at noticeable frequencies. In order of occurrence these were:

1. NDVI$_{max}$:greening − NDVI$_{sum}$:no change
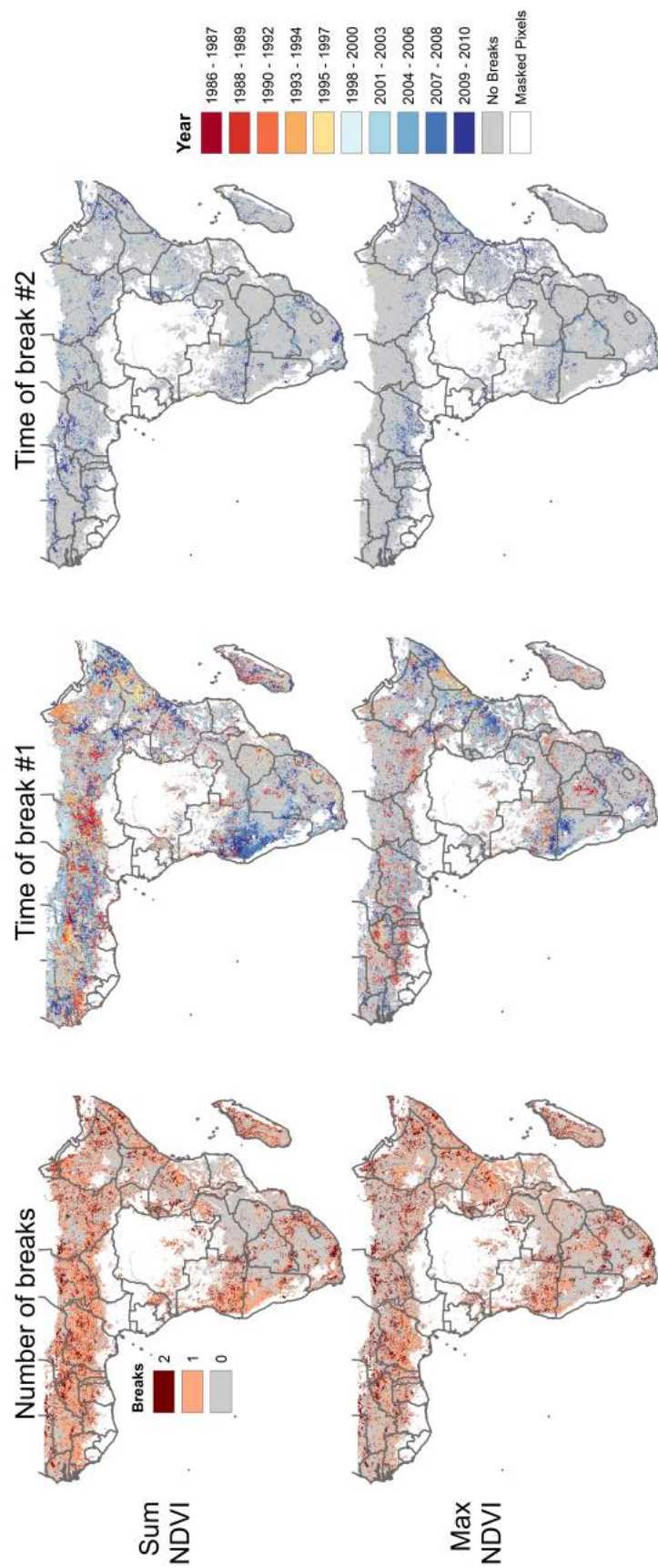
Figure 6.4: Number and timings of breakpoints for the NDVI time-series. All breakpoints are shown regardless of segment length or significance. Only significant breaks ($P < 0.05$) leading to segments longer than seven years are considered.
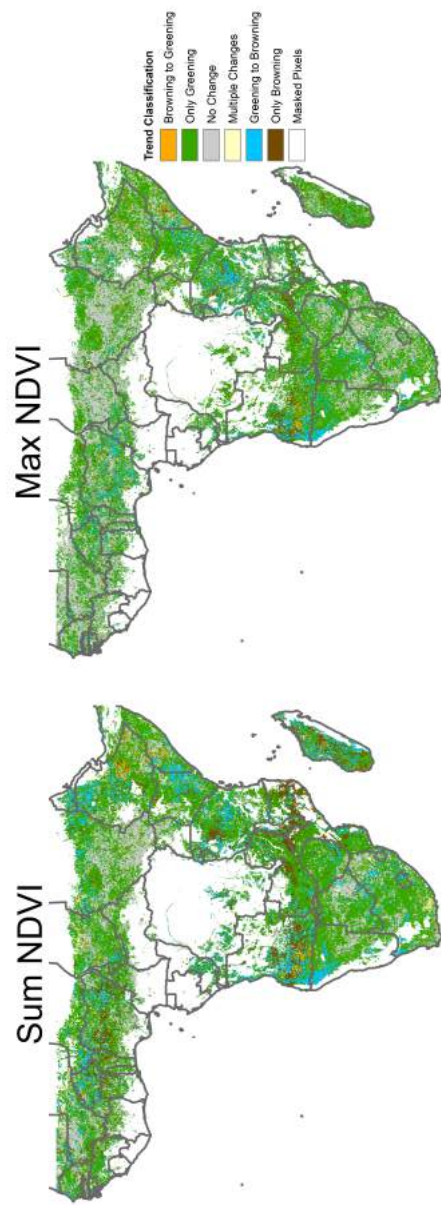
Figure 6.5: Classified NDVI trend maps, based on the breakpoints analysis. Only significant ($P < 0.05$) segments that last a minimum of seven years are considered.

111
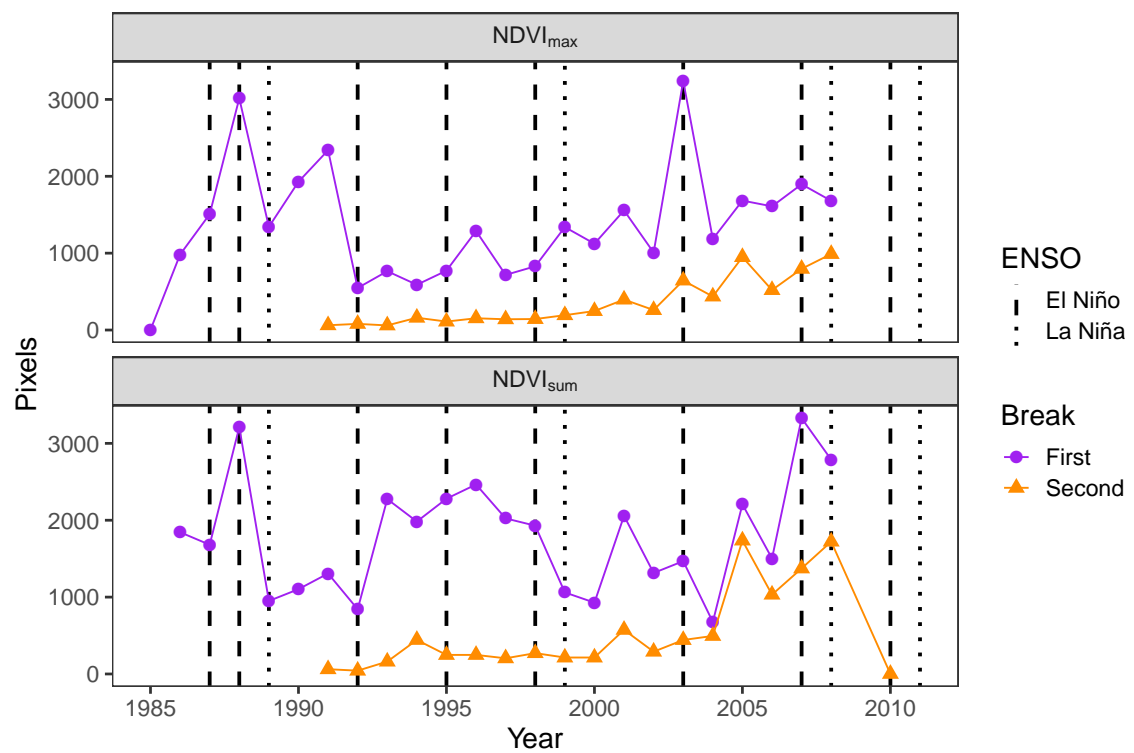
Figure 6.6: Time-series of the number of pixels undergoing a breakpoint, with ENSO years highlighted

2. $NDVI_{max}$:no change – $NDVI_{sum}$:browning

3. $NDVI_{max}$:greening – $NDVI_{sum}$:no change

(Figure 6.2 and 6.3). Divergence types one and two (consistent $NDVI_{max}$ with increasing or decreasing $NDVI_{sum}$) are spatially located in southern Africa (Namibia and Botswana) and across the Sahel. These most likely indicate areas where the overall vegetation productivity has increased or decreased but the amplitude has remained constant, such as grasslands experiencing a lengthening or shortening of the growing season but no peak productivity change. The third type of divergence (max:greening - sum:no change) is predominantly located in South Africa, Ethiopia, and Tanzania. An increase in peak (amplitude) NDVI whilst the annual integral remains constant is more likely to be indicitive of land cover or ecosystem function changes; such as, shrub encroachment or agricultural expansion. (Fensholt et al. 2015) These phenonema have been reported for the highlighted areas and are discussed in Section 6.4.

For complex ecological systems, using a simple linear model, which returns a single slope value, for a 34 year time-series is likely to be overly simplistic and fail to consider ecologically significant trajectory changes. To address this, we complemented the monotonic analysis with a trend breaks model, allowing the series to be segmented into multiple change periods with varying trajectories.

Trend Breaks

Semi-arid regions, in particular the western Sahel and Sudanese zones, contain a majority of pixels that display multiple breakpoints. This was expected for number of reasons. Firstly, the Sahel experienced increasing annual rainfall amounts during the earlier period of our analysis, which later abated (Nicholson et al. 1998). Secondly, semi-arid regions are characterised by highly variable rainfall and multi-year droughts, such as those that occurred in east Africa in the 2000s. Finally, as semi-arid regions have lower NDVI values, smaller shifts are required to instigate a significant trend change. The $NDVI_{max}$ series had relatively fewer breakpoints than $NDVI_{sum}$. This potentially indicates a near continuous increase in the maximum photosynthetic capacity, whilst the total vegetation productivity is more variable.

The detected breakpoints can be spatially and temporally grouped in to a number of clusters. Firstly, around 1988 in the western and central Sahel for both metrics, and the Kalahari for $NDVI_{max}$. Secondly, between 1991 and 1997 an increasing

113

number of breaks were detected in the far eastern Sahel and the Horn of Africa for NDVI$_{sum}$. Finally, eastern Africa, especially Kenya and Tanzania, northern Namibia, and southern Angola underwent breaks for NDVI$_{max}$ in 2003, and in 2007 for NDVI$_{sum}$. These clusters can be attributed to the role of large-scale drivers. The first Sahelian cluster has been previously discussed as a response to regional rainfall trends (Herrmann et al. 2005). The second, east African, cluster coincides with the commencement of a pronounced decline in regional rainfall in early-mid 1990s, a trend that has accelerated post-2000 (Lyon and DeWitt 2012). This decline is mainly concentrated in the longer of the two rainfall seasons, this explains the divergence between NDVI$_{max}$ and NDVI$_{sum}$, as the cumulative value is more likely to be affected than the max. No comparable climate factor can explain the shift in Angola-Namibia; however, NDVI trend breaks were observed in the same region by De Jong, Verbesselt, Zeileis and Schaepman (2013). One potential contributing factor to breaks in 2007 could be artefacts from the decommissioning of NOAA-14, which having been launched in 1994 was the longest operating NOAA satellite. Secondary breaks displayed less homogeneity; increasing in frequency from the early 1990s, with only a slight peak in 2005, predominantly in arid regions. Low spatial homogeneity in breakpoints post-2000 was also noted by De Jong, Verbesselt, Zeileis and Schaepman (2013). Interestingly, 1997-1999, when major El Niño and La Niña events occurred, do not display a noticeably larger number of breakpoints. However, other weaker ENSO events are apparent, in particular: 1988, 2003, and 2007. The 1991 Mount Pinatubo eruption does not appear to have resulted in an increase in change points, most likely due to a low sensitivity of savannahs to insolation levels (De Jong, Schaepman, Furrer, Bruin and Verburg 2013). Nevertheless, the absence of an volcanic effect, which is understandable from an ecological point of view,can be attributed to the fact that the aerosol correction procedure in the GIMMS$_{3g}$ dataset is effective (Pinzon and Tucker 2014).

Our breakpoints analysis results in noticeably fewer pixels with directional changes than a similar procedure by De Jong, Verbesselt, Zeileis and Schaepman (2013) (Figure 6.4). This can be attributed to the different approaches for classifying trend breaks. We limited our analysis to segments with a minimum length of seven years, whereas De Jong, Verbesselt, Zeileis and Schaepman (2013) used a seasonal trend model, whilst applying a threshold of a 0.25%/year NDVI change for 3.5 years to indicate non-stable trends. Both methods use a $P < 0.05$ MOSUM test. These differences make our trend classification more indicative of the overall long-term direction of the time-series, whereas the method of De Jong, Verbesselt, Zeileis and

Schaepman (2013) is more suited to detect minor shifts or fluctuations, such as the 'burst' type events they considered. Similarly, de Jong et al. (2012) identified a far higher number of breakpoints in semi-arid Africa using a Breaks For Additive Season and Trend (BFAST) approach (Verbesselt, Hyndman, Newnham and Culvenor 2010), with South Africa, Botswana, and Somalia featuring up to four changes. This was possible as they considered 4-year trend segments, designed to detect the effect of drought events and climate oscillations, whereas our study is focussed on more broad trends. The segment length requirement also explains why we did not identify many changes around major El Niño/ La Niña episodes (Figure 6.4), as these events result in short-term anomalies, which, despite having major impacts on NDVI values, do not persist long enough for inclusion (Brown et al. 2010).

The observed dynamism across our study area highlights the need to consider non-linear or segmented time-series approaches when analysing Earth-observation data. As the length of the satellite-derived data record increases, more areas are likely to reverse or alter their trend trajectory. Monotonic and linear methods have well established limitations, such as susceptibility to outliers and an inertness to late-occurring shifts, that make their use on long time-series less helpful (Wessels et al. 2012, De Beurs and Henebry 2005, De Jong, Verbesselt, Zeileis and Schaepman 2013). The trend-break method implemented here is mathematically comparable to BFAST and LandTrendR which are increasingly being used to detect trends (Kennedy et al. 2010, Forkel et al. 2013). However, there exists a wide-range of statistical methods that may also be beneficial, such as, Generalised Additive Models (GAMs), which fit the response as a smooth function of time with less assumptions and are capable of detecting periods of significant change in noisy series (Wood 2006).

Ecological Interpretation

The dominant trend dynamic identified for African savannahs was that of greening (Figure 6.2 & 6.5). This is in agreement with other studies that have used both NDVI and ecosystem models (Fensholt et al. 2012, Hickler et al. 2005, De Jong, Schaepman, Furrer, Bruin and Verburg 2013). As greening occurs almost pan-continentally, large-scale drivers should be considered as driving factors. Over the past 40 years, biogeochemical changes, such as increases in reactive nitrogen deposition and elevated atmospheric CO_2, have occurred, which increase the maximum potential vegetation production (Los 2013, Donohue et al. 2013). Furthermore, the climatic

constraints on plant growth have weakened, as rainfall has generally increased, whilst air temperature changes have been relatively minor (De Jong, Schaepman, Furrer, Bruin and Verburg 2013, Myneni et al. 1997). Combined, these factors would lead to an assumption of increasing vegetation turnover and production, especially for semi-arid regions, where constrains on plant growth are higher (Poulter et al. 2014). However, how this increase materialises is unclear, with a potential proliferation of woody cover at the expense of grasslands occurring (Stevens et al. 2016, Eldridge et al. 2011). Areas of reported shrub encroachment coincide with divergent trends in our linear models, particularly increases in the $NDVI_{max}$ but no change in the $NDVI_{sum}$.

The largest area of browning, identified by all analyses, is a latitudinal transect extending from southern Angola, through to Zambia to northern Mozambique, and Madagascar (Figures 6.2 & 6.5). Ecologically, this zone marks a transition from southern African savannah to semi-tropical woodland. This region is notable for the range and dynamism of land use/land cover changes. The end of the 1975 to 2002 Angolan civil war facilitated an increase in agriculture, which materialised through intensification of cropping frequency, within shifting cultivation (Schneibel, Frantz, Röder, Stellmes, Fischer and Hill 2017, Schneibel, Stellmes, Röder, Frantz, Kowalski, Haß and Hill 2017). Further agricultural expansion has occurred in Zambia, as part of an up-serge in soybean plantations (Gasparri et al. 2016). These changes have driven declines in Net Primary Production (NPP) and forest cover, as identified by Zhu and Southworth (2013), Brink and Eva (2009), Hansen et al. (2013). Yet, in recent years, woody biomass has increased, due to rapid regrowth and shrub expansion (McNicol et al. 2018, Tian et al. 2017). Reconciling these dynamic processes within 8 km resolution pixels, is a challenging endeavour. Over the long-term (1980-present), it is plausible that forest degradation, through agricultural expansion and charcoal harvesting, has driven browning trends, with recent regrowth leading to browning-greening reversals, whereas, woody regrowth in recent years may have contributed to browning-greening trend reversals.

The most dynamic region featuring trend reversals and divergence in the linear models is East Africa, in particular, Tanzania, but also Kenya and Ethiopia (Figures 6.2 & 6.5). Analysis in this area may be complicated by the bimodal rainfall regimes, as the maximum and sum-NDVI will be less correlated. The wider Eastern-African region, as noted by Vrieling et al. (2013), is experiencing significant decreases in the length of the growing season(s), with vegetation senescence

occurring up to one month earlier by 2010 than in the early 1980s. The most pronounced declines in growth season length, in western Tanzania, show a strong geographic alignment with a number of our identified browning pixels (Vrieling et al. 2013). The NDVI$_{sum}$ series, analysed by both monotonic and breakpoint analyses, highlighted this area as consistently browning (Figures 6.2 & 6.5). This contrasts with the NDVI$_{max}$, which showed a higher rate of no-change pixels when assessed as a monotonic slope. However, when assessed using the breakpoints analysis, a trend reversal from greening to browning occurs in the early 2000s (Figure 6.4). These differences support a phenology-based explanation: initially, the NDVI$_{max}$ will be unaffected by early senescence, until sufficient reductions have occurred, whereas the NDVI$_{sum}$ will respond more rapidly.

Sahelian and East African browning, identified in both analyses, show an alignment with regions of high and rapidly increasing population (Figure 6.2 & 6.5). Population growth was identified by Brandt et al. (2017) as a localised constraint on continental-scale woody cover increases between 1992-2011. The mechanism for this decrease was postulated as increasing demand for fuelwood and agricultural land, driving the degradation of woodlands and clearing of savannahs. This agrees with Tian et al. (2017), who identified declining woody biomass in Kenya. Interestingly, neither Brandt et al. (2017) or Tian et al. (2017) mapped a decrease in woodland condition in the Miombo woodlands of Angola-Zambia, as reported by Schneibel, Frantz, Röder, Stellmes, Fischer and Hill (2017) and Schneibel, Stellmes, Röder, Frantz, Kowalski, Haß and Hill (2017), and where our analysis highlighted extensive browning. This discrepancy may be due to the coarse resolution of the radar data used by Brandt and Tian, or alternatively this coarse scale may result in losses being balanced by shrub encroachment and regrowth. Population growth and agricultural expansion in the Sahel may result in divergent trends in woody coverage, depending on aridity. In the humid areas, cropland results in fewer trees and shrubs, than the surrounding savannah; conversely, in the arid, northern Sahel, farmlands have higher levels of woody cover than surrounding areas, as this resource is used as windbreaks and fencing (Brandt et al. 2018). From our analysis, browning pixels were predominantly located in the southern Sahel, especially for NDVI$_{max}$, coinciding with agricultural expansion in this region.

6.5   Conclusion

We used multiple time-series analysis to investigate the trends and dynamics of African savannahs for the 1982-2015 period. By aggregating the AVHRR GIMMS NDVI data set into two annual metrics (maximum and sum) we aimed to identify a range of environmental change processes. The overarching trends of African savannahs across our study period is of vegetation greening. This has occurred across all regions, even when different precipitation patterns have occurred. This would indicate the role of pan-continental driver(s). There are numerous ongoing trends which are beneficial for plant growth that could contribute to this, such as elevated CO_2 levels, nitrogen deposition, and increased temperatures. Areas of browning predominantly occurred in areas where either population growth had been high, or where phenological change has curtailed the growth season.

Chapter 7

Synthesis

The overarching aim of this thesis was to improve the capacity of Earth-observation for monitoring the ecosystem dynamics and health of semi-arid savannah ecosystems. This was approached through five research chapters, each of which addressed a distinct aspect of Earth-observation in semi-arid environments. The key findings of each chapter are as follows:

Chapter Two reviewed the use of NDVI trends to assess land degradation and desertification. This review covered the historical context of the NDVI, EO-based time-series analysis, and land degradation monitoring frameworks. Key knowledge gaps that remained unresolved or controversial were highlighted, these include: i) quantifying the robustness of trend techniques, ii) detecting degradation at minor intensities, and iii) improving the ecological interpretation of trends.

Chapter Three investigates the mapping of grass biomass by combining *in situ* field data with coarse-resolution NDVI metrics. A statistical downscaling procedure was applied to MODIS and AVHRR data to generate a 1 km resolution NDVI data set. These data were combined with a spatially dense 18-year grass biomass field dataset in a machine learning framework. The spatial and temporal consistency of the NDVI-biomass relationships were tested using spatio-temporal cross validation and feature selection procedures. Many of the models tested had good overall predictive performance, but accuracies declined when subject to target-orientated validation stratergies designed to identify over-fitting. Results showed that spatial overfitting in models is driven by the inclusion of auxiliary variables (e.g elevation), whilst temporal over-fitting was caused by annual variation in the NDVI-biomass relationship - which was attributed to varying species composition. In summary, predicting grass biomass from NDVI is not a simple process, and care must be taken to ensure any developed models are robust to spatial and temporal artefacts in the training data.

Chapter Four tested the utility of Landsat-based spectral-temporal metrics and ALOS PALSAR global mosaics for mapping regional-scale woody cover in the Limpopo Province of South Africa, for 2010. A machine learning framework was used to compare the accuracies of Random Forest models developed with i) seasonal Landsat metrics, ii) multi-seasonal Landsat metrics, and, iii) combined Landsat-PALSAR data. Furthermore, a statistical variable selection method, the recursive feature elimination (RFE), was used as a automated alternative to user-defined models. All tests were undertaken at four aggregation levels (30, 60, 90, and 120 m - pixels) to test the impact of spatial resolution on results. These test showed that combining Landsat and PALSAR data was beneficial for woody cover mapping. Whereas multi-sensor models were only marginally more effective than multi-temporal Landsat metrics using wet and dry season data. When using a single period of imagery the highest accuracies were obtained by the dry season. The RFE was effective at selected accurate models and generated the best overall model, but this was only slightly more accurate than other methods.

Chapter Five modelled changes in woody cover against a suite of explanatory variable, to test competing theories on the drivers of shrub encroachment. Carbon fertilisation-driver shrub encroachment was the theory most supported by the observed trends. This was inferred by the proportionally large increases in woody cover in areas with low wet season rainfall and low initial woody coverage. These findings support the theory that increasing atmospheric CO_2 levels are improving the water use efficiency of woody plants, allowing the expansion of woody cover in areas previously limited by water availability.

Chapter Six presents an NDVI trend-based assessment of vegetation in pan-African savannahs. A 34-year NDVI dataset was processed into two metrics: the annual sum and maximum values. These metrics were input into two trend analysis frameworks: a linear regression against time, and a structural breaks method that allows for directional changes in the trend direction. The overall result of these analyses was of near ubiquitous vegetation greening, with a majority of the land area experiencing only positive NDVI trends. The most conspicuous areas of either divergence between the metrics or negative trends were a latitudinal transect from Angola to Mozambique and the horn of Africa. Browning in east Africa may be caused by phenological change and a shortening of the growing season. While negative trends in Angola-Mozambique overlap with areas of continuing woodland degradation.

7.1 Is a Land Degradation Monitoring System Feasible?

A major environmental concern for savannah and dryland systems globally is land degradation; defined by the United Nations as *"the reduction in the capacity of the land to perform ecosystem goods, functions and services that support society and development"* (Safriel and Adeel 2005). As discussed in Chapter Two (Higginbottom and Symeonakis 2014), the mapping of land degradation using Earth-observation has typically focused on either trends in vegetation greenness (e.g. (Fensholt et al. 2012, Wessels et al. 2007)) or multi-criteria analysis of different indicators (e.g. (Symeonakis and Drake 2004, Le et al. 2012)). Given the range of Earth-observation data now available and demonstration of the effective mapping of many savannah attributes, it is theoretically feasible that a land degradation monitoring system could be developed, as comparable systems have been demonstrated in forest regions (Hansen et al. 2013, 2016). However, the key limitation to such a system is not technical but theoretical. The generally accepted definition of land degradation, provided by the UN, is not easily translated into objective measures that can be repeatedly monitored over large scales. For example, in grass dominated savannahs bush encroachment is considered a negative process as it depletes the potential grazing resource, which falls under the *'services that support society and development'* clause of the UN definition (O'Connor et al. 2014, Anadón et al. 2014) . Conversely, in miombo woodlands, a reduction in woody canopy cover would be a negative indicator, as fuelwood resources, which are also a service for society and development, decrease (Schneibel, Frantz, Röder, Stellmes, Fischer and Hill 2017). Therefore, the same trajectory in a single objective indicator, such as woody cover, could have a minimum of two divergent interpretations depending on the locality.

Earth-observation has a clear and continually improving ability to map many savannah attributes (Main et al. 2016, Mathieu et al. 2013). The conversion of these indicators into a land degradation framework is, however, a fundamentally subjective process (Warren 2002). Over large spatial and temporal scales, these decisions may render any derived product or indicator unhelpful at a local level, where the undertaken decisions are not consistent with regional ecology or livelihoods (Wessels 2009). A more appropriate framework may be a focus on generating large-scale maps of desirable indicators, such as land cover or biomass, which can be used by local actors in unique contexts, thus avoiding subjective decision on condition assessment.

7.2   Potential Future Developments

Land Cover Mapping

Mapping of land use and land cover change will greatly benefit from the launch of new sensors and the ongoing increase of open data policies. Whereas this applies to LULCC studies in general, savannahs especially will benefit, due to their strong seasonal signal and subtle spectral differences between land cover types (Hüttich et al. 2009). The density of observations currently being acquired by Landsat 8 and Sentinel 2 allows, when combined as a virtual constellation, a data point every 2.9 days, on average (Li and Roy 2017). This temporal frequency will allow the fitting of seasonal curves to quantify land cover, this approach has improved fidelity compared to the epochal metrics used in Chapters Three, Four, and Seven (Roy and Yan 2018). Greater precision, especially of seasonal timings, should allow mapping at a species level opposed to broad physiological classes. Further improvements are also being realised through multi-sensor fusion. In Chapter Three and Seven, the benefit of combining data from the L-band radar ALOS PALSAR with Landsat metrics was demonstrated. Baumann et al. (2018) recently combined temporally dense observation from Landsat 8 and the C-band radar Sentinel 1 for the South American Chaco region, this fusion was effective at mapping both shrub and tree cover as separate factional cover fields. Radar data have historically been expensive and their usage therefore limited. The recent rectification of in this situation, typified by ALOS PALSAR and Sentinel 1, will allow radar data to be processed in bulk and combined with complimentary sensors (Reiche et al. 2015).

Primary Production and Biomass

This thesis addressed two themes concerning primary production and biomass motoring: 1) the mapping of biomass using NDVI and field data, and 2) using trends in NDVI as an indicator of ecosystem condition. Therefore, two distinct areas exist that may benefit from further research.

The prediction of Gross Primary Production - and therefore biomass - from optical sensors has fundamental limitations, as photosynthesis is inferred from absorbed light measurements, not quantified directly. This limitation can be eased by narrow spectral bands that are well placed in the red-edge region, such as with Sentinel 2 (Drusch et al. 2012). However, this does not address the issue that photosynthesis is still not directly measured. An alternative to optical Earth-observation,

for GPP monitoring, is to monitor the light emitted by chlorophyll molecules as they transition from an excited to non-excited state. This *chlorophyll fluorescence* more closely relates to photosynthetic activity than ratios of absorbed spectral wavelengths. There are currently limited spaceborne sensors in operation capable of measuring activity in this spectral region, and these are typically coarse-resolution atmospheric or soil moisture orientated missions (Meroni et al. 2009). Nevertheless, the Solar-Induced chlorophyll Fluorescence (SIF) readings obtained by these sensors have produced good relationships with GPP and areas of dense cropland (Frankenberg et al. 2011). The European Space Agency has plans for the launch of a bespoke SIF mission, Fluorescence Explorer (FLEX), for 2022, which will provide valuable insights on photosynthetic processes (Drusch et al. 2017).

Trend analysis of NDVI has a range of statistical and ecological concerns, which are reviewed in detail in Chapter Two (Higginbottom and Symeonakis 2014). The key issues that were identified during review were 1) an absence of methods to ensure the robustness of trend techniques, and 2) uncertainty over the ecological interpretation of trends. To date, only Wessels et al. (2012) has attempted to develop a process to overcome the first issue, and this has not been generally adopted, despite acknowledgement of the underlying issue. Regarding issue two, since the publication of Chapter Two in 2014, it has become more common for studies to employ trend analysis on different metrics, with potential divergences being indicative of ecosystem changes (Fensholt et al. 2015). Nevertheless, ecological interpretation of NDVI trends is still highly subjective and uncertain, and merits further study.

Machine (Deep?) Learning and Earth-Observation

Several chapters of this thesis would not have been possible without the development of machine learning (ML) methods, such as random forest and cubist (Kuhn and Johnson 2013). These techniques have conferred considerable benefits to the Earth-observation community, by increasing the accuracy of land use/land cover change products, relative to older approaches. The proliferation of machine learning software is one contributor to the high accuracies reported by contemporary EO studies; which, with few exceptions, typically range from 75-90%. However, compared to more traditional statistics, these methods are highly opaque, operating as a "black-box" whereby the underlying mechanism for prediction is not readily available. Given that machine learning is not a geographic discipline, this black-box

process may prove problematic. EO data is inherently spatial, and therefore, is associated with issues such as spatial autocorrelation and non-stationarity (Lennon 2000*b*, Meyer et al. 2016). How ML handles such problems is not clear; as ML, by design, strives for statistical performance whilst operating in a black-box, it is possible – or likely– that spatially-based biases and errors may be propagated. Chapter three identified that ML approaches would "learn" spatial autocorrelation structures present in field biomass data, and incorporate this into predictive models using NDVI, therefore, exaggerating the accuracy of the model relationship. Several recent studies have moved beyond ML and applied novel *deep learning* procedures to EO imagery (Kemker et al. 2018). This family of methods is based on using multi-layered neural networks for pattern analysis and detections. Again, these technologies have been developed in a non-spatial statistical field, which does not have the considerations of geographic data. Therefore, novel statistical developments have great potential for EO analysis, but they require assessment and proving in a geographic data framework to ensure suitability. Without such quality assurance there is a strong likelihood that classical statistical issues such as spatial autocorrelation and non-stationarity may incur unforeseen errors.

Cloud Computing, Open Source Software, and Earth-Observation

Nearly all analyses in this thesis were conducted in an open-source software environment, mainly R or Python (R Core Team 2015*b*, Bivand et al. 2018). The ability of scientists to access and share open-source software has led to major strides for technique development in recent years. Remote sensing is, in essence, a computation discipline with a common source of data. This makes it well placed to benefit from the sharing and community-based development of analysis techniques. For example, Chapter Six used an open-source, time-series algorithm initially developed for application in Alaska (Forkel et al. 2013). The sharing of this software has resulted in considerably more benefit to the EO community than any single applied study could have done. Many of the most cited remote sensing papers of the past 15 years have described new software or algorithms e.g. Zhu and Woodcock (2012), Kennedy et al. (2007), Verbesselt, Hyndman, Newnham and Culvenor (2010). The development of cloud-based analysis platforms, such as Google Earth Engine, has the potential to further increase the benefits obtained from open-source software (Gorelick et al. 2017). By hosting imagery in the cloud, it is possible to reverse the traditional analysis framework, now algorithms can be developed and "taken

to the data" without the need to download the raw data (Hansen et al. 2013). This means analysis can be repeated anywhere in the world (with an internet connection). This paradigm shift has enormous potential to allow the results of studies to be widely shared, and validated. As EO data is increasingly a fixture of ecological analysis (Kennedy et al. 2014), the ability to validate and test the replicability of results is crucial, particularly when considered in light of the replication crisis in other disciplines (e.g. psychology, (Shrout and Rodgers 2018)). The combination of open-source software and cloud computing, therefore, has the potential to expand the reach, robustness and usability of EO analysis.

References

Ahlcrona, E. et al. (1988), *The impact of climate and man on land transformation in Central Sudan. Applications of remote sensing.*, number 103.

Alcaraz-Segura, D., Chuvieco, E., Epstein, H. E., Kasischke, E. S. & Trishchenko, A. (2010), 'Debating the greening vs. browning of the north american boreal forest: differences between satellite datasets', *Global Change Biology* **16**(2), 760–770.

Alcaraz-Segura, D., Liras, E., Tabik, S., Paruelo, J. & Cabello, J. (2010), 'Evaluating the consistency of the 1982–1999 ndvi trends in the iberian peninsula across four time-series derived from the avhrr sensor: Ltdr, gimms, fasir, and pal-ii', *Sensors* **10**(2), 1291–1314.

Anadón, J. D., Sala, O. E., Turner, B. & Bennett, E. M. (2014), 'Effect of woody-plant encroachment on livestock production in north and south america', *Proceedings of the National Academy of Sciences* **111**(35), 12948–12953.

Appelhans, T., Detsch, F., Nauss, T. et al. (2015), 'remote: Empirical orthogonal tele-connections in r', *J. Stat. Softw* **65**(10), 1–9.

Archer, E. (2004), 'Beyond the "climate versus grazing" impasse: Using remote sensing to investigate the effects of grazing system choice on vegetation cover in the eastern karoo', *Journal of Arid Environments* **57**(3), 381–408.

Archer, S. (1994), 'Woody plant encroachment into southwestern grasslands and savannas: rates, patterns and proximate causes', *Ecological implications of livestock herbivory in the West* **1**.

Archibold, O. W. (2012), *Ecology of world vegetation*, Springer Science & Business Media.

Armston, J. D., Denham, R. J., Danaher, Scarth, T. J., Moffiet, P. F. & Trevor, N. (2009), 'Prediction and validation of foliage projective cover from landsat-5 tm and landsat-7 etm+ imagery', *Journal of Applied Remote Sensing* **3**(033540).

Asner, G. P. (2014), 'Satellites and psychology for improved forest monitoring', *Proceedings of the National Academy of Sciences* **111**(2), 567–568.

Asner, G. P., Knapp, D. E., Balaji, A. & Páez-Acosta, G. (2009), 'Automated mapping of tropical deforestation and forest degradation: Claslite', *Journal of Applied Remote Sensing* **3**(1), 033543.

Atzberger, C. & Eilers, P. (2011), 'Evaluating the effectiveness of smoothing algorithms in the absence of ground reference measurements', *International Journal of Remote Sensing* **32**, 13.

Aubréville, A. et al. (1949), 'Climats, forêts et désertification de l'afrique tropicale'.

Bai, J. & Perron, P. (2003), 'Computation and analysis of multiple structural change models', *Journal of applied econometrics* **18**(1), 1–22.

Bai, Z. G., Dent, D. L., Olsson, L. & Schaepman, M. E. (2008), 'Proxy global assessment of land degradation', *Soil use and management* **24**(3), 223–234.

Baldi, G., Nosetto, M. D., Aragón, R., Aversa, F., Paruelo, J. M. & Jobbágy, E. G. (2008), 'Long-term satellite ndvi data sets: evaluating their ability to detect ecosystem functional changes in south america', *Sensors* **8**(9), 5397–5425.

Bastin, J.-F., Berrahmouni, N., Grainger, A., Maniatis, D., Mollicone, D., Moore, R., Patriarca, C., Picard, N., Sparrow, B., Abraham, E. M. et al. (2017), 'The extent of forest in dryland biomes', *Science* **356**(6338), 635–638.

Baumann, M., Levers, C., Macchi, L., Bluhm, H., Waske, B., Gasparri, N. I. & Kuemmerle, T. (2018), 'Mapping continuous fields of tree and shrub cover across the gran chaco using landsat 8 and sentinel-1 data', *Remote Sensing of Environment* **216**, 201–211.

Beck, H. E., McVicar, T. R., van Dijk, A. I., Schellekens, J., de Jeu, R. A. & Bruijnzeel, L. A. (2011), 'Global evaluation of four avhrr–ndvi data sets: Intercomparison and assessment against landsat imagery', *Remote Sensing of Environment* **115**(10), 2547–2563.

Birth, G. & McVey, G. (1968), 'Measuring the color of growing turf with a reflectance spectrophotometer', *Agronomy Journal* **60**(6), 640–643. cited By 148.

Bivand, R., Keitt, T. & Rowlingson, B. (2018), *rgdal: Bindings for the 'Geospatial' Data Abstraction Library*. R package version 1.3-1.
URL: *https://CRAN.R-project.org/package=rgdal*

Bond, W. J. & Keeley, J. E. (2005), 'Fire as a global âĂŸherbivoreâĂŹ: the ecology and evolution of flammable ecosystems', *Trends in ecology & evolution* **20**(7), 387–394.

Bond, W. J. & Midgley, G. F. (2012), 'Carbon dioxide and the uneasy interactions of trees and savannah grasses', *Phil. Trans. R. Soc. B* **367**(1588), 601–612.

Bradshaw, C. J. & Brook, B. W. (2014), 'Human population reduction is not a quick fix for environmental problems', *Proceedings of the National Academy of Sciences* **111**(46), 16610–16615.

Brandt, M., Hiernaux, P., Tagesson, T., Verger, A., Rasmussen, K., Diouf, A. A., Mbow, C., Mougin, E. & Fensholt, R. (2016), 'Woody plant cover estimation in drylands from earth observation based seasonal metrics', *Remote Sensing of Environment* **172**, 28–38.

Brandt, M., Mbow, C., Diouf, A. A., Verger, A., Samimi, C. & Fensholt, R. (2015), 'Ground-and satellite-based evidence of the biophysical mechanisms behind the greening sahel', *Global change biology* **21**(4), 1610–1620.

Brandt, M., Rasmussen, K., Hiernaux, P., Herrmann, S., Tucker, C. J., Tong, X., Tian, F., Mertz, O., Kergoat, L., Mbow, C. et al. (2018), 'Reduction of tree cover in west african woodlands and promotion in semi-arid farmlands', *Nature Geoscience* **11**(5), 328.

Brandt, M., Rasmussen, K., Peñuelas, J., Tian, F., Schurgers, G., Verger, A., Mertz, O., Palmer, J. R. & Fensholt, R. (2017), 'Human population growth offsets climate-driven increase in woody vegetation in sub-saharan africa', *Nature ecology & evolution* **1**(4), 0081.

Brandt, M., Romankiewicz, C., Spiekermann, R. & Samimi, C. (2014), 'Environmental change in time series–an interdisciplinary study in the sahel of mali and senegal', *Journal of Arid Environments* **105**, 52–63.

Brandt, M., Verger, A., Diouf, A. A., Baret, F. & Samimi, C. (2014), 'Local vegetation trends in the sahel of mali and senegal using long time series fapar satellite products and field measurement (1982–2010)', *Remote Sensing* **6**(3), 2408–2434.

Breiman, L. (2001), 'Random forests', *Machine learning* **45**(1), 5–32.

Brenning, A. (2012), Spatial cross-validation and bootstrap for the assessment of prediction rules in remote sensing: The r package sperrorest, *in* 'Geoscience and Remote Sensing Symposium (IGARSS), 2012 IEEE International', IEEE, pp. 5372–5375.

Brink, A. B. & Eva, H. D. (2009), 'Monitoring 25 years of land cover change dynamics in africa: A sample based remote sensing approach', *Applied Geography* **29**(4), 501–512.

Brown, M. E., de Beurs, K. & Vrieling, A. (2010), 'The response of african land surface phenology to large scale climate oscillations', *Remote Sensing of Environment* **114**(10), 2286–2296.

Brown, M. E., Pinzón, J. E., Didan, K., Morisette, J. T. & Tucker, C. J. (2006), 'Evaluation of the consistency of long-term ndvi time series derived from avhrr, spot-vegetation, seawifs, modis, and landsat etm+ sensors', *IEEE Transactions on Geoscience and Remote Sensing* **44**(7), 1787–1793.

Bucini, G., Hanan, N., Boone, R., Smit, I., Saatchi, S., Lefsky, M. & Asner, G. (2010), Woody fractional cover in kruger national park, south africa: remote-sensing-based maps and ecological insights, *in* M. J. Hill & N. P. Hanan, eds, 'Ecosystem function in savannas: measurement and modeling at landscape to global scales', CRC Press, Boca Raton, Florida, chapter 11, pp. 219–238.

Buitenwerf, R., Bond, W., Stevens, N. & Trollope, W. (2012), 'Increased tree densities in south african savannas:> 50 years of data suggests co2 as a driver', *Global Change Biology* **18**(2), 675–684.

Carlson, T. N. & Ripley, D. A. (1997), 'On the relation between ndvi, fractional vegetation cover, and leaf area index', *Remote sensing of Environment* **62**(3), 241–252.

Charney, J. (1975), 'Dynamics of deserts and drought in the sahel', *Quart. J. Roy. Meteor. Soc* **101**, 193–202.

Charney, J., Quirk, W. J., Chow, S.-H. & Kornfield, J. (1977), 'Comparative study of the effects of albedo change on drought in semi-arid regions.', *Journal of the Atmospheric Sciences* **34**(9), 1366–1385.

Chartres, C. (1987), 'Australia's land resources at risk', *Land degradation: problems and policies* pp. 7–26.

Cracknell, A. P. (2001), 'The exciting and totally unanticipated success of the avhrr in applications for which it was never intended', *Advances in Space Research* **28**(1), 233–240.

Cuni-Sanchez, A., White, L. J., Calders, K., Jeffery, K. J., Abernethy, K., Burt, A., Disney, M., Gilpin, M., Gomez-Dans, J. L. & Lewis, S. L. (2016), 'African savanna-forest boundary dynamics: A 20-year study', *PLoS One* **11**(6), e0156934.

Cutler, M., Boyd, D., Foody, G. & Vetrivel, A. (2012), 'Estimating tropical forest biomass with a combination of sar image texture and landsat tm data: An assessment of predictions between regions', *ISPRS Journal of Photogrammetry and Remote Sensing* **70**, 66–77.

Dardel, C., Kergoat, L., Hiernaux, P., Grippa, M., Mougin, E., Ciais, P. & Nguyen, C.-C. (2014), 'Rain-use-efficiency: What it tells us about the conflicting sahel greening and sahelian paradox', *Remote Sensing* **6**(4), 3446–3474.

De Beurs, K. & Henebry, G. (2005), 'A statistical framework for the analysis of long image time series', *International Journal of Remote Sensing* **26**(8), 1551–1573.

de Jong, R., de Bruin, S., de Wit, A., Schaepman, M. & Dent, D. (2011), 'Analysis of monotonic greening and browning trends from global ndvi time-series', *Remote Sensing of Environment* **115**(2), 692–702.

de Jong, R., de Bruin, S., Schaepman, M. & Dent, D. (2011), 'Quantitative mapping of global land degradation using earth observations', *International Journal of Remote Sensing* **32**(21), 6823–6853.

De Jong, R., Schaepman, M. E., Furrer, R., Bruin, S. & Verburg, P. H. (2013), 'Spatial relationship between climatologies and changes in global vegetation activity', *Global change biology* **19**(6), 1953–1964.

de Jong, R., Verbesselt, J., Schaepman, M. E. & Bruin, S. (2012), 'Trend changes in global greening and browning: contribution of short-term trends to longer-term change', *Global Change Biology* **18**(2), 642–655.

De Jong, R., Verbesselt, J., Zeileis, A. & Schaepman, M. (2013), 'Shifts in global vegetation activity trends', *Remote Sensing* **5**(3), 1117–1133.

Deering, D. (1978), 'Rangeland reflectance characteristics measured by aircraft and spacecraft sensors', *Rangeland Reflectance Characteristics Measured by Aircraft and Spacecraft Sensors* . cited By 118.

Detsch, F. (2018), *gimms: Download and Process GIMMS NDVI3g Data*. R package version 1.1.0.
URL: *https://CRAN.R-project.org/package=gimms*

Detsch, F., Otte, I., Appelhans, T. & Nauss, T. (2016), 'A comparative study of cross-product ndvi dynamics in the kilimanjaro region-a matter of sensor, degradation calibration, and significance', *Remote Sensing* **8**(2), 159.

Diffenbaugh, N. S. & Giorgi, F. (2012), 'Climate change hotspots in the cmip5 global climate model ensemble', *Climatic change* **114**(3-4), 813–822.

D'Odorico, P., Bhattachan, A., Davis, K., Ravi, S. & Runyan, C. (2013), 'Global desertification: Drivers and feedbacks', *Advances in Water Resources* **51**, 326–344.

Donohue, R. J., Roderick, M. L., McVicar, T. R. & Farquhar, G. D. (2013), 'Impact of co2 fertilization on maximum foliage cover across the globe's warm, arid environments', *Geophysical Research Letters* **40**(12), 3031–3035.

Donohue, R., Mcvicar, T. & Roderick, M. (2009), 'Climate-related trends in australian vegetation cover as inferred from satellite observations, 1981-2006', *Global Change Biology* **15**(4), 1025–1039.

Dregne, H. (1986), 'Desertification of arid lands', *Physics of Desertification* pp. 4–34.

Drusch, M., Del Bello, U., Carlier, S., Colin, O., Fernandez, V., Gascon, F., Hoersch, B., Isola, C., Laberinti, P., Martimort, P. et al. (2012), 'Sentinel-2: Esa's optical high-resolution mission for gmes operational services', *Remote Sensing of Environment* **120**, 25–36.

Drusch, M., Moreno, J., Del Bello, U., Franco, R., Goulas, Y., Huth, A., Kraft, S., Middleton, E. M., Miglietta, F., Mohammed, G. et al. (2017), 'The fluorescence explorer mission conceptâĂŤesaâĂŹs earth explorer 8', *IEEE Transactions on Geoscience and Remote Sensing* **55**(3), 1273–1284.

Eisfelder, C., Kuenzer, C. & Dech, S. (2012), 'Derivation of biomass information for semi-arid areas using remote-sensing data', *International Journal of Remote Sensing* **33**(9), 2937–2984.

Eklundh, L. & Olsson, L. (2003), 'Vegetation index trends for the african sahel 1982-1999', *Geophysical Research Letters* **30**(8), 13–1.

Eldridge, D. J., Bowker, M. A., Maestre, F. T., Roger, E., Reynolds, J. F. & Whitford, W. G. (2011), 'Impacts of shrub encroachment on ecosystem structure and functioning: towards a global synthesis', *Ecology Letters* **14**(7), 709–722.

Ellis, E. C., Klein Goldewijk, K., Siebert, S., Lightman, D. & Ramankutty, N. (2010), 'Anthropogenic transformation of the biomes, 1700 to 2000', *Global ecology and biogeography* **19**(5), 589–606.

Evans, J. & Geerken, R. (2004), 'Discrimination between climate and human-induced dryland degradation', *Journal of Arid Environments* **57**(4), 535–554.

Farrar, T., Nicholson, S. & Lare, A. (1994), 'The influence of soil type on the relationships between ndvi, rainfall, and soil moisture in semiarid botswana. ii. ndvi response to soil oisture', *Remote Sensing of Environment* **50**(2), 121–133.

Fensholt, R., Horion, S., Tagesson, T., Ehammer, A., Ivits, E. & Rasmussen, K. (2015), 'Global-scale mapping of changes in ecosystem functioning from earth observation-based trends in total and recurrent vegetation', *Global ecology and biogeography* **24**(9), 1003–1017.

Fensholt, R., Langanke, T., Rasmussen, K., Reenberg, A., Prince, S. D., Tucker, C., Scholes, R. J., Le, Q. B., Bondeau, A., Eastman, R. et al. (2012), 'Greenness in semi-arid areas across the globe 1981–2007âĂŤan earth observing satellite based analysis of trends and drivers', *Remote sensing of environment* **121**, 144–158.

Fensholt, R. & Rasmussen, K. (2011), 'Analysis of trends in the sahelian 'rain-use efficiency' using gimms ndvi, rfe and gpcp rainfall data', *Remote Sensing of Environment* **115**(2), 438–451.

Fensholt, R., Rasmussen, K., Kaspersen, P., Huber, S., Horion, S. & Swinnen, E. (2013), 'Assessing land degradation/recovery in the african sahel from long-term earth observation based primary productivity and precipitation relationships', *Remote Sensing* **5**(2), 664–686.

Fensholt, R., Sandholt, I., Rasmussen, M. S., Stisen, S. & Diouf, A. (2006), 'Evaluation of satellite based primary production modelling in the semi-arid sahel', *Remote Sensing of Environment* **105**(3), 173–188.

Foody, G. M. & Boyd, D. S. (2013), 'Using volunteered data in land cover map validation: Mapping west african forests', *IEEE Journal of Selected Topics in Applied Earth Observations and Remote Sensing* **6**(3), 1305–1312.

Forkel, M., Carvalhais, N., Verbesselt, J., Mahecha, M. D., Neigh, C. S. & Reichstein, M. (2013), 'Trend change detection in ndvi time series: Effects of inter-annual variability and methodology', *Remote Sensing* **5**(5), 2113–2144.

Frankenberg, C., Fisher, J. B., Worden, J., Badgley, G., Saatchi, S. S., Lee, J.-E., Toon, G. C., Butz, A., Jung, M., Kuze, A. et al. (2011), 'New global observations of the terrestrial carbon cycle from gosat: Patterns of plant fluorescence with gross primary productivity', *Geophysical Research Letters* **38**(17).

Frantz, D., Röder, A., Stellmes, M. & Hill, J. (2017), 'Phenology-adaptive pixel-based compositing using optical earth observation imagery', *Remote sensing of environment* **190**, 331–347.

from Jed Wing, M. K. C., Weston, S., Williams, A., Keefer, C., Engelhardt, A., Cooper, T., Mayer, Z., Kenkel, B., the R Core Team, Benesty, M., Lescarbeau, R., Ziem, A., Scrucca, L., Tang, Y., Candan, C. & Hunt., T. (2017), *caret: Classification and Regression Training*. R package version 6.0-76.
URL: *https://CRAN.R-project.org/package=caret*

Gasch, C. K., Hengl, T., Gräler, B., Meyer, H., Magney, T. S. & Brown, D. J. (2015), 'Spatio-temporal interpolation of soil water, temperature, and electrical conductivity in 3d+ t: The cook agronomy farm data set', *Spatial Statistics* **14**, 70–90.

Gasparri, N. I., Kuemmerle, T., Meyfroidt, P., le Polain de Waroux, Y. & Kreft, H. (2016), 'The emerging soybean production frontier in southern africa: conservation challenges and the role of south-south telecouplings', *Conservation Letters* **9**(1), 21–31.

Gaughan, A. E., Stevens, F. R., Gibbes, C., Southworth, J. & Binford, M. W. (2012), 'Linking vegetation response to seasonal precipitation in the okavango–kwando–zambezi catchment of southern africa', *International journal of remote sensing* **33**(21), 6783–6804.

Gherardi, L. A. & Sala, O. E. (2015), 'Enhanced precipitation variability decreases grass-and increases shrub-productivity', *Proceedings of the National Academy of Sciences* **112**(41), 12735–12740.

Giannini, A., Saravanan, R. & Chang, P. (2003), 'Oceanic forcing of sahel rainfall on interannual to interdecadal time scales', *Science* **302**(5647), 1027–1030.

Glenn, E., Smith, M. S. & Squires, V. (1998), 'On our failure to control desertification: implications for global change issues, and a research agenda for the future', *Environmental Science & Policy* **1**(2), 71–78.

Good, S. P. & Caylor, K. K. (2011), 'Climatological determinants of woody cover in africa', *Proceedings of the National Academy of Sciences* **108**(12), 4902–4907.

Gorelick, N., Hancher, M., Dixon, M., Ilyushchenko, S., Thau, D. & Moore, R. (2017), 'Google earth engine: Planetary-scale geospatial analysis for everyone', *Remote Sensing of Environment* **202**, 18–27.

Grainger, A. (2015), 'Is land degradation neutrality feasible in dry areas?', *Journal of Arid Environments* **112**, 14–24.

Griffiths, P., Kuemmerle, T., Kennedy, R. E., Abrudan, I. V., Knorn, J. & Hostert, P. (2012), 'Using annual time-series of landsat images to assess the effects of forest restitution in post-socialist romania', *Remote Sensing of Environment* **118**, 199–214.

Griffiths, P., van der Linden, S., Kuemmerle, T. & Hostert, P. (2013), 'A pixel-based landsat compositing algorithm for large area land cover mapping', *IEEE Journal of Selected Topics in Applied Earth Observations and Remote Sensing* **6**(5), 2088–2101.

Guerschman, J. P., Hill, M. J., Renzullo, L. J., Barrett, D. J., Marks, A. S. & Botha, E. J. (2009), 'Estimating fractional cover of photosynthetic vegetation, non-photosynthetic vegetation and bare soil in the australian tropical savanna region upscaling the eo-1 hyperion and modis sensors', *Remote Sensing of Environment* **113**(5), 928–945.

Guyon, I. & Elisseeff, A. (2003), 'An introduction to variable and feature selection', *Journal of machine learning research* **3**(Mar), 1157–1182.

Guyon, I., Weston, J., Barnhill, S. & Vapnik, V. (2002), 'Gene selection for cancer classification using support vector machines', *Machine learning* **46**(1-3), 389–422.

Hanan, N., Prevost, Y., Diouf, A. & Diallo, O. (1991), 'Assessment of desertification around deep wells in the sahel using satellite imagery', *Journal of Applied Ecology* **28**(1), 173–186.

Hansen, M. C., Krylov, A., Tyukavina, A., Potapov, P. V., Turubanova, S., Zutta, B., Ifo, S., Margono, B., Stolle, F. & Moore, R. (2016), 'Humid tropical forest disturbance alerts using landsat data', *Environmental Research Letters* **11**(3), 034008.

Hansen, M. C., Potapov, P. V., Moore, R., Hancher, M., Turubanova, S., Tyukavina, A., Thau, D., Stehman, S., Goetz, S., Loveland, T. et al. (2013), 'High-resolution global maps of 21st-century forest cover change', *Science* **342**(6160), 850–853.

Hargrove, W. W., Spruce, J. P., Gasser, G. E., Hoffman, F. M. et al. (2009), 'Toward a national early warning system for forest disturbances using remotely sensed canopy phenology.', *PE&RS, Photogrammetric Engineering & Remote Sensing* **75**(10), 1150–1156.

Haywood, J., Jones, A., Bellouin, N. & Stephenson, D. (2013), 'Asymmetric forcing from stratospheric aerosols impacts sahelian rainfall', *Nature Climate Change* **3**(7), 660–665.

Hein, L. & De Ridder, N. (2006), 'Desertification in the sahel: A reinterpretation', *Global Change Biology* **12**(5), 751–758.

Hein, L., De Ridder, N., Hiernaux, P., Leemans, R., De Wit, A. & Schaepman, M. (2011), 'Desertification in the sahel: Towards better accounting for ecosystem dynamics in the interpretation of remote sensing images', *Journal of Arid Environments* **75**(11), 1164–1172.

Hellden, U. (1984), 'Remote sensing for drought impact assessment - a study of land transformation in kordofan, sudan', *Advances in Space Research* **4**(11), 165–168.

Hellden, U. (1991), 'Desertification - time for an assessment?', *Ambio* **20**(8).

Helldén, U. & Tottrup, C. (2008), 'Regional desertification: A global synthesis', *Global and Planetary Change* **64**(3), 169–176.

Herold, M., Mayaux, P., Woodcock, C., Baccini, A. & Schmullius, C. (2008), 'Some challenges in global land cover mapping: An assessment of agreement and accuracy in existing 1 km datasets', *Remote Sensing of Environment* **112**(5), 2538–2556.

Herrmann, S., Anyamba, A. & Tucker, C. (2005), 'Recent trends in vegetation dynamics in the african sahel and their relationship to climate', *Global Environmental Change* **15**(4), 394–404.

Herrmann, S. M. & Hutchinson, C. F. (2005), 'The changing contexts of the desertification debate', *Journal of Arid Environments* **63**(3), 538–555.

Herrmann, S. M. & Tappan, G. G. (2013), 'Vegetation impoverishment despite greening: A case study from central senegal', *Journal of Arid Environments* **90**, 55–66.

Herrmann, S., Sall, I. & Sy, O. (2014), 'People and pixels in the sahel: a study linking coarse-resolution remote sensing observations to land users' perceptions of their changing environment in senegal', *Ecology and Society* **19**(3).

Heumann, B., Seaquist, J., Eklundh, L. & JÃűnsson, P. (2007), 'Avhrr derived phenological change in the sahel and soudan, africa, 1982-2005', *Remote Sensing of Environment* **108**(4), 385–392.

Hickler, T., Eklundh, L., Seaquist, J., Smith, B., Ardo, J., Olsson, L., Sykes, M. & Sjostrom, M. (2005), 'Precipitation controls sahel greening trend', *Geophysical Research Letters* **32**(21), 1–4.

Higginbottom, T. P. & Symeonakis, E. (2014), 'Assessing land degradation and desertification using vegetation index data: Current frameworks and future directions', *Remote Sensing* **6**(10), 9552–9575.

Higginbottom, T. P., Symeonakis, E., Meyer, H. & van der Linden, S. (2018), 'Mapping fractional woody cover in semi-arid savannahs using multi-seasonal composites from landsat data', *ISPRS Journal of Photogrammetry and Remote Sensing* **139**, 88–102.

Hijmans, R. J., van Etten, J., Mattiuzzi, M., Sumner, M., Greenberg, J. A., Lamigueiro, O. P., Bevan, A., Racine, E. B., Shortridge, A. & Hijmans, M. R. J. (2015), 'raster: Geographic data analysis and modeling', *R package version 2.3-40* .

Hill, J., Stellmes, M., Udelhoven, T., Röder, A. & Sommer, S. (2008), 'Mediterranean desertification and land degradation: mapping related land use change syndromes based on satellite observations', *Global and Planetary Change* **64**(3), 146–157.

Holben, B. N. (1986), 'Characteristics of maximum-value composite images from temporal avhrr data', *International journal of remote sensing* **7**(11), 1417–1434.

Horion, S., Prishchepov, A. V., Verbesselt, J., de Beurs, K., Tagesson, T. & Fensholt, R. (2016), 'Revealing turning points in ecosystem functioning over the northern eurasian agricultural frontier', *Global change biology* **22**(8), 2801–2817.

Huber, S., Fensholt, R. & Rasmussen, K. (2011), 'Water availability as the driver of vegetation dynamics in the african sahel from 1982 to 2007', *Global and Planetary Change* **76**(3-4), 186–195.

Huete, A., Didan, K., Miura, T., Rodriguez, E. P., Gao, X. & Ferreira, L. G. (2002), 'Overview of the radiometric and biophysical performance of the modis vegetation indices', *Remote sensing of environment* **83**(1), 195–213.

Hulme, M. (2001), 'Climatic perspectives on sahelian desiccation: 1973–1998', *Global environmental change* **11**(1), 19–29.

Hüttich, C., Gessner, U., Herold, M., Strohbach, B. J., Schmidt, M., Keil, M. & Dech, S. (2009), 'On the suitability of modis time series metrics to map vegetation types in dry savanna ecosystems: A case study in the kalahari of ne namibia', *Remote sensing* **1**(4), 620–643.

Hüttich, C., Herold, M., Wegmann, M., Cord, A., Strohbach, B., Schmullius, C. & Dech, S. (2011), 'Assessing effects of temporal compositing and varying observation periods for large-area land-cover mapping in semi-arid ecosystems: Implications for global monitoring', *Remote Sensing of Environment* **115**(10), 2445–2459.

IEA (2010), 'World energy outlook', *Paris: International Energy Agency* .

Jacob, A. L., Wilson, S. J. & Lewis, S. L. (2014), 'Forests are more than sticks of carbon', *Nature* **507**(7492), 306.

James, G., Witten, D., Hastie, T. & Tibshirani, R. (2013), *An introduction to statistical learning*, Springer.

Janzen, H. (2006), 'The soil carbon dilemma: Shall we hoard it or use it?', *Soil Biology and Biochemistry* **38**(3), 419–424.

Jenkins, C. N., Pimm, S. L. & Joppa, L. N. (2013), 'Global patterns of terrestrial vertebrate diversity and conservation', *Proceedings of the National Academy of Sciences* **110**(28), E2602–E2610.

Jeong, S.-J., Ho, C.-H., Brown, M., Kug, J.-S. & Piao, S. (2011), 'Browning in desert boundaries in asia in recent decades', *Journal of Geophysical Research Atmospheres* **116**(2).

John, R., Chen, J., Giannico, V., Park, H., Xiao, J., Shirkey, G., Ouyang, Z., Shao, C., Lafortezza, R. & Qi, J. (2018), 'Grassland canopy cover and aboveground biomass in mongolia and inner mongolia: Spatiotemporal estimates and controlling factors', *Remote Sensing of Environment* **213**, 34–48.

Jordan, C. (1969), 'Derivation of leaf area index from quality of light on the forest floor', *Ecology* **50**(4), 663–666. cited By 745.

Joseph, J. & Devadas (2015), 'Detection of rooftop regions in rural areas using support vector machine', *International Journal of Science Research Engineering* **4**, 549–553.

Kaspersen, P. S., Fensholt, R. & Huber, S. (2011), 'A spatiotemporal analysis of climatic drivers for observed changes in sahelian vegetation productivity (1982–2007)', *International Journal of Geophysics* **2011**.

Kemker, R., Salvaggio, C. & Kanan, C. (2018), 'Algorithms for semantic segmentation of multispectral remote sensing imagery using deep learning', *ISPRS Journal of Photogrammetry and Remote Sensing* **145**, 60–77.

Kendall, M. G. (1938), 'A new measure of rank correlation', *Biometrika* **30**(1/2), 81–93.

Kennedy, R. E., Andrefouet, S., Cohen, W. B., Gomez, C., Griffiths, P., Hais, M., Healey, S. P., Helmer, E. H., Hostert, P., Lyons, M. B. et al. (2014), 'Bringing an ecological view of change to landsat-based remote sensing', *Frontiers in Ecology and the Environment* **12**(6), 339–346.

Kennedy, R. E., Cohen, W. B. & Schroeder, T. A. (2007), 'Trajectory-based change detection for automated characterization of forest disturbance dynamics', *Remote Sensing of Environment* **110**(3), 370–386.

Kennedy, R. E., Yang, Z. & Cohen, W. B. (2010), 'Detecting trends in forest disturbance and recovery using yearly landsat time series: 1. landtrendrâĂŤtemporal segmentation algorithms', *Remote Sensing of Environment* **114**(12), 2897–2910.

Kgope, B. S., Bond, W. J. & Midgley, G. F. (2010), 'Growth responses of african savanna trees implicate atmospheric [co2] as a driver of past and current changes in savanna tree cover', *Austral Ecology* **35**(4), 451–463.

Kottek, M., Grieser, J., Beck, C., Rudolf, B. & Rubel, F. (2006), 'World map of the köppen-geiger climate classification updated', *Meteorologische Zeitschrift* **15**(3), 259–263.

Krausmann, F., Erb, K.-H., Gingrich, S., Haberl, H., Bondeau, A., Gaube, V., Lauk, C., Plutzar, C. & Searchinger, T. D. (2013), 'Global human appropriation of net primary production doubled in the 20th century', *Proceedings of the national academy of sciences* **110**(25), 10324–10329.

Kuhn, M. & Johnson, K. (2013), *Applied predictive modeling*, Springer.

Kuhn, M. & Quinlan, R. (2017), *Cubist: Rule- And Instance-Based Regression Modeling*. R package version 0.2.1.
URL: *https://CRAN.R-project.org/package=Cubist*

Laliberte, A. S., Rango, A., Havstad, K. M., Paris, J. F., Beck, R. F., McNeely, R. & Gonzalez, A. L. (2004), 'Object-oriented image analysis for mapping shrub encroachment from 1937 to 2003 in southern new mexico', *Remote Sensing of Environment* **93**(1), 198–210.

Lamprey, H. (1975), *Report on the Desert Encroachment Reconnaissance in Northern Sudan* . cited By 29.

Le Houerou, H. (1984), 'Rain use efficiency: a unifying concept in arid-land ecology.', *Journal of Arid Environments* **7**(3), 213–247.

Le, Q. B., Tamene, L. & Vlek, P. L. (2012), 'Multi-pronged assessment of land degradation in west africa to assess the importance of atmospheric fertilization in masking the processes involved', *Global and Planetary Change* **92**, 71–81.

Lehmann, E. A., Caccetta, P., Lowell, K., Mitchell, A., Zhou, Z.-S., Held, A., Milne, T. & Tapley, I. (2015), 'Sar and optical remote sensing: Assessment of complementarity and interoperability in the context of a large-scale operational forest monitoring system', *Remote Sensing of Environment* **156**, 335–348.

Lennon, J. J. (2000*a*), 'Red-shifts and red herrings in geographical ecology', *Ecography* pp. 101–113.

Lennon, J. J. (2000*b*), 'RedâǍŘshifts and red herrings in geographical ecology', *Ecography* **23**(1), 101–113.

Leutner, B. & Horning, N. (2016), *RStoolbox: Tools for Remote Sensing Data Analysis*. R package version 0.1.4.
URL: *https://CRAN.R-project.org/package=RStoolbox*

Li, J. & Roy, D. P. (2017), 'A global analysis of sentinel-2a, sentinel-2b and landsat-8 data revisit intervals and implications for terrestrial monitoring', *Remote Sensing* **9**(9), 902.

Liaw, A. & Wiener, M. (2002), 'Classification and regression by randomforest', *R news* **2**(3), 18–22.

Lillesand, T., Kiefer, R. & Chipman, J. (2004), 'Remote sensing and image interpretation. new york'.

Los, S. (2013), 'Analysis of trends in fused avhrr and modis ndvi data for 1982–2006: Indication for a co2 fertilization effect in global vegetation', *Global Biogeochemical Cycles* **27**(2), 318–330.

Lucas, R. M., Cronin, N., Moghaddam, M., Lee, A., Armston, J., Bunting, P. & Witte, C. (2006), 'Integration of radar and landsat-derived foliage projected cover for woody regrowth mapping, queensland, australia', *Remote Sensing of Environment* **100**(3), 388–406.

Lunetta, R. S. & Elvidge, C. D. (1999), *Remote sensing change detection*, Vol. 310, Taylor & Francis.

Lyon, B. & DeWitt, D. G. (2012), 'A recent and abrupt decline in the east african long rains', *Geophysical Research Letters* **39**(2).

MacKellar, N., New, M. & Jack, C. (2014), 'Observed and modelled trends in rainfall and temperature for south africa: 1960-2010', *South African Journal of Science* **110**(7-8), 1–13.

Main, R., Mathieu, R., Kleynhans, W., Wessels, K., Naidoo, L. & Asner, G. P. (2016), 'Hyper-temporal c-band sar for baseline woody structural assessments in deciduous savannas', *Remote Sensing* **8**(8), 661.

Malingreau, J.-P. & Tucker, C. (1988), 'Large-scale deforestation in the southeastern amazon basin of brazil', *AMBIO* **17**(1), 49–55.

Mann, H. B. (1945), 'Nonparametric tests against trend', *Econometrica: Journal of the Econometric Society* pp. 245–259.

Martiny, N., Camberlin, P., Richard, Y. & Philippon, N. (2006), 'Compared regimes of ndvi and rainfall in semi-arid regions of africa', *International Journal of Remote Sensing* **27**(23), 5201–5223.

Masek, J. G., Vermote, E. F., Saleous, N. E., Wolfe, R., Hall, F. G., Huemmrich, K. F., Gao, F., Kutler, J. & Lim, T.-K. (2006), 'A landsat surface reflectance dataset for north america, 1990-2000', *IEEE Geoscience and Remote Sensing Letters* **3**(1), 68–72.

Mathieu, R., Naidoo, L., Cho, M. A., Leblon, B., Main, R., Wessels, K., Asner, G. P., Buckley, J., Van Aardt, J., Erasmus, B. F. N. & Smit, I. P. J. (2013), 'Toward structural assessment of semi-arid african savannahs and woodlands: The potential of multitemporal polarimetric radarsat-2 fine beam images', *Remote Sensing of Environment* **138**, 215–231.

Mbow, C., Fensholt, R., Rasmussen, K. & Diop, D. (2013), 'Can vegetation productivity be derived from greenness in a semi-arid environment? evidence from ground-based measurements', *Journal of Arid Environments* **97**, 56–65.

McNicol, I. M., Ryan, C. M. & Mitchard, E. T. (2018), 'Carbon losses from deforestation and widespread degradation offset by extensive growth in african woodlands', *Nature communications* **9**(1), 3045.

Meroni, M., Rossini, M., Guanter, L., Alonso, L., Rascher, U., Colombo, R. & Moreno, J. (2009), 'Remote sensing of solar-induced chlorophyll fluorescence: Review of methods and applications', *Remote Sensing of Environment* **113**(10), 2037–2051.

Meyer, H. (2018), *CAST: 'caret' Applications for Spatial-Temporal Models*. R package version 0.1.0.
URL: *https://CRAN.R-project.org/package=CAST*

Meyer, H., Katurji, M., Appelhans, T., Müller, M. U., Nauss, T., Roudier, P. & Zawar-Reza, P. (2016), 'Mapping daily air temperature for antarctica based on modis lst', *Remote Sensing* **8**(9), 732.

Meyer, H., Reudenbach, C., Hengl, T., Katurji, M. & Nauss, T. (2018), 'Improving performance of spatio-temporal machine learning models using forward feature selection and target-oriented validation', *Environmental Modelling & Software* **101**, 1–9.

Miehe, S., Kluge, J., Von Wehrden, H. & Retzer, V. (2010), 'Long-term degradation of sahelian rangeland detected by 27 years of field study in senegal', *Journal of Applied Ecology* **47**(3), 692–700.

Mitchard, E., Saatchi, S., Woodhouse, I., Nangendo, G., Ribeiro, N., Williams, M., Ryan, C., Lewis, S., Feldpausch, T. & Meir, P. (2009), 'Using satellite radar backscatter to predict aboveground woody biomass: A consistent relationship across four different african landscapes', *Geophysical Research Letters* **36**(23).

Mitchard, E. T. & Flintrop, C. M. (2013), 'Woody encroachment and forest degradation in sub-saharan africa's woodlands and savannas 1982–2006', *Phil. Trans. R. Soc. B* **368**(1625), 20120406.

Monteith, J. L. & Moss, C. (1977), 'Climate and the efficiency of crop production in britain', *Philosophical Transactions of the Royal Society of London B: Biological Sciences* **281**(980), 277–294.

Moore, R. & Hansen, M. (2011), Google earth engine: a new cloud-computing platform for global-scale earth observation data and analysis, *in* 'AGU Fall Meeting Abstracts'.

Mucina, L., Rutherford, M. C. et al. (2006), *The vegetation of South Africa, Lesotho and Swaziland.*, South African National Biodiversity Institute.

Müller, H., Rufin, P., Griffiths, P., Siqueira, A. J. B. & Hostert, P. (2015), 'Mining dense landsat time series for separating cropland and pasture in a heterogeneous brazilian savanna landscape', *Remote Sensing of Environment* **156**, 490–499.

Myneni, R. B., Keeling, C., Tucker, C. J., Asrar, G. & Nemani, R. R. (1997), 'Increased plant growth in the northern high latitudes from 1981 to 1991', *Nature* **386**(6626), 698.

Nagol, J. R., Vermote, E. F. & Prince, S. D. (2009), 'Effects of atmospheric variation on avhrr ndvi data', *Remote Sensing of Environment* **113**(2), 392–397.

Nagol, J. R., Vermote, E. F. & Prince, S. D. (2014), 'Quantification of impact of orbital drift on inter-annual trends in avhrr ndvi data', *Remote Sensing* **6**(7), 6680–6687.

Naidoo, L., Mathieu, R., Main, R., Kleynhans, W., Wessels, K., Asner, G. & Leblon, B. (2015), 'Savannah woody structure modelling and mapping using multi-frequency (x-, c-and l-band) synthetic aperture radar data', *ISPRS Journal of Photogrammetry and Remote Sensing* **105**, 234–250.

Naidoo, L., Mathieu, R., Main, R., Wessels, K. & Asner, G. P. (2016), 'L-band synthetic aperture radar imagery performs better than optical datasets at retrieving woody fractional cover in deciduous, dry savannahs', *International Journal of Applied Earth Observation and Geoinformation* **52**, 54–64.

Naito, A. T. & Cairns, D. M. (2011), 'Patterns and processes of global shrub expansion', *Progress in Physical Geography* **35**(4), 423–442.

Nicholson, S., Davenport, M. & Malo, A. (1990), 'A comparison of the vegetation response to rainfall in the sahel and east africa, using normalized difference vegetation index from noaa avhrr', *Climatic Change* **17**(2-3), 209–241.

Nicholson, S. E. (2000), 'The nature of rainfall variability over africa on time scales of decades to millenia', *Global and planetary change* **26**(1-3), 137–158.

Nicholson, S. E., Tucker, C. J. & Ba, M. (1998), 'Desertification, drought, and surface vegetation: an example from the west african sahel', *Bulletin of the American Meteorological Society* **79**(5), 815–829.

Nicholson, S. & Farrar, T. (1994), 'The influence of soil type on the relationships between ndvi, rainfall, and soil moisture in semiarid botswana. i. ndvi response to rainfall', *Remote Sensing of Environment* **50**(2), 107–120.

O'Connor, T. G., Puttick, J. R. & Hoffman, M. T. (2014), 'Bush encroachment in southern africa: changes and causes', *African Journal of Range & Forage Science* **31**(2), 67–88.

Oldeman, L., Hakkeling, R. & Sombrock, W. (1991), 'Global assessment of soil degradation (glasod)', *Global Assessment of Soil Degradation* .

Olson, D. M., Dinerstein, E., Wikramanayake, E. D., Burgess, N. D., Powell, G. V., Underwood, E. C., D'amico, J. A., Itoua, I., Strand, H. E., Morrison, J. C. et al. (2001), 'Terrestrial ecoregions of the world: A new map of life on eartha new global map

of terrestrial ecoregions provides an innovative tool for conserving biodiversity', *BioScience* **51**(11), 933–938.

Olsson, A. D., van Leeuwen, W. J. & Marsh, S. E. (2011), 'Feasibility of invasive grass detection in a desertscrub community using hyperspectral field measurements and landsat tm imagery', *Remote Sensing* **3**(10), 2283–2304.

Otterman, J. (1981), 'Satellite and field studies of man's impact on the surface in arid regions.', *Tellus* **33**(1), 68–77.

Otterman, J. & Tucker, C. (1985), 'Satellite measurements of surface albedo and temperatures in semi- desert.', *Journal of Climate and Applied Meteorology* **24**(3), 228–235.

Pal, M. & Foody, G. M. (2010), 'Feature selection for classification of hyperspectral data by svm', *IEEE Transactions on Geoscience and Remote Sensing* **48**(5), 2297–2307.

Pearson, R. & Miller, L. (1972), 'Remote mapping of standing crop biomass for estimation of the productivity of the shortgrass prairie', *In Proceedings of the Eighth International Symposium on Remote Sensing of Environment* . cited By 1.

Peng, S., Chen, A., Xu, L., Cao, C., Fang, J., Myneni, R., Pinzon, J., Tucker, C. & Piao, S. (2011), 'Recent change of vegetation growth trend in china', *Environmental Research Letters* **6**(4).

Pereira, M. G., Sena, J. A., Freitas, M. A. V. & Da Silva, N. F. (2011), 'Evaluation of the impact of access to electricity: A comparative analysis of south africa, china, india and brazil', *Renewable and Sustainable Energy Reviews* **15**(3), 1427–1441.

Pettorelli, N. (2013), *The Normalized Difference Vegetation Index*.

Pflugmacher, D., Cohen, W. B. & Kennedy, R. E. (2012), 'Using landsat-derived disturbance history (1972–2010) to predict current forest structure', *Remote Sensing of Environment* **122**, 146–165.

Philippon, N., Jarlan, L., Martiny, N., Camberlin, P. & Mougin, E. (2007), 'Characterization of the interannual and intraseasonal variability of west african vegetation between 1982 and 2002 by means of noaa avhrr ndvi data', *Journal of Climate* **20**(7), 1202–1218.

Piao, S., Fang, J., Liu, H. & Zhu, B. (2005), 'Ndvi-indicated decline in desertification in china in the past two decades', *Geophysical Research Letters* **32**(6), 1–4.

Piao, S., Fang, J., Zhou, L., Ciais, P. & Zhu, B. (2006), 'Variations in satellite-derived phenology in china's temperate vegetation', *Global Change Biology* **12**(4), 672–685.

Pinzon, J. & Tucker, C. (2014), 'A non-stationary 1981-2012 avhrr ndvi3g time series', *Remote Sensing* **6**(8), 6929–6960.

Pollard, S., Shackleton, C. & Carruthers, J. (2003), Beyond the fence: people and the lowveld landscape, *in* J. T. Du Toit, K. H. Rogers & H. C. Biggs, eds, 'The Kruger experience: Ecology and management of savanna heterogeneity', Island Press, Washington, chapter 7, pp. 422–446.

Poulter, B., Frank, D., Ciais, P., Myneni, R. B., Andela, N., Bi, J., Broquet, G., Canadell, J. G., Chevallier, F. & Liu, Y. Y. (2014), 'Contribution of semi-arid ecosystems to interannual variability of the global carbon cycle', *Nature* **509**(7502), 600–603.

Prince, S. (1991), 'Satellite remote sensing of primary production: comparison of results for sahelian grasslands 1981-1988', *International Journal of Remote Sensing* **12**(6), 1301–1311.

Prince, S. & Astle, W. (1986), 'Satellite remote sensing of rangelands in botswana i. landsat mss and herbaceous vegetation', *International Journal of Remote Sensing* **7**(11), 1533–1553.

Prince, S., Becker-Reshef, I. & Rishmawi, K. (2009), 'Detection and mapping of long-term land degradation using local net production scaling: Application to zimbabwe', *Remote Sensing of Environment* **113**(5), 1046–1057.

Prince, S. D., Colstoun, D., Brown, E. & Kravitz, L. (1998), 'Evidence from rain-use efficiencies does not indicate extensive sahelian desertification', *Global Change Biology* **4**(4), 359–374.

Prince, S. D., Wessels, K. J., Tucker, C. J. & Nicholson, S. E. (2007), 'Desertification in the sahel: a reinterpretation of a reinterpretation', *Global Change Biology* **13**(7), 1308–1313.

Prince, S. & Tucker, C. (1986), 'Satellite remote sensing of rangelands in botswana ii. noaa avhrr and herbaceous vegetation', *International Journal of Remote Sensing* **7**(11), 1555–1570.

Prothero, R. (1974), 'Some perspectives on drought in north-west nigeria', *African Affairs* **73**(291), 162–169.

R Core Team (2015*a*), *R: A Language and Environment for Statistical Computing*, R Foundation for Statistical Computing, Vienna, Austria.
URL: *https://www.R-project.org/*

R Core Team (2015*b*), *R: A Language and Environment for Statistical Computing*, R Foundation for Statistical Computing, Vienna, Austria.
URL: *http://www.R-project.org/*

R Core Team (2017), *R: A Language and Environment for Statistical Computing*, R Foundation for Statistical Computing, Vienna, Austria.
URL: *https://www.R-project.org/*

Ravi, S., Breshears, D. D., Huxman, T. E. & D'Odorico, P. (2010), 'Land degradation in drylands: Interactions among hydrologic–aeolian erosion and vegetation dynamics', *Geomorphology* **116**(3-4), 236–245.

Reiche, J., Verbesselt, J., Hoekman, D. & Herold, M. (2015), 'Fusing landsat and sar time series to detect deforestation in the tropics', *Remote Sensing of Environment* **156**, 276–293.

Reynolds, J. F., Grainger, A., Stafford Smith, D. M., Bastin, G., Garcia-Barrios, L., FernÃąndez, R. J., Janssen, M. A., JÃijrgens, N., Scholes, R. J., Veldkamp, A., Verstraete, M. M., Von Maltitz, G. & Zdruli, P. (2011), 'Scientific concepts for an integrated analysis of desertification', *Land Degradation Development* **22**(2), 166–183.
URL: *http://dx.doi.org/10.1002/ldr.1104*

Richard, Y., Martiny, N., Rouault, M., Philippon, N., Tracol, Y. & Castel, T. (2012), 'Multi-month memory effects on early summer vegetative activity in semi-arid south africa and their spatial heterogeneity', *International journal of remote sensing* **33**(21), 6763–6782.

Röder, A., Udelhoven, T., Hill, J., Del Barrio, G. & Tsiourlis, G. (2008), 'Trend analysis of landsat-tm and-etm+ imagery to monitor grazing impact in a rangeland ecosystem in northern greece', *Remote Sensing of Environment* **112**(6), 2863–2875.

Roques, K., O'connor, T. & Watkinson, A. (2001), 'Dynamics of shrub encroachment in an african savanna: relative influences of fire, herbivory, rainfall and density dependence', *Journal of Applied Ecology* **38**(2), 268–280.

Rosenqvist, A., Shimada, M., Ito, N. & Watanabe, M. (2007), 'Alos palsar: A pathfinder mission for global-scale monitoring of the environment', *IEEE Transactions on Geoscience and Remote Sensing* **45**(11), 3307–3316.

Rouse, J., Haas, R., Schell, J. & Deering, D. (1973), 'Monitoring vegetation systems in the great plains with erts', *Third ERTS Symposium* **1**, 309–317. cited By 2152.

Roy, D. P., Ju, J., Kline, K., Scaramuzza, P. L., Kovalskyy, V., Hansen, M., Loveland, T. R., Vermote, E. & Zhang, C. (2010), 'Web-enabled landsat data (weld): Landsat etm+ composited mosaics of the conterminous united states', *Remote Sensing of Environment* **114**(1), 35–49.

Roy, D. P., Ju, J., Mbow, C., Frost, P. & Loveland, T. (2010), 'Accessing free landsat data via the internet: Africa's challenge', *Remote Sensing Letters* **1**(2), 111–117.

Roy, D. P., Wulder, M., Loveland, T., Woodcock, C., Allen, R., Anderson, M., Helder, D., Irons, J., Johnson, D., Kennedy, R. et al. (2014), 'Landsat-8: Science and product vision for terrestrial global change research', *Remote Sensing of Environment* **145**, 154–172.

Roy, D. & Yan, L. (2018), 'Robust landsat-based crop time series modelling', *Remote Sensing of Environment* .

Running, S. W., Nemani, R. R., Heinsch, F. A., Zhao, M. et al. (2004), 'A continuous satellite-derived measure of global terrestrial primary production', *Bioscience* **54**(6), 547.

Ruppert, J. C., Holm, A., Miehe, S., Muldavin, E., Snyman, H. A., Wesche, K. & Linstädter, A. (2012), 'Meta-analysis of anpp and rain-use efficiency confirms indicative value for degradation and supports non-linear response along precipitation gradients in drylands', *Journal of Vegetation Science* **23**(6), 1035–1050.

Safriel, U. & Adeel, Z. (2005), Dryland systems.âĂŰ, *in* . N. A. R. Hassan, R. Scholes, ed., 'Ecosystems and Human Well-being: Current State and Trends', Island Press, Washington, DC.

Sankaran, M., Hanan, N. P., Scholes, R. J., Ratnam, J., Augustine, D. J., Cade, B. S., Gignoux, J., Higgins, S. I., Le Roux, X., Ludwig, F. et al. (2005), 'Determinants of woody cover in african savannas', *Nature* **438**(7069), 846.

Sankaran, M., Ratnam, J. & Hanan, N. (2008), 'Woody cover in african savannas: the role of resources, fire and herbivory', *Global Ecology and Biogeography* **17**(2), 236–245.

Scheftic, W., Zeng, X., Broxton, P. & Brunke, M. (2014), 'Intercomparison of seven ndvi products over the united states and mexico', *Remote Sensing* **6**(2), 1057–1084.

Schneibel, A., Frantz, D., Röder, A., Stellmes, M., Fischer, K. & Hill, J. (2017), 'Using annual landsat time series for the detection of dry forest degradation processes in south-central angola', *Remote Sensing* **9**(9), 905.

Schneibel, A., Stellmes, M., Röder, A., Frantz, D., Kowalski, B., Haß, E. & Hill, J. (2017), 'Assessment of spatio-temporal changes of smallholder cultivation patterns in the angolan miombo belt using segmentation of landsat time series', *Remote Sensing of Environment* **195**, 118–129.

Scholes, R. & Archer, S. (1997), 'Tree-grass interactions in savannas 1', *Annual review of Ecology and Systematics* **28**(1), 517–544.

Scholes, R., Gureja, N., Giannecchinni, M., Dovie, D., Wilson, B., Davidson, N., Piggott, K., McLoughlin, C., Van der Velde, K., Freeman, A. et al. (2001), 'The environment and vegetation of the flux measurement site near skukuza, kruger national park', *Koedoe* **44**(1), 73–83.

Seaquist, J., Hickler, T., Eklundh, L., ArdÃŰ, J. & Heumann, B. (2009), 'Disentangling the effects of climate and people on sahel vegetation dynamics', *Biogeosciences* **6**(3), 469–477.

Sen, P. K. (1968), 'Estimates of the regression coefficient based on kendall's tau', *Journal of the American Statistical Association* **63**(324), 1379–1389.

Shimada, M., Itoh, T., Motooka, T., Watanabe, M., Shiraishi, T., Thapa, R. & Lucas, R. (2014), 'New global forest/non-forest maps from alos palsar data (2007âĂŞ2010)', *Remote Sensing of Environment* **155**, 13–31.

Shimada, M. & Ohtaki, T. (2010), 'Generating large-scale high-quality sar mosaic datasets: Application to palsar data for global monitoring', *IEEE Journal of Selected Topics in Applied Earth Observations and Remote Sensing* **3**(4), 637–656.

Shrout, P. E. & Rodgers, J. L. (2018), 'Psychology, science, and knowledge construction: Broadening perspectives from the replication crisis', *Annual review of psychology* **69**, 487–510.

Sinclair, A. & Fryxell, J. (1985), 'The sahel of africa: ecology of a disaster.', *Canadian Journal of Zoology* **63**(5), 987–994.

Singh, A. (1989), 'Review article digital change detection techniques using remotely-sensed data', *International journal of remote sensing* **10**(6), 989–1003.

Skole, D. & Tucker, C. (1993), 'Tropical deforestation and habitat fragmentation in the amazon: Satellite data from 1978 to 1988', *Science* **260**(5116), 1905–1910.

Skowno, A. L., Thompson, M. W., Hiestermann, J., Ripley, B., West, A. G. & Bond, W. J. (2017), 'Woodland expansion in south african grassy biomes based on satellite observations (1990–2013): general patterns and potential drivers', *Global change biology* **23**(6), 2358–2369.

Sonnenschein, R., Kuemmerle, T., Udelhoven, T., Stellmes, M. & Hostert, P. (2011), 'Differences in landsat-based trend analyses in drylands due to the choice of vegetation estimate', *Remote sensing of environment* **115**(6), 1408–1420.

Spiekermann, R., Brandt, M. & Samimi, C. (2015), 'Woody vegetation and land cover changes in the sahel of mali (1967–2011)', *International Journal of Applied Earth Observation and Geoinformation* **34**, 113–121.

Spruce, J. P., Sader, S., Ryan, R. E., Smoot, J., Kuper, P., Ross, K., Prados, D., Russell, J., Gasser, G., McKellip, R. et al. (2011), 'Assessment of modis ndvi time series data products for detecting forest defoliation by gypsy moth outbreaks', *Remote sensing of environment* **115**(2), 427–437.

Staben, G., Lucieer, A., Evans, K., Scarth, P. & Cook, G. (2016), 'Obtaining biophysical measurements of woody vegetation from high resolution digital aerial photography in tropical and arid environments: Northern territory, australia', *International Journal of Applied Earth Observation and Geoinformation* **52**, 204–220.

Staver, A. C., Botha, J. & Hedin, L. (2017), 'Soils and fire jointly determine vegetation structure in an african savanna', *New Phytologist* **216**(4), 1151–1160.

Stebbing, E. P. (1935), 'The encroaching sahara: the threat to the west african colonies', *The Geographical Journal* **85**(6), 506–519.

Stellmes, M., Udelhoven, T., Röder, A., Sonnenschein, R. & Hill, J. (2010), 'Dryland observation at local and regional scaleâĂŤcomparison of landsat tm/etm+ and noaa avhrr time series', *Remote Sensing of Environment* **114**(10), 2111–2125.

Stevens, N., Erasmus, B., Archibald, S. & Bond, W. (2016), 'Woody encroachment over 70 years in south african savannahs: overgrazing, global change or extinction aftershock?', *Phil. Trans. R. Soc. B* **371**(1703), 20150437.

Stevens, N., Lehmann, C. E., Murphy, B. P. & Durigan, G. (2017), 'Savanna woody encroachment is widespread across three continents', *Global change biology* **23**(1), 235–244.

Stringer, L., Dougill, A., Thomas, A., Spracklen, D., Chesterman, S., Speranza, C. I., Rueff, H., Riddell, M., Williams, M., Beedy, T. et al. (2012), 'Challenges and opportunities in linking carbon sequestration, livelihoods and ecosystem service provision in drylands', *Environmental science & policy* **19**, 121–135.

Symeonakis, E. & Drake, N. (2004), 'Monitoring desertification and land degradation over sub-saharan africa', *International Journal of Remote Sensing* **25**(3), 573–592.

Theil, H. (1992), A rank-invariant method of linear and polynomial regression analysis, *in* 'Henri TheilâĂŹs contributions to economics and econometrics', Springer, pp. 345–381.

Thomas, D. S., Middleton, N. J. et al. (1994), *Desertification: exploding the myth.*, John Wiley and Sons.

Tian, F., Brandt, M., Liu, Y. Y., Rasmussen, K. & Fensholt, R. (2017), 'Mapping gains and losses in woody vegetation across global tropical drylands', *Global change biology* **23**(4), 1748–1760.

Townshend, J. (1994), 'Global data sets for land applications from the advanced very high resolution radiometer: An introduction', *International Journal of Remote Sensing* **15**(17), 3319–3332.

Trollope, W. (1990), 'Development of a technique for assessing veld condition in the kruger national park using key grass species', *Journal of the Grassland Society of southern Africa* **7**(1), 46–51.

Tsalyuk, M., Kelly, M. & Getz, W. M. (2017), 'Improving the prediction of african savanna vegetation variables using time series of modis products', *ISPRS Journal of Photogrammetry and Remote Sensing* **131**, 77–91.

Tsoar, H. & Karnieli, A. (1996), 'What determines the spectral reflectance of the negev-sinai sand dunes', *International Journal of Remote Sensing* **17**(3), 513–525.

Tucker, C., Dregne, H. & Newcomb, W. (1991), 'Expansion and contraction of the sahara desert from 1980 to 1990', *Science* **253**(5017), 299–301.

Tucker, C. J. (1979), 'Red and photographic infrared linear combinations for monitoring vegetation', *Remote sensing of Environment* **8**(2), 127–150.

Tucker, C. J., Townshend, J. R. & Goff, T. E. (1985), 'African land-cover classification using satellite data', *Science* **227**(4685), 369–375.

Tucker, C., Justice, C. & Prince, S. (1986), 'Monitoring the grasslands of the sahel 1984-1985', *International Journal of Remote Sensing* **7**(11), 1571–1581.

Tucker, C., Miller, L. D. & Pearson, R. (1973), 'Measurement of the combined effect of green biomass, chlorophyll, and leaf water on canopy spectroreflectance of the shortgrass prairie', *Remote Sensing of Earth Resources* .

Tucker, C., Pinzon, J., Brown, M., Slayback, D., Pak, E., Mahoney, R., Vermote, E. & El Saleous, N. (2005), 'An extended avhrr 8-km ndvi dataset compatible with modis and spot vegetation ndvi data', *International Journal of Remote Sensing* **26**(20), 4485–4498.

Tucker, C., Vanpraet, C., Sharman, M. & Van Ittersum, G. (1985), 'Satellite remote sensing of total herbaceous biomass production in the senegalese sahel: 1980-1984', *Remote Sensing of Environment* **17**(3), 233–249.

UN (2016), 'Human development index'.

UNCCD (1994), *United Nations Convention to Combat Desertification in Those Countries Experiencing Serious Drought and/or Desertification, Particularly in Africa* .

UNCCD (2002), *Recommendations and Conclusions of the African Regional Conference Preparatory to the First Session of the Committee for the Review of the Implementation of the United Nations Convention to Combat Desertification (UNCCD-CRIC1)* .

Urbazaev, M., Thiel, C., Mathieu, R., Naidoo, L., Levick, S. R., Smit, I. P., Asner, G. P. & Schmullius, C. (2015), 'Assessment of the mapping of fractional woody cover in southern african savannas using multi-temporal and polarimetric alos palsar l-band images', *Remote Sensing of Environment* **166**, 138–153.

Van Auken, O. (2009), 'Causes and consequences of woody plant encroachment into western north american grasslands', *Journal of Environmental Management* **90**(10), 2931–2942.

Van den Dool, H. (2007), *Empirical methods in short-term climate prediction*, Oxford University Press.

Van den Dool, H., Saha, S. & Johansson, Å. (2000), 'Empirical orthogonal teleconnections', *Journal of Climate* **13**(8), 1421–1435.

Verbesselt, J., Hyndman, R., Newnham, G. & Culvenor, D. (2010), 'Detecting trend and seasonal changes in satellite image time series', *Remote sensing of Environment* **114**(1), 106–115.

Verbesselt, J., Hyndman, R., Zeileis, A. & Culvenor, D. (2010), 'Phenological change detection while accounting for abrupt and gradual trends in satellite image time series', *Remote Sensing of Environment* **114**(12), 2970–2980.

Verbesselt, J., Zeileis, A. & Herold, M. (2012), 'Near real-time disturbance detection using satellite image time series', *Remote Sensing of Environment* **123**, 98–108.

Verger, A., Baret, F., Weiss, M., Lacaze, R., Makhmara, H. & Vermote, E. (2012), 'Long term consistent global geov1 avhrr biophysical products', *In Proceedings of the 1st EARSeL Workshop on Temporal Analysis of Satellite Images* pp. 1–6.

Verrôn, S., Paruelo, J. & Oesterheld, M. (2006), 'Assessing desertification', *Journal of Arid Environments* **66**(4), 751–763.

Verstraete, M., Hutchinson, C., Grainger, A., Stafford Smith, M., Scholes, R., Reynolds, J., Barbosa, P., Léon, A. & Mbow, C. (2011), 'Towards a global drylands observing system: observational requirements and institutional solutions', *Land Degradation & Development* **22**(2), 198–213.

Verstraete, M. M., Scholes, R. J. & Smith, M. S. (2009), 'Climate and desertification: looking at an old problem through new lenses', *Frontiers in Ecology and the Environment* **7**(8), 421–428.

Vrieling, A. (2006), 'Satellite remote sensing for water erosion assessment: A review', *Catena* **65**(1), 2–18.

Vrieling, A., De Leeuw, J. & Said, M. Y. (2013), 'Length of growing period over africa: Variability and trends from 30 years of ndvi time series', *Remote Sensing* **5**(2), 982–1000.

Walter, H. (1939), 'Grasland, savanne und busch der arideren teile afrikas in ihrer ökologischen bedingtheit', *Jahrbücher für Wissenschaftliche Botanik* **87**, 750–860.

Ward, D. (2005), 'Do we understand the causes of bush encroachment in african savannas?', *African Journal of Range and Forage Science* **22**(2), 101–105.

Warner, T. A., Foody, G. M. & Nellis, M. D. (2009), *The SAGE handbook of remote sensing*, Sage Publications.

Warren, A. (2002), 'Land degradation is contextual', *Land Degradation & Development* **13**(6), 449–459.

Wessels, K. (2009), 'Letter to the editor: Comments on 'proxy global assessment of land degradation' by bai et al. (2008)', *Soil Use and Management* **25**(1), 91–92.

Wessels, K. J., Colgan, M. S., Erasmus, B. F. N., Asner, G. P., Twine, W. C., Mathieu, R., Van Aardt, J. A. N., Fisher, J. T. & Smit, I. P. J. (2013), 'Unsustainable fuelwood extraction from south african savannas', *Environmental Research Letters* **8**(1).

Wessels, K. J., Prince, S., Zambatis, N., MacFadyen, S., Frost, P. & Van Zyl, D. (2006), 'Relationship between herbaceous biomass and 1-km2 advanced very high resolution radiometer (avhrr) ndvi in kruger national park, south africa', *International Journal of Remote Sensing* **27**(05), 951–973.

Wessels, K., Prince, S., Malherbe, J., Small, J., Frost, P. & VanZyl, D. (2007), 'Can human-induced land degradation be distinguished from the effects of rainfall variability? a case study in south africa', *Journal of Arid Environments* **68**(2), 271–297.

Wessels, K., Van Den Bergh, F. & Scholes, R. (2012), 'Limits to detectability of land degradation by trend analysis of vegetation index data', *Remote sensing of Environment* **125**, 10–22.

White, J., Wulder, M., Hobart, G., Luther, J., Hermosilla, T., Griffiths, P., Coops, N., Hall, R., Hostert, P., Dyk, A. et al. (2014), 'Pixel-based image compositing for large-area dense time series applications and science', *Canadian Journal of Remote Sensing* **40**(3), 192–212.

White, M. A. & Nemani, R. R. (2006), 'Real-time monitoring and short-term forecasting of land surface phenology', *Remote Sensing of Environment* **104**(1), 43–49.

Whittaker, R. & Marks, P. (1975), 'Methods of assessing primary productivity. ch. 4 in h. leith and rh whittaker. eds. primary productivity of the biosphere'.

Williamson, J. C., Bestelmeyer, B. T. & Peters, D. P. (2012), 'Spatiotemporal patterns of production can be used to detect state change across an arid landscape', *Ecosystems* **15**(1), 34–47.

Wood, S. (2006), *Generalized Additive Models: An Introduction with R*, Chapman and Hall/CRC.

Wood, S. N. (2003), 'Thin-plate regression splines', *Journal of the Royal Statistical Society (B)* **65**(1), 95–114.

Wood, S. N. (2011), 'Fast stable restricted maximum likelihood and marginal likelihood estimation of semiparametric generalized linear models', *Journal of the Royal Statistical Society (B)* **73**(1), 3–36.

Woodcock, C. E., Allen, R., Anderson, M., Belward, A., Bindschadler, R., Cohen, W., Gao, F., Goward, S. N., Helder, D., Helmer, E. et al. (2008), 'Free access to landsat imagery', *Science* **320**(5879), 1011–1011.

Woodcock, C. E. & Strahler, A. H. (1987), 'The factor of scale in remote sensing', *Remote sensing of Environment* **21**(3), 311–332.

World Bank (2013), 'Tourism in africa: Harnessing tourism for growth and improved livelihoods', *World Bank: New York* .

Wulder, M. A., Masek, J. G., Cohen, W. B., Loveland, T. R. & Woodcock, C. E. (2012), 'Opening the archive: How free data has enabled the science and monitoring promise of landsat', *Remote Sensing of Environment* **122**, 2–10.

Wulder, M. A., White, J. C., Loveland, T. R., Woodcock, C. E., Belward, A. S., Cohen, W. B., Fosnight, E. A., Shaw, J., Masek, J. G. & Roy, D. P. (2016), 'The global landsat archive: Status, consolidation, and direction', *Remote Sensing of Environment* **185**, 271–283.

Xian, G., Homer, C., Meyer, D. & Granneman, B. (2013), 'An approach for characterizing the distribution of shrubland ecosystem components as continuous fields as part of nlcd', *ISPRS journal of photogrammetry and remote sensing* **86**, 136–149.

Zeileis, A., Kleiber, C., Krämer, W. & Hornik, K. (2003), 'Testing and dating of structural changes in practice', *Computational Statistics & Data Analysis* **44**(1-2), 109–123.

Zhang, J., Feng, L. & Yao, F. (2014), 'Improved maize cultivated area estimation over a large scale combining modis–evi time series data and crop phenological information', *ISPRS Journal of Photogrammetry and Remote Sensing* **94**, 102–113.

Zhong, L., Gong, P. & Biging, G. S. (2014), 'Efficient corn and soybean mapping with temporal extendability: A multi-year experiment using landsat imagery', *Remote Sensing of Environment* **140**, 1–13.

Zhu, L. & Southworth, J. (2013), 'Disentangling the relationships between net primary production and precipitation in southern africa savannas using satellite observations from 1982 to 2010', *Remote Sensing* **5**(8), 3803–3825.

Zhu, Z., Bi, J., Pan, Y., Ganguly, S., Anav, A., Xu, L., Samanta, A., Piao, S., Nemani, R. R. & Myneni, R. B. (2013), 'Global data sets of vegetation leaf area index (lai) 3g and fraction of photosynthetically active radiation (fpar) 3g derived from global inventory modeling and mapping studies (gimms) normalized difference vegetation index (ndvi3g) for the period 1981 to 2011', *Remote Sensing* **5**(2), 927–948.

Zhu, Z. & Woodcock, C. E. (2012), 'Object-based cloud and cloud shadow detection in landsat imagery', *Remote Sensing of Environment* **118**, 83–94.

Zhu, Z., Woodcock, C. E. & Olofsson, P. (2012), 'Continuous monitoring of forest disturbance using all available landsat imagery', *Remote Sensing of Environment* **122**, 75–91.